Development of a Turbulent Flotation Model from First Principles

Hyunsun Do

Dissertation submitted to the faculty of the
Virginia Polytechnic Institute and State University
in partial fulfillment of the requirements for the degree of

Doctor of Philosophy

In

Engineering Mechanics

Roe-Hoan Yoon, Chair
Gerald H. Luttrell
Scott L. Hendricks
Pavlos P. Vlachos
Sunghwan Jung

June 8, 2010
Blacksburg, Virginia

Keywords: flotation modeling, surface force, hydrophobic force, extended DLVO, foam drainage, foam film, critical rupture thickness

Development of a Turbulent Flotation Model from First Principles

Hyunsun Do

ABSTRACT

Flotation is a process of separating particulate materials of different surface properties in a hydrodynamic environment, and is used extensively for separating different minerals from each other in the mining industry. In this process, air bubbles are introduced at the bottom of a particulate suspension (pulp), so that bubbles coated with hydrophobic particles rise to the top and form a froth phase while hydrophobic particles stay in suspension. The selectivity of the flotation process is determined by the hydrophobicity of the particulate materials involved, while the kinetics of the process is controlled by the hydrodynamic conditions and the disjoining pressures in the thin aqueous films between air bubbles and particles.

In the present work, a mathematical model for the flotation process has been developed by considering both the hydrodynamic and surface chemical parameters. The model can describe the events occurring in both the pulp and froth phases of a mechanically-agitated flotation cell. The pulp-phase model is based on predicting the kinetics of bubble-particle attachment using the DLVO extended to include contributions from hydrophobic force and the theory of turbulent collision. The froth-phase model is based on predicting the rate of bubble-particle detachment by considering bubble coarsening and water recovery. The predictions from the overall flotation model are in general agreement with the results obtained in single-bubble flotation experiments and the flotation test results reported in literature. Since the model has been developed largely from first principles, it has predictive and diagnostic capabilities.

ACKNOWLEDGEMENT

Truthful acknowledgement cannot be described by words. In addition, this page is too small to write down all the names I love, and to whom I owe so many things. If you are reading this now, you are one of them. Thank you. Thank you for being my '*you*'. You have made me who I am.

I exceptionally name only two persons. I thank my advisor Dr. Roe-Hoan Yoon for his patience, guidance, and so many life lessons in the pursuit of my degree. I also thank my wife Sung Min for her endless love and support.

TABLE OF CONTENTS

LIST OF FIGURES

Chapter 2

A flotation model under turbulent flow conditions

Chapter 3

Induction time measurement for single-particle flotation

Chapter 4

Developing a drainage model in foams incorporating hydrophobic force

Chapter 5

Predicting the critical rupture thickness of free foam films

Chapter 6

Developing a froth-phase recovery model from first principles

LIST OF TABLES

Chapter 5

Predicting the critical rupture thickness of free foam films

Chapter 1. Introduction

1. Fundamentals on Flotation Modeling

Flotation is a process for separating finely divided solids from each other using air bubbles under hydrodynamic environment [1]. Regarding its application in the mining industry, it has been used for more than 100 years for separating valuable minerals from raw ore. This popularity is due to its low operation cost, simplicity and versatility. Virtually any mineral present in an ore can be separated from other minerals by flotation. Minerals to be floated must be either naturally hydrophobic or rendered hydrophobic by judicious use of hydrophobizing reagents (collectors). Therefore, when bubbles are introduced into the bottom of a flotation cell in which an ore pulp is contained, hydrophobic mineral particles are selectively attached to the bubbles while hydrophilic mineral particles are left unattached. The bubble-particle aggregates formed as a result of the attachment process then rise to the top of the slurry and exit the flotation cell, and thereby be separated from the hydrophilic minerals left in the cell.

For the bubble-particle attachment to occur, the Gibbs free energy change (ΔG) must be negative. The free energy change associated with the attachment process can be by considering the changes in interfacial tensions at the solid-liquid, solid-vapor, and liquid-vapor interfaces [2]. By relating the changes in interfacial tensions to the Young's equation, one obtains the flowing relation,

$$\Delta G = \gamma_{lv}(\cos\theta - 1) < 0 \qquad (1)$$

as the thermodynamic criterion for bubble-particle attachment, or flotation. In Eq. (1), γ_{lv} is the interfacial tension between liquid and vapor, and θ is the contact angle at the three phase contact. From this relation it is clear that the process of bubble-particle attachment is thermodynamically possible only when the contact angle is greater than zero. The larger the value of θ is, the more negative the value of ΔG becomes. Therefore the contact angle has often been used as a measure of floatability. Parameters such as θ or γ_{lv} vary depending on the chemical conditions such as collector and concentrations employed during flotation.

While the thermodynamic criterion for floatation is determined by chemistry parameters, hydrodynamic parameters such as bubble size, particle size, and energy dissipation rate in a flotation cell also affect the process. Flotation machines are designed to optimize the hydrodynamic conditions to maximize bubble-particle collision, which is a prerequisite for the attachment process discussed above, and to keep particles in suspension and move forward from one cell to another. It is difficult, however, to experimentally measure collision frequencies as it is a stochastic process particularly under turbulent flow conditions.

Many investigators developed collision models and used them to predict coagulation of colloidal particles [3-9]. The various collision models developed to date are of different forms, but may be represented in the following generalized form:

$$Z_{12} = CN_1N_2(d_{12})^n \quad (2)$$

in which Z_{12} is the number of collisions between species **1** and species **2**, N_1 and N_2 are the number densities of particles **1** and **2**, d_{12} is the sum of the radius of the two particles, which is referred to as collision radius, and C and *n* are parameters varying with the boundary conditions involved in the derivation of the models. It is a challenge to use Eq. (2) developed for the interaction between small, colloidal size particles in liquid or gaseous phases for flotation, in which **1** is solid and **2** is air bubble and particle sizes are well beyond the length scales involved colloidal and aerosol interactions. Many investigators adapted Eq. (2) for the bubble-particle interactions in flotation by introducing adjustable parameters such as probability (or efficiency) of collision (P_c), attachment (P_a) and detachment (P_d) [10-12]. Modeling flotation is complicated further by the fact that bubble-particle aggregates form a froth phase (three-phase foam) on top of the flotation pulp and that some of the bubble-particle aggregates break up during the course of entering and rising in the froth phase. Thus, it would be necessary to consider the probability of the hydrophobic particles not being dropped out of the froth phase and exit the flotation cell and be recovered in the forth launder (P_f).

Many investigators showed that flotation can be represented as first-order rate process, in which case the following flotation rate equation may be used [13, 14]:

$$\frac{dN_1}{dt} = -kN_1 = -Z_{12}P \quad (3)$$

Eq. (3) states that the rate of flotation is proportional to the number density (N_1) of particles in a flotation cell and flotation time *t*, with *k* being the flotation rate constant. Its shows also that flotation rate is simply the product of collision frequency (Z_{12}) and the probability of flotation (P). Sutherland [13] proposed that P should be a function of various subprocesses discussed above, *i.e.*, P_c, P_a, P_d, and P_f. Most of the investigators derived the probability functions of some of these sub-processes by considering hydrodynamic parameters. Others, however, considered both hydrodynamic and surface chemistry parameters [9, 14-16]

So far, most researchers on flotation modeling laid foundations for predicting flotation rate either by using chemistry or hydrodynamic parameters. Not many studied the effects of both parameters partuclarly for the flotation under turbulent flow conditions. Serious attempts to account for both parameters were few [9, 16]. More recently, however, increasing number of researchers have challenged the subject of modeling flotation by taking advantages of the recent advances in fluid mechanics, particularly CFD simulations, and in colloid chemistry, particularly on the role of hydrophobic force in the thin films of water between air bubble and particles, which are referred to as wetting films. Recent interest in flotation model development may stem also from ever increasing demands for natural resources. Developing a good flotation model should lead to the development of a computer simulator that can be used to optimize the process, train plant operators and engineers, and help better understand the complex three-phase phenomenon.

2. Research Objectives

The objectives of the present work are restated as follows:

1) To develop a turbulent flotation model from first principles by considering both chemistry and hydrodynamic parameters.

2) To study bubble-particle attachment kinetics by conducting induction time measurements under different chemical and hydrodynamic conditions.

3) To develop a foam drainage model from first principles and compare the model predictions with experimental results.

4) To develop a model to predict the critical rupture thicknesses for free foam films, and use the model to predict bubble coarsening in foam columns.

5) To develop a froth recovery model and incorporate it into the flotation model to be developed in Chapter 1.

3. Literature Review

The first aggregation kinetics model was in higher order since it was derived for colloidal particles subject to Brownian motion [17]. However, flotation system is less influenced by Brownian motion, and accordingly many investigators used the first order equation shown in Eq.(3) [9, 12-16, 18-22].

Equation (3) is interpreted such that the rate constant k indicates how fast the floatable particles are recovered. So many various parameters are involved in the constant, but largely, it has been found a function of the number of bubble-particle collisions taking place (Z_{12}), and the probability (P) of the collision's follow-up sub-processes, *i.e*.

$$k = f(Z_{12}, P) \tag{4}$$

Z_{12} is termed as collision frequency. As the name purports, Z_{12} presents the number of encounters between bubbles (subscript 2) and particles (subscript 1) occurring in their relative motions. Regarding this, earlier models in the literature used the simple idea that a bubble meets particles in the way when it sweeps through, and reached an approximate relation of Z_{12} with bubble size and superficial gas flow rate [12, 15]. According to the relation the frequency increases as gas flow rate increases, and inversely to the bubble size. However, this relation may not fit well for turbulent flow conditions.

In turbulent flow environment, modeling Z_{12} and P will be substantially different from what is for relatively quiescent flow conditions because bubbles and particles may influence each other's adjacent streamlines. In fact, researchers like Pyke *et al*.[9] extended to turbulent flow conditions the model originally derived from the streamline assumption around a bubble in quiescent flow

[22]. On the other hand, Sherrell and Yoon [16] suspected this idea and incorporated turbulence properties into calculating *P* based on surface energy estimate. The model, however, showed a result indicating that flotation kinetics is controlled more by bubble-particle detachment, rather than attachment [21].

Turbulence is composed of eddies of various length scales. Turbulent kinetic energy is known to be distributed along these different length scales, and the energy input at the largest scale is transferred successively to smaller scales until it dissipates out. One of the most significant properties of turbulence is the energy dissipation (or specific energy input), ε_{sp}. It involves along with the liquid viscosity in determining the statistically universal form of the dissipation length scale [23]. In some turbulent systems where inertial effects are ignored, the root mean squared (r.m.s) value of fluid's velocity gradients is proportional to the square root of the ratio of energy dissipation to liquid viscosity [24]. In such systems, collision frequencies are derived using the relation [3, 8]. For the case of systems where inertial effects are not ignored, collisions are not due to shear mechanism only. Therefore, Abrahamson [4] implied the r.m.s velocities of suspended particles 1 and 2 directly into the model as the following.

$$Z_{12} = 2^{3/2}\pi^{1/2}N_1N_2d_{12}^2\sqrt{\overline{u_1}^2 + \overline{u_2}^2} \tag{5}$$

with notations meaning the same as in Eq.(2). $\overline{u_1}^2$ and $\overline{u_2}^2$ are the mean squared fluctuation velocities. This has been frequently referenced in describing aggregations in flotation systems. In the application of mineral flotation, Schubert [25] regarded the particles as minerals (subscript 1) and bubbles (subscript 2), and replaced the velocity term with the one proposed by Liepe and Moeckel [26]. Recently, Brady *et al*.[27] verified experimentally several models describing particle velocities in homogeneous turbulence. In their model comparison, Liepe and Moeckel [26]'s expression fit best for describing particle velocities. This information may be useful in modeling bubble-particle interactions in flotation system. However, there exists a limitation that the models are valid only for homogenous turbulence. In practical flotation tank, it is well known that near-impeller regions have higher energy dissipations than the remainders, and even with certain ratio relative to the average energy dissipation [9, 28, 29]

In turbulent flow conditions, neither the probability *P* of sub-processes nor the number of collisions is independent of hydrodynamic influence. On the other hand, unlike the collision frequency, surface chemistry also plays equivalently important role in evaluating *P*. The most important phenomenon implied in *P* is the bubble-particle attachment. Luttrell and Yoon [11] suggested the following expression for estimating the probability of bubble-particle attachment, P_a.

$$P_a = \exp\left(-E_1/E_k\right) \tag{6}$$

,where E_1 is the energy barrier or activation energy for bubble-particle attachment determined by colloidal forces, and E_k is the kinetic energy of collision. For objects in liquid medium, the hydrodynamic resistance increases as two surfaces approach closer [30, 31]. Due to this resistance, the kinetic energy exerted on particles in flotation system should reduce at sufficiently small separation distance to a comparable degree to the order of activation energy.

In aggregation kinetics modeling, Derjaguin and Dukhin [14] were the first who used surface forces in modeling bubble-particle interactions. Their work, however, was intriguing for mineral processing applications because what they considered were only repulsive forces while for mineral flotation to occur attractive force is responsible [32]. Therefore, Luttrell and Yoon [11] modified the classical DLVO theory that is used to describe the bubble-particle interaction energy. After adding attractive energy term due to hydrophobic force, the extended DLVO theory is as follows.

$$V_T = V_E + V_D + V_H \tag{7}$$

,where V_T is the total potential energy summed up by the potential energies due to electrostatic repulsion(V_E), Van der Waals dispersion (V_D), and hydrophobic force attraction (V_H). The value of energy barrier E_1 in Eq.(6) is found at the local maximum of the potential *vs*. separation distance curve portrayed by Eq.(7). Regarding the term V_H, no general analytical expressions is available because the origin of hydrophobic force is still at a loss. However, the evidences for its existence can be found easily in other literature [33-35].

Similar to P_a, the probability of detachment was also suggested as follows [15].

$$P_d = \exp\left(-(W_a + E_1)/E'_k\right) \tag{8}$$

,where W_a is the work of adhesion and E_k' is the detachment kinetic energy. The work of adhesion is derived from the force balance on the particle area in contact with bubble surface, and accordingly surface tension, contact area, and contact angles are involved.

After Sutherland [13]'s pioneering work, most of flotation models adopted the idea of the sub-process probability P as a product of collision (P_c), attachment (P_a), and detachment probability (P_d) as follows.

$$P = P_c P_a (1 - P_d) \tag{9}$$

Many flotation models in the literature estimate flotation rate constants based on this relationship. However, it may be appropriate only for describing batch flotation test where 100% recovery of mineral within the froth is usually assumed [36, 37]. The rate constants obtained in this way may be regarded 'apparent' rate constant since the pulp-to-froth transport process of particles collected in the pulp is ignored.

To be realistic, the transfer process needs to be considered. Noting that froth-pulp interface behaves like a barrier before the bubble-particle aggregates transfer, the probability of aggregates being transferred into froth (P_f) is incorporated with P as follows.

$$P = P_c P_a (1 - P_d) P_f \tag{10}$$

The same idea dates back as old as the work by Schumann [38]. However, the post-attachment sub-processes were not specified as the author simply put them in one parameter defined as froth stability factor. Clear distinction was not made until Tomlinson and Flemming's work [20] where the authors first suggested P_f as a probability of the attached particle reaching the pulp-froth interface without detachment. A clearer picture to this statistical aspect has been shown by Waters *et al*. recently [39]. In their experiment, the authors used positron emission particle tracking method to follow particles in flotation cells, and observed particles entering the froth after attaching to an air bubble, detaching from the froth, and re-entering. For all this experimental advances, incorporating P_f into P doesn't seem easy either empirically or analytically, because of the complex characteristics of froth [16, 20, 38]. According to the recent work by Koh and Schwarz [40, 41], froth phase is a significant contributor to the overall recovery. Aided by a Computational Fluid Dynamics (CFD) program for the first time, they could predict the temporal changes of total particle numbers in a lab-scale cell, which were used to infer the flotation rate constant.

As it was well reviewed in other literature, kinetic modeling of flotation critically depends on the assumptions made for the mixing conditions of the flow in the cell [42, 43]. Typically, two perfectly mixed flow regimes are defined: pulp and froth phase. With this regard, the first order kinetic modeling is valid only in the pulp phase, and the process in the froth phase needs to be studied separately if interested. Nevertheless, many researchers did not account for this in modeling flotation. At best, froth recovery was investigated separately while setting the 'apparent' rate constant proportional to froth recovery [12, 44-46]. In other words,

$$k = k_p R_f \tag{11}$$

,where k is the overall (apparent) flotation rate constant, k_p is the rate constant concerning the collection mechanism in pulp phase only, and R_f is defined as the froth recovery factor. R_f is interpreted as the fraction of particles recovered after they are transferred into froth [12]. While k is inferred from the recovery data in flotation tests, k_p is evaluated by extrapolating rate constants plot obtained from the same recovery data with various froth depths. However, the relation in Eq.(11) is not strictly valid because it is derived assuming the particles collection in the pulp phase is a first order process with 100% maximum recovery, that is ideal case [36, 43].

Many researchers do not differentiate k with k_p in interpreting recovery data. One common mistake is that they obtain the "apparent" rate constant k from recovery data, then wrongfully use it for validating the model derived for pulp phase only [9, 47, 48]. To conduct more precise validation, the overall recovery data needs to be directly compared with the model prediction, not the rate constant. Finch and Dobby [12] suggested the following to estimate the overall flotation recovery when the recovery in the pulp phase and froth phase are discrete.

$$R = \frac{R_c R_f}{R_c R_f + 1 - R_c} \tag{12}$$

,where R is the overall recovery, and R_c and R_f ar the recovery in the pulp and froth phase respectively. R_c can be estimated using the rate constant k_p, and R_f needs to be defined independently.

The fractional recovery in the froth phase, R_f, may be modeled in a broader sense by the following aspects. Since air bubbles are hydrophobic [49] as well as mineral particles, the mechanisms governing froth recovery can be attributed to attachment. This is called true froth recovery because only hydrophobic particles are recovered along with the surviving bubble-particle aggregates from the froth. Because froth bubbles are hydrophobic and in 3 phase some researchers could model the recovery in empirical ways only [50, 51]. However, more analytical froth recovery model may be developed by investigating liquid drainage and bubble coarsening in froth. It is well known that non-hydrophobic particles are also recovered from froth, being carried by the froth without attachment. This is called entrainment, and it is not directly related to the chemistry but well known to play significant roles in the fine mineral particles recovery [52, 53].

Recovery mechanisms in relation with froth structure may be more simplified if one is to apply the same physical interpretations to foams. *Foams* is the term used to distinguish the 2 phase system from the 3 phase (*froths*) [54]. A foam is a two-phase system where gas cells are enclosed by liquid, and accordingly the structure looks like a network of pipe-like channels (called Plateau Border) and thin film walls (called lamellae) [55]. The drainage along this structure has been a popular research topic for a long time because foams are commonly observed in many practical applications. Most of foam drainage models in the literature assume that liquids in foams flow mainly through the channels, and set the following continuity equation as the basis for the model [56-60]

$$\frac{\partial \varepsilon}{\partial t} + \frac{\partial (\varepsilon u)}{\partial x} = 0 \tag{11}$$

,where ε is the liquid fraction defined as the ratio of wet area over the whole column cross-sectional area and u is the average velocity of the flow through plateau borders. This equation basically states that the rate of change of the liquid mass flow inside the volume is balanced by the changes induced by the flow velocity through the surface area. Knowing that the pressure difference between liquid and gas bubble is described by the Young's equation, an expression for u can be found after manipulating the Euler equation [59, 60]. The models in the literature were derived only for dry and stable foams. In reality, however, foam bubbles grow, break and coalesce into larger sizes. Those models fail to comprise the coalescence of bubbles. Combining coalescence with drainage model is challenging because the factors causing foam's instability are not clear yet. The most convincing factor so far is the hydrophobic force in foam films. In many experiments on foam films drainage, it has been shown that foam films thin faster than the prediction by the Reynolds lubrication equation and it was ascribed to the hydrophobic force [61, 62]. Thin water films tend to rupture at different thicknesses for different surfactant concentrations or certain chemical conditions. This particular thickness is termed as critical rupture thickness h_{cr}. The film thinning rate down to h_{cr} in those systems is well predictable with the help of the extended DLVO theory [62], but a good theory to predict the approximate time of rupture or corresponding rupture thickness is still missing. Majority of researchers on film rupture models think that the rupture results from capillary waves due to the forces at the water-air interface [63-65], but those models also deviate from actual observations when hydrophobic force is influential [61, 66].

4. Dissertation Outline

The results of the present work are presented in five chapters in the same order as listed under Research Objectives.

Chapter 1 gives an overview and justification of the present research along with literature review.

Chapter 2 presents the model developed in the present work. The model consists of two parts, including i) the model describing the bubble-particle attachment and detachment processes occurring in the pulp phase of a flotation cell and ii) the transport of resulting bubble-particle aggregates and entrained particles through the froth phase.

Chapter 3 shows i) the effects of chemical and hydrodynamic parameters affecting flotation, and ii) the role of surface forces affecting the kinetics of bubble-particle attachment by conducing induction time measurements.

Chapter 4 describes a foam drainage model derived from first principles. The model can predict bubble coarsening as functions of the hydrophobic force parameter (K_{232}), which in turn is a function of surfactant (frother) additions.

Chapter 5 gives a theoretical model that can predict the critical rupture thickness of free foam films.

Chapter 6 presents derivation of thefroth recovery model that is used in Chapter 1.

Chapter 7 suggests possible future work in developing a comprehensive flotation model.

All of the chapters have been written in journal paper formats for publications with appropriate amendments in the near future.

5. References

1. Gaudin, A.M., *Flotation*. 1957: McGraw Hill.
2. Laskowski, J., ed. *The relationship between floatability and hydrophobicity*. Advances in Mineral Processing, ed. P. Somasundaran. 1986, SME publication.
3. Saffman, P.G.a.T., J.S., *On the collision of drops in turbulent coluds.* Journal of Fluid Mechanics, 1956. **1**: p. 16-30.
4. Abrahamson, J., *Collision rates of small particles in a vigorously turbulent fluid.* Chemical Engineering Science, 1975. **30**(11): p. 1371-1379.
5. Levins, D.M. and J.R. Glastonbury, *Particle-liquid hydrodynamics and mass transfer in a stirred vessel.* Chemical Engineering Research and Design, 1972. **50A**: p. 32-41.
6. Kruis, F.E. and K.A. Kusters, *The collision rate of particles in turbulent flow.* Chemical Engineering Communications, 1997. **158**: p. 201-230.

7. Bloom, F. and T.J. Heindel, *On the structure of collision and detachment frequencies in flotation models.* Chemical Engineering Science, 2002. **57**(13): p. 2467-2473.
8. Camp, P.R. and P.C. Stein, *Velocity gradients and internal work in fluid motion.* Journal of the Boston Society of Civil Engineers, 1943. **30**(4): p. 219-237.
9. Pyke, B., D. Fornasiero, and J. Ralston, *Bubble particle heterocoagulation under turbulent conditions.* Journal of Colloid and Interface Science, 2003. **265**(1): p. 141-151.
10. Weber, M.E. and D. Paddock, *Interceptional and gravitational collision efficiencies for single collectors at intermediate Reynolds numbers.* Journal of Colloid and Interface Science, 1983. **94**(2): p. 328-335.
11. Luttrell, G.H. and R.-H. Yoon, *A hydrodynamic model for bubble-particle attachment.* Journal of Colloid and Interface Science, 1992. **154**(1): p. 129-137.
12. Finch, J.A. and G.S. Dobby, *Column flotation*. 1990: Pergamon press.
13. Sutherland, K.L., *Physical Chemistry of Flotation. XI. Kinetics of the Flotation Process.* The Journal of Physical and Colloid Chemistry, 1948. **52**(2): p. 394-425.
14. Derjaguin, B.V. and S.S. Dukhin, *Theory of flotation of small and medium-size particles.* Transactions of Institutions of Mining and Metallurgy, 1961. **70**: p. 221-246.
15. Yoon, R.-H. and L. Mao, *Application of Extended DLVO Theory, IV: Derivation of Flotation Rate Equation from First Principles.* Journal of Colloid and Interface Science, 1996. **181**(2): p. 613-626.
16. Sherrell, I. and R.-H. Yoon. *Development of a turbulent flotation model*. in *Centenary of flotation symposium*. 2005. Barisbane, Australia.
17. Smoluchowski, M., *Mathematical theory of the kinetics of the coagulation of colloidal particle.* Z. phys. Chem, 1917. **92**: p. 129.
18. Kelsall, D.F., *Application of probability assessment of flotation systems.* Transactions of Institutions of Mining and Metallurgy, 1961. **70**(3): p. 191.
19. Arbiter, N. and C.C. Harris, *Flotation kinetics*, in *Froth Flotation 50th Anniversary Volume*, D.W. Fuerstenau, Editor. 1962, AIME. p. 215-246.
20. Tomlinson, H.S. and M.B. Flemming, *Flotation rate studies*, in *6th International Mineral Processing Congress*. 1963. p. 563.
21. Sherrell, I., *Development of a flotation rate equation from first principles under turbulent flow conditions*, in *Mining and Minerals Engineering*. 2004, Virginia Tech: Blacksburg.
22. Ralston, J., S.S. Dukhin, and N.A. Mishchuk, *Inertial hydrodynamic particle-bubble interaction in flotation.* International Journal of Mineral Processing, 1999. **56**(1-4): p. 207-256.
23. Kolmogorov, A.N., *Dissipation of energy in locally isotropic turbulence (in russian).* Dokl. Alad. Nauk SSSR, 1941. **32**: p. 19-21.
24. Taylor, G.I., *Statistical theory of turbulence: Parts I-III.* Proceedings of Royal Society, Series A, 1935. **151**: p. 421-464.
25. Schubert, H., *On the turbulence-controlled microprocesses in flotation machines.* International Journal of Mineral Processing, 1999. **56**(1-4): p. 257-276.
26. Liepe, F. and H.O. Moeckel, *Untersuchungen zum Stoffvereinigen in Flüssiger Phase.* Chemical Technology, 1976. **28**.
27. Brady, M.R., et al., *Evaluation of multiphase flotation models in grid turbulence via Particle Image Velocimetry.* International Journal of Mineral Processing, 2006. **80**(2-4): p. 133-143.

28. Lu, S., Y. Ding, and J. Guo, *Kinetics of fine particle aggregation in turbulence.* Advances in Colloid and Interface Science, 1998. **78**(3): p. 197-235.
29. Okamoto, Y., M. Nishikawa, and K. Hashimoto, *Energy dissipation rate distribution in mixing vessels and its effects on liquid-liquid dispersion and solid-liquid mass transfer.* International Chemical Engineering, 1981. **21**(1): p. 88-94.
30. Goren, S.L. and M.E. O'Neill, *On the hydrodynamic resistance to a particle of a dilute suspension when in the neighbourhood of a large obstacle.* Chemical Engineering Science, 1971. **26**(3): p. 325-338.
31. Davis, R.H., J.A. Schonberg, and J.M. Rallison, *The lubrication force between two viscous drops.* Physics of Fluids A: Fluid Dynamics, 1989. **1**(1): p. 77-81.
32. Yoon, R.H., *The role of hydrodynamic and surface forces in bubble-particle interaction.* International Journal of Mineral Processing, 2000. **58**(1-4): p. 129-143.
33. Yoon, R.-H. and S.A. Ravishankar, *Long-Range Hydrophobic Forces between Mica Surfaces in Dodecylammonium Chloride Solutions in the Presence of Dodecanol.* Journal of Colloid and Interface Science, 1996. **179**(2): p. 391-402.
34. Christenson, H.K. and P.M. Claesson, *Cavitation and the Interaction Between Macroscopic Hydrophobic Surfaces.* Science, 1988. **239**(4838): p. 390-392.
35. Stevens, H., et al., *Effects of Degassing on the Long-Range Attractive Force between Hydrophobic Surfaces in Water.* Langmuir, 2005. **21**(14): p. 6399-6405.
36. Yianatos, J.B., et al., *Froth recovery of industrial flotation cells.* Minerals Engineering, 2008. **21**(12-14): p. 817-825.
37. Mathe, Z.T., M.C. Harris, and C.T. O'Connor, *A review of methods to model the froth phase in non-steady state flotation systems.* Minerals Engineering, 2000. **13**(2): p. 127-140.
38. Schumann, R., *Flotation kinetics: I. Moethods for steady state study of flotation problems.* Journal of physical chemistry, 1942. **46**: p. 891-902.
39. Waters, K.E., et al., *Positron emission particle tracking as a method to map the movement of particles in the pulp and froth phases.* Minerals Engineering, 2008. **21**(12-14): p. 877-882.
40. Koh, P.T.L. and M.P. Schwarz, *CFD modelling of bubble-particle collision rates and efficiencies in a flotation cell.* Minerals Engineering, 2003. **16**(11): p. 1055-1059.
41. Koh, P.T.L. and M.P. Schwarz, *CFD modelling of bubble-particle attachments in flotation cells.* Minerals Engineering, 2006. **19**(6-8): p. 619-626.
42. Harris, C.C., *Multiphase models of flotation machine behaviour.* International Journal of Mineral Processing, 1978. **5**(2): p. 107-129.
43. Yianatos, J.B., *Fluid Flow and Kinetic Modelling in Flotation Related Processes: Columns and Mechanically Agitated Cells--A Review.* Chemical Engineering Research and Design, 2007. **85**(12): p. 1591-1603.
44. Vera, M.A., J.P. Franzidis, and E.V. Manlapig, *Simultaneous determination of collection zone rate constant and froth zone recovery in a mechanical flotation environment.* Minerals Engineering, 1999. **12**(10): p. 1163-1176.
45. Seaman, D.R., J.P. Franzidis, and E.V. Manlapig, *Bubble load measurement in the pulp zone of industrial flotation machines--a new device for determining the froth recovery of attached particles.* International Journal of Mineral Processing, 2004. **74**(1-4): p. 1-13.
46. Alexander, D.J., J.P. Franzidis, and E.V. Manlapig, *Froth recovery measurement in plant scale flotation cells.* Minerals Engineering, 2003. **16**(11): p. 1197-1203.

47. Duan, J., D. Fornasiero, and J. Ralston, *Calculation of the flotation rate constant of chalcopyrite particles in an ore.* International Journal of Mineral Processing, 2003. **72**(1-4): p. 227-237.
48. Ralston, J., et al. *Flotation rate constant prediction for metal sulfide particles*. in *Centenay of flotation symposium*. 2005. Brisbane, Australia.
49. Craig, V.S.J., B.W. Ninham, and R.M. Pashley, *The effect of electrolytes on bubble coalescence in water.* The Journal of Physical Chemistry, 1993. **97**(39): p. 10192-10197.
50. Gorain, B.K., et al., *The effect of froth residence time on the kinetics of flotation.* Minerals Engineering, 1998. **11**(7): p. 627-638.
51. Mathe, Z.T., et al., *Review of froth modelling in steady state flotation systems.* Minerals Engineering, 1998. **11**(5): p. 397-421.
52. Maachar, A. and G.S. Dobby, *Measurement of feed water recovery and entrainment solids recovery in flotation columns.* Canadian Metallurgical Quarterly, 1992. **31**(3): p. 167-172.
53. Savassi, O.N., et al., *An empirical model for entrainment in industrial flotation plants.* Minerals Engineering, 1998. **11**(3): p. 243-256.
54. Pugh, R.J., *Experimental techniques for studying the structure of foams and froths.* Advances in Colloid and Interface Science, 2005. **114-115**: p. 239-251.
55. Weaire, D. and S. Hutzler, *The physics of foams*. 1999: Oxford university press.
56. Leonard, R.A. and R. Lemlich, *A study of interstitial liquid flow in foam. Part I. Theoretical model and application to foam fractionation.* AIChE Journal, 1965. **11**(1): p. 18-25.
57. Koehler, S.A., S. Hilgenfeldt, and H.A. Stone, *A Generalized View of Foam Drainage: Experiment and Theory.* Langmuir, 2000. **16**(15): p. 6327-6341.
58. Verbist, G., D. Weaire, and A.M. Kraynik, *The foam drainage equation.* Journal of Physics: Condensed Matter, 1996. **8**(21): p. 3715-3731.
59. Gol'dfarb, I.I., K.B. Kann, and I.R. Shreiber, *Liquid flow in foams.* Fluid Dynamics, 1988. **23**(2): p. 244-249.
60. Verbist, G. and D. Weaire, *A Soluble Model for Foam Drainage.* EPL (Europhysics Letters), 1994. **26**(8): p. 631-634.
61. Angarska, J.K., et al., *Detection of the Hydrophobic Surface Force in Foam Films by Measurements of the Critical Thickness of the Film Rupture.* Langmuir, 2004. **20**(5): p. 1799-1806.
62. Wang, L. and R.-H. Yoon, *Hydrophobic forces in thin aqueous films and their role in film thinning.* Colloids and Surfaces A: Physicochemical and Engineering Aspects, 2005. **263**(1-3): p. 267-274.
63. Vrij, A., *Possible mechanism for the spontaneous rupture of thin, free liquid films.* Discussions of Faraday Society, 1966. **42**: p. 23-33.
64. Ruckenstein, E. and R.K. Jain, *Spontaneous rupture of thin liquid films.* Journal of Chemical Society, Faraday Transactions 2, 1974. **70**: p. 132-147.
65. Ivanov, I.B., et al., *Theory of the critical thickness of rupture of thin liquid films.* Transactions of Faraday Society, 1970. **66**: p. 1262-1273.
66. Wang, L. and R.-H. Yoon, *Effects of surface forces and film elasticity on foam stability.* International Journal of Mineral Processing, 2008. **85**(4): p. 101-110.

CHAPTER 2

A FLOTATION MODEL UNDER TURBULENT FLOW CONDITIONS

ABSTRACT

Flotation is designed to separate hydrophobic and hydrophilic particles by selectively attaching the former on the surfaces of air bubbles. The process has been modeled by many investigators mostly using parameters affecting the hydrodynamics of bubble-particle interactions occurring in the pulp phase of a flotation cell, while the efficiency of the process is critically affected by various chemical parameters, particularly the hydrophobicity of particles. In a previous work, the effect of particle hydrophobicity was incorporated into a flotation model using the DLVO theory extended to include the contributions from hydrophobic force. However, the model was applicable only for the bubble-particle interactions occurring under laminar flow conditions without consideration of the separation processes occurring in the froth phase formed on top of the pulp phase. In the present communication, a comprehensive flotation model has been developed to describe the events occurring both in the pulp and froth phases of a flotation cell operating under turbulent flow conditions. The model predictions are consistent with typical industrial mineral flotation results reported in the literature.

1. INTRODUCTION

Froth flotation is an important separation process that is widely used in the minerals, coal, oil, recycling, and environmental industries. It is designed to separate hydrophobic particles from hydrophilic ones by selectively attaching the former to the surface of rising stream of air bubbles in aqueous media (pulp), leaving the latter behind. The air bubbles carrying the hydrophobic particles form a froth (three-phase foam) phase, in which some of the particles drop back to the pulp phase due to bubble coarsening and drainage. The parameters affecting the process may be divided into hydrodynamic (*e.g.*, bubble size, particle size, turbulence, energy dissipation) and chemical parameters (*e.g.*, hydrophobicity, surface tension, ζ-potentials). Most of the models derived until recently incorporated only the hydrodynamic parameters, which made it impossible to predict the efficiency of separation. In general, hydrodynamic parameters affect recovery, while chemical parameters control both recovery and separation efficiency.

The first theory of modeling flotation was developed by Sutherland [1] based on Gaudin's hypothesis [2, 3]. The theory described the process as dependent on the probabilities of bubble-particle collision, attachment and detachment occurring under the environment of inviscid fluid. Some models also took similar approach with more detailed considerations in the interpretation of bubble-particle attachment. For example, Derjaguin and Dukhin [4] considered interfacial forces in determining the flotation rate of fine particles settling onto a rising bubble in a quiescent flow. As interests extended to the aggregation of larger particles, the hydrodynamic effect of particle inertia was also incorporated with flotation kinetics by other researchers [5-8]. Finch and Dobby [7] developed their flotation model using Weber and Paddock's theory on collection efficiency [6], where only hydrodynamic effect of small stokes number particles and intermediate Reynolds number flow was investigated. The bubble-particle attachment efficiency was determined by the induction time (the time required for film rupture) and particle's sliding time on bubble surface.

While Finch and Dobby [7] modeled flotation kinetics in hydrodynamics' aspects only, Yoon and Mao [9] derived a first-order flotation rate equation using both the hydrodynamic and chemical parameters. The model estimated kinetic energies of particles using the empirical flow streamline around a bubble derived for intermediate Reynolds numbers by Yoon and Luttrell [8]. In an attempt to derive the model from first principles, the model was limited to describing frothless flotation under laminar flow conditions. On the other hand, most of the industrial flotation machines operate under turbulent flow conditions, and the froth phase plays a critical role in determining the efficiency of hydrophobic and hydrophilic separation and also the recovery, particularly that of coarse particles.

In flotation, turbulence plays an important role. It is used to disperse air in water, induce bubble-particle collision, keep solid particles in suspension, and to transport the suspension from one flotation cell to another. Recently, Pyke *et al*. [10] derived a flotation model for such environment. Their model was in essence the extended version of Ralston *et al*.[11]'s flotation model to turbulent flow conditions. In the latter, the authors used the BBO equation to describe the particle moving along the streamline around a bubble. The collision efficiency and attachment efficiency were calculated based on the induction time and the angle of bubble-particle contact obtained by solving the BBO equation.

On the other hand, Sherrell and Yoon [12] suspected Pyke *et al.*'[10]s approach realizing that flow streamlines may be affected by turbulent flows in the presence of particles of high inertia. Therefore, Sherrell and Yoon [12] extended Yoon and Mao's [9] model to turbulent flow conditions, with the aspect of bubble-particle interaction energies in turbulence. The model, however, showed a result indicating that flotation kinetics is controlled more by bubble-particle detachment, rather than attachment [13]. More recently, Koh and Schwarz [14, 15] applied Yoon and Luttrell [8]'s sub-process probabilities into their flotation model. Aided by a Computational Fluid Dynamics (CFD) program for the first time, they could predict the temporal changes of total particle numbers in a lab-scale cell, which were used to infer the flotation rate constant. Their results showed that froth phase is a significant contributor to the overall recovery.

As well as the models stated above, most of the flotation models [10, 11, 16-18] addressing turbulence used the collision model derived by Abrahamson [19], which was based on the assumption of infinite Stokes number (*i.e.*, bubbles and particles are in random motion independently of fluid flow) and, hence, of hardcore collision. During the process of bubble-particle collision, a particle can approach the surface of an air bubble within the distance range where surface forces can affect the attachment process. Derjaguin and Dukhin [4] were in fact the first to consider the effects of surface forces in flotation. They suggested that during the course of bubble-particle interaction, a particle passes through three successive zones, *i.e.*, hydrodynamic, diffusio-phoretic and wetting zones. As the particle reaches the wetting zone, it would experience three surface forces, namely, electrostatic, van der Waals dispersion, and *structural* forces. The structural force was considered hydrophilic, which was considered repulsive but becomes zero when bubble-particle adhesion is to occur. In a later publication, Derjaguin and Dukhin [20] suggested that the bubble-particle adhesion can occur without penetrating the wetting film, a process referred to as 'contactless flotation'.

Mika and Fuerstenau [21] developed a detailed flotation model by considering various sub-processes, including collision, attachment and detachment. These authors considered that the attachment sub-process is controlled by the double-layer and dispersion forces, and that the wetting film is thinned by turbulent force. They also noted that the diffusiophoretic phenomena suggested by Derjaguin and Dukhin [4] cannot be justified when the essentially turbulent character of the fluid in the neighborhood of the bubble is recognized.

It is interesting to note here that all of the surface forces by Derjagiun and Dukhin [4, 20] and Mika and Fuerstenau [21] are repulsive under typical flotation conditions. It is likely that electrostatic forces are repulsive as both bubbles and particles are often negatively charged particularly in alkaline solutions. Knowing that the van der Waals dispersion forces are also repulsive in bubble-particle interactions, as are the hydrophilic structural (or hydration) forces, it is difficult to explain the process of bubble-particle attachment. It was probably these reasons that Derjagiun and Dukhin suggested the concept of contactless flotation, which means that bubble-particle attachment can occur without forming a three-phase contact. This mechanism may provide an explanation for the flotation of submicron particles but not for the flotation of larger particles that are commonly processed in the minerals and coal industries. If the wetting film between bubble and particle does not rupture, the energy of holding a particle onto the surface of a bubble, which is proportional to the area of the three-phase contact, becomes too

weak to withstand the turbulence created in an industrial flotation machine. Furthermore, the repulsive surface forces will create a large energy barrier, which should cause the process to be slow. In colloid chemistry, coagulation is considered to be 'slow' or 'fast' depending on the presence or absence of energy barrier, respectively [22-24]. In flotation, the bubble-particle adhesion is a fast process, with the wetting films rupturing within the time frame of tens of milliseconds or less [25, 26].

Israelachvili and Pashley's work [27] on surface force measurements may shed a light to the dilemma in explaining flotation, that is, the bubble-particle adhesion is fast despite the high energy barrier. These investigators measured the surface forces between two mica surfaces hydrophobized by cetyltrimethylammounium bromide (CTAB), and discovered a hitherto unknown attractive force that was approximately ten times stronger than the van der Waals force. The follow-up experiments conducted by numerous other investigators also showed the presence of the extraneous force, which was appropriately referred to as hydrophobic force, as described in a recent review paper by Christenson and Claesson [28]. It was shown that the hydrophobic force increases with increasing water contact angle [29, 30]. Other investigators showed, on the other hand, that the long-range attractions measured between hydrophobic surfaces are due to bridging bubbles [31, 32]. In support of this mechanism, Tyrell and Attard [33] and Ishida *et al*. [34] observed nanobubbles on hydrophobic surfaces by means of atomic force microscope (AFM), while Mao *et al*.[35] failed to detect nanobubbles (or vapor cavities) on hydrophobic surfaces by means of ellipsometry. Also, Sakamoto *et al*. [36] showed that the long-range attractions observed with silica surfaces coated with octadecyltrimethyl ammonium chloride (C_{18}TAC) disappeared completely when the force measurements were conducted in degassed solutions. Zhang, *et al.* [37] showed, however, that the measurements conducted under the same conditions showed long-range attractions both in air-saturated and degassed solutions. Meyer *et al.* [38] also observed strong attractive forces between mica surfaces in degassed C_{18}TAC solutions.

The role of the hydrophobic force in flotation may be to reduce the energy barrier for bubble-particle interaction so that flotation can become a fast process. It was shown previously that coagulation of hydrophobic particles requires much less kinetic energy than required to overcome the energy barriers calculated using the DLVO theory [39-41]. In relating the kinetic energy of bubble-particle collision to the energy barrier, it is important to consider the hydrodynamic resistance to film thinning, which causes deceleration of the particles approaching bubbles in close proximity [9, 42, 43].

It was the objective of the proposed work to derive a turbulent flotation model using both hydrodynamic and chemical parameters based on the concepts presented above. The model describes the events occurring in the pulp phase and froth phase separately. The model predictions are compared with the general trends reported in the literature with regards to the effects of particle size, bubble size, energy input, particle hydrophobicity, surface tension, and the ζ-potentials of particles and bubbles, all of which are recognized as important parameters affecting flotation.

2. MODEL

2.1 Collision Frequency

The process of flotation commences with bubble-particle collision, followed by adhesion. Camp and Stein [44] were the first to derive a collision model under turbulent flow consitions,

$$Z_{12} = \frac{4}{3} N_1 N_2 d_{12}^3 \sqrt{\frac{\varepsilon}{\nu}} \tag{1}$$

where Z_{12} is the collision frequency between particles 1 and 2, N_1 and N_2 are the number densities of particles, d_{12} (= r_1 + r_2) is the collision radius with r_1 and r_2 being the radii of the particles, ε the energy dissipation rate, and ν is the kinematic viscosity of the medium. Eq. (1) is of the same form as Smoluchowski's model [24] which was derived for collision under laminar flow conditions. The model derived by Saffman and Turner [45] was the same as Eq. (1) with a slightly different constant, *i.e.*, $\sqrt{8\pi/15}$ rather than 4/3. These models are applicable for small particles that follow fluid flow, which makes it difficult to be used for modeling flotation involving coarse particles.

Abrahamson [19] derived a turbulent collision model based on the assumption that particle velocities are independent of fluid flow. The simplest form of his model is given by

$$Z_{12} = 2^{3/2} \pi^{1/2} N_1 N_2 d_{12}^2 \sqrt{\bar{u}_1{}^2 + \bar{u}_2{}^2} \tag{2}$$

where $\sqrt{\overline{U_1^2}}$ and $\sqrt{\overline{U_2^2}}$ represent the root-mean-square (RMS) velocity fluctuations of the particles 1 and 2, respectively. Eq. (2) was derived with an infinite Stokes number, which makes it applicable for large particles. For small particles, however, an appropriate correction may be necessary.

2.2 Flotation Kinetics

Eq. (2) can be used as a basis for writing a second-order flotation rate equation as follows,

$$\frac{dN_1}{dt} = -Z_{12} P \tag{3}$$

where P is the probability of flotation, which may be considered a product of collision (P_c), adhesion (P_a) and detachment (P_d) probabilities [1]:

$$P = P_c P_a (1 - P_d) \tag{4}$$

Use of Eq. (4) for a flotation model presumes that bubble-particle aggregates formed in the pulp phase enter the froth phase automatically, which is unlikely.

When a bubble-particle aggregate rises in a flotation pulp, it will encounter the froth-pulp interface and may break up depending on the hydrodynamic conditions at the interface. Thus, it

would be necessary to consider the probability of bubble-particle aggregates successfully entering the froth phase (P_f). Therefore, Eq. (4) may be rewritten as follows,

$$P = P_c P_a (1 - P_d) P_f \tag{5}$$

as suggested by Schumann [46] and Tomlinson and Flemming [47].

Substituting Eqs. (2) and (5) into Eq. (3), one obtains,

$$\frac{dN_1}{dt} = -2^{3/2}\pi^{1/2} N_1 N_2 (r_1 + r_2)^2 \sqrt{\bar{u}_1{}^2 + \bar{u}_2{}^2} P_c P_a (1 - P_d) P_f \tag{6}$$

which is a second-order rate equation with respect to N_1 and N_2. If $N_2 >> N_1$ or N_2 remains constant during flotation, one can write a pseudo-first-order flotation rate equation as follows:

$$\frac{dN_1}{dt} = -k_p N_1 \tag{7}$$

where

$$k_p = 2^{3/2}\pi^{1/2} N_2 (r_1 + r_2)^2 \sqrt{\bar{u}_1{}^2 + \bar{u}_2{}^2} P_c P_a (1 - P_d) P_f \tag{8}$$

In the present work, the particle RMS velocities were calculated using the following empirical relation [18, 48]:

$$\sqrt{\bar{u}_1{}^2} = 0.4 \frac{\varepsilon^{4/9} d_1^{7/9}}{\nu^{1/3}} \left(\frac{\rho_1 - \rho_3}{\rho_3}\right)^{2/3} \tag{9}$$

in which ε is energy dissipation rate, d_1 particle diameter, ν kinematic viscosity, ρ_1 particle density, and ρ_3 is water density. Recently, Brady *et al*. [49] measured particle velocities using a digital particle image velocimetry (PIV) technique and compared the results with those calculated using Eq. (9). For 80 μm particles under grid turbulence, the errors were within 12%.

On the other hand, the mean squared velocity of bubbles, $\bar{u}_2{}^2$, were calculated using the following relationship [50]:

$$\bar{u}_2{}^2 = C_0 (\varepsilon d_2)^{2/3} \tag{10}$$

where d_2 is bubble diameter and C_0 (=2) is a constant.

2.3. Probabilities of Attachment and Detachment

In the flotation model developed by Yoon and Mao [9] for laminar flow conditions, the probability of attachment, P_a, was considered to be a function of the energy barrier (E_1) for bubble-particle attachment and the kinetic energy of attachment (E_k) as follows,

$$P_a = \exp\left(-E_1/E_k\right) \quad (11)$$

while P_d is a function of E_1, work of adhesion (W_a), and the kinetic energy of detachment (E'_k) as follows:

$$P_d = \exp\left(-(W_a + E_1)/E'_k\right) \quad (12)$$

It was shown that [9]

$$W_a = \gamma_{lv}\pi r_1^2(1-\cos\theta)^2 \quad (13)$$

where γ_{lv} is the surface tension of water and θ is the water contact angle of the particle with radius r_1.

Eq. (11) is analogous to the Arrhenius equation for chemical kinetics and to coagulation models for colloidal particles. Derjaguin *et al*. [51] derived an expression for coagulation efficiency, which is an exponential function of $-E_1/k_bT$, where the denominator represents the kinetic energy due to thermal motion. For the heterocoagulation of macroscopic particles, *i.e*., between bubbles and particles in flotation, it would be appropriate to substitute the k_bT with the kinetic energies (E_k) due to hydrodynamic interactions. The use of Eq. (11) implicitly recognizes that bubbles and particles in a flotation cell have distributed kinetic energies.

The approach taken in this communication to determining P_a is distinguished from that of Ralston *et al.* [17, 52] who used induction time rather than E_1. In their approach, it is assumed that bubble-particle attachment occurs when the sliding time of a particle on the surface of a bubble is longer than the induction time. The induction time, which is defined as the minimum time required for bubble-particle attachment, is usually determined experimentally, although a predictive model is available [53, 54].

2.4. Energy Barrier

In the present work, the energy barrier (E_1) has been determined using the extended DLVO theory,

$$V = V_E + V_D + V_H \quad (14)$$

where V is the free energy of interaction between bubble and particle, V_E the contribution from electrostatic interaction, V_D the same from van der Waals-dispersion interaction, and V_H is from hydrophobic interaction. Under most flotation conditions particularly at alkaline pH, both V_E and V_D are repulsive, while V_H is attractive as shown in Fig. 1.

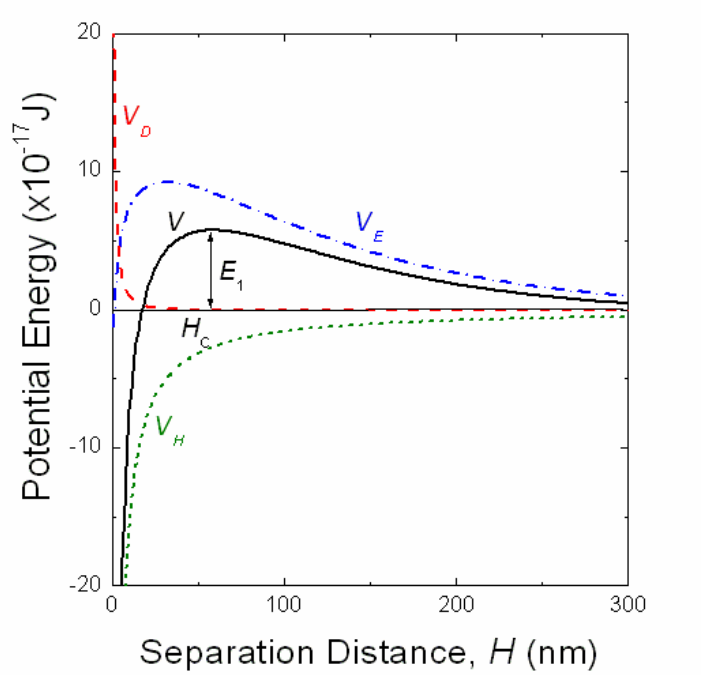

Fig.1. A plot of Eq. (14) with Ψ_1 = -63.9 mV, Ψ_1 = -32.8 mV, A_{132} = -7.08 x10^{-20} J, K_{132} = 4.14 x10^{19} J, r_1 = 0.05mm, r_2 = 0.5 m. E_1 represents the energy barrier for bubble particle attachment and H_c is the critical rupture thickness of the wetting film.

The electrostatic interaction energy (V_E) can be calculated using the model derived by Hogg, Healey and Fuerstenau [55],

$$V_E = \frac{\pi\epsilon_0\epsilon r_1 r_2(\Psi_1^2+\Psi_2^2)}{(r_1+r_2)}\left[\frac{\Psi_1^2\Psi_2^2}{\Psi_1^2+\Psi_2^2}\ln\left(\frac{1+e^{-\kappa H}}{1-e^{-\kappa H}}\right)+\ln(1+e^{-2\kappa H})\right] \quad (15)$$

where ϵ_0 is the permittivity in vacuum, ϵ the dielectric constant of the medium, Ψ_1 and Ψ_2 are the double layer potentials for particle and bubble, respectively, κ the inverse Debye length, and H is the closest separation distance between particle and bubble. As an approximation, Ψ_1 and Ψ_2 may be substituted by ζ–potentials.

The dispersion interaction energy can be calculated using the following relation [56],

$$V_D = -\frac{A_{132}r_1r_2}{6H(r_1+r_2)}\left[1-\frac{1+2bl}{1+bc/H}\right] \quad (16)$$

where A_{132} is the Hamaker constant for the interaction between particle **1** and bubble **2** in a medium **3**. The second term of Eq. (16) is a correction factor for the retardation effect, where b (= 3x10^{-17} s for most materials) is a parameter characterizing materials of interacting particles, l (= 3.3x10^{15} s^{-1} for water) is a parameter characterizing the medium, and c is the speed of light [9].

The hydrophobic interaction energy (V_H) between bubble and particle may be calculated using the following equation [9]

$$V_H = -\frac{r_1 r_2 K_{132}}{6(r_1+r_2)H} \tag{17}$$

which is of the same form as Eq. (16). The hydrophobic interaction constant, K_{132}, can be obtained using the combining law [57]:

$$K_{132} = \sqrt{K_{131}K_{232}} \tag{18}$$

in which K_{131} and K_{232} represent the hydrophobic force constant between two particles **1** and the bubbles **2** in a medium **3**, respectively.

Many investigators showed that the long-range attractive force between two hydrophobic surfaces increases with increasing hydrophobicity. Pazhianur and Yoon [29] showed that K_{131} increases with increasing water contact angle (θ), a measure of hydrophobicity. The log K_{131} vs. θ plots given by these investigators may be used to obtain the values of the hydrophobic force constants from the contact angles that can be readily measured in experiment. The plot shows three different regions of contact angles, in which one can obtain the value of K_{131} from θ using the following relation:

$$K_{131} = ae^{b_k\theta} \tag{19}$$

in which a and b_k are fitting parameters whose values are: $a = 2.732\text{x}10^{-21}$ and $b_k = 0.04136$ at $\theta < 86.89°$; $a = 4.888\text{x}10^{-44}$, $b_k = 0.6441$ at $86.89° < \theta < 92.28°$; and $a = 6.327\text{x}10^{-27}$, $b_k = 0.2172$ at $\theta > 92.28°$.

The values of K_{131} obtained using Eq. (19) were then combined with the value of $K_{232} = 2.5\text{x}10^{-18}$, representing the hydrophobic force constant of the bubble-bubble interactions occurring in the absence of surfactant, to obtain the value of K_{132} using Eq. (18). It was shown previously that K_{232} decreases with increasing concentration of surfactants (cationic, anionic, and non-ionic)[58, 59].

2.5 Kinetic Energy for Attachment

To calculate P_a using Eq. (11), it is necessary to know the kinetic energy, E_k, of the particles colliding with bubbles. The kinetic energy may be calculated using the following equation,

$$E_k = 0.5m_1\bar{u}_1{}^2 \tag{20}$$

where m_1 is particle mass, $\bar{u}_1{}^2$ is the mean-square velocity of the particle relative to fluids that can be obtained from Eq. (9). As a particle approaches a bubble, the distance (H) separating the

two decreases with time. In time, the particle will reach the critical rupture distance (H_c), where the wetting film ruptures spontaneously to form a three-phase contact line. It is necessary, therefore, to compare E_k with the energy barrier E_1 at H_c, which in turn requires the velocity of the particle at the rupture thickness rather than in the bulk of the solution. According to the Reynolds lubrication theory, a spherical particle of radius r_1 should experience a hydrodynamic resistance force, F_{hyd}, during the approach:

$$F_{hyd} = 6\pi\mu r_1 U\beta \tag{21}$$

where U is the velocity of the sphere at H, μ the viscosity, and β is a drag coefficient in the boundary layer. For a small sphere approaching a large sphere, Goren and O'Neil [60] calculated the values of β numerically, which may be represented by the following relationship found by Luttrell and Yoon [61, 62],

$$\beta = 0.37(r_1/H)^{0.83} \tag{22}$$

By equating the hydrodynamic resistance force ($F_{hyd} = 6\pi\mu r_1 U_H\beta$) at H_c to the Stokes drag force ($F_{drag} = 6\pi\mu r_1\sqrt{\bar{u}_1{}^2}$), one obtains the following relation [61],

$$U_{H_c} = \sqrt{\bar{u}_1{}^2}/\beta \tag{23}$$

which may be used to determine the velocity of the particles (U_{H_c}) colliding with bubbles at H_c. It is this velocity rather than the velocity in the bulk solution that is used to calculate E_k.

2.6 Kinetic Energy for Detachment

It has been suggested that particles are detached from bubbles by the centrifugal force in a vortex rotating in a turbulent flow [63, 64]. The shear rate in a vortex has been given as $\sqrt{\varepsilon/\nu}$ by Camp and Stein [44] (see Eq. (1)). The following equation may thus be used to calculate the kinetic energy for detachment,

$$E'_k = 0.5m_1\left((d_1 + d_2)\sqrt{\varepsilon/\nu}\right)^2 \tag{24}$$

2.7 Energy Dissipation Rate in two different region

Energy dissipation rate plays a critical role in determining the particle and bubble velocities and the detachment kinetic energy, as shown in Eqs. (9), (10) and (24). One could use a mean energy dissipation rate ($\bar{\varepsilon}$), which can be obtained by dividing the power input (W) with the mass (M) of the slurry in a flotation cell, for the values of ε in these equations. It has been shown, however, that the value of ε in the vicinity of an impeller (or a rotor-stator mechanism) is much larger than in the bulk of a flotation pulp [10, 65, 66]. Therefore, it would be more realistic to subdivide the volume of a flotation cell into two different zones, *i.e.*, one near an impeller where bubbles are generated (bubble generation zone), and the other away from it where bubbles

and particles may interact with each other (collection zone). One can then use the following relation,

$$\bar{\varepsilon} = \frac{W}{M}(f_b\varphi_b + f_c\varphi_c) = f_b\varepsilon_b + f_c\varepsilon_c \tag{25}$$

where φ_b and φ_c are the multiplication factors representing the intensity of agitation in the bubble generation and collection zone, respectively; f_b and f_c are the respective volume fractions; and ε_b and ε_c are the dissipation rates. In the present work, it is assumed that φ_b=15, φ_c=0.5, and the corresponding volume fractions are: f_b=0.035 and f_c=0.965.

It has been assumed that bubble-particle attachment is controlled by ε_c, bubble-particle detachment by $\bar{\varepsilon}$, and bubble generation by ε_b. In the present work, the bubble generation model

$$d_2 = \left(\frac{2.11\gamma_{lv}}{\rho_3\varepsilon_b^{0.66}}\right)^{0.6} \tag{26}$$

reported by Schulze [64] was used. According to this model, bubble size decreases approximately as $\varepsilon_b^{-0.4}$ and $\gamma_{lv}^{0.6}$.

2.8 Probability of Collision

The Abrahamson's collision model (Eq. (2)) was derived with an assumption of infinitely large Stokes number. Therefore, bubbles and particles move independently of fluid flow, in which case collision probability (P_c) should be unity. This may be the case with particles larger than approximately 100 μm at energy dissipation rates in the order usually found in pumping fluids in industry [19]. Much of the particles subjected to flotation are finer than 100 μm, and the energy dissipation rates in the collection zones are substantially lower. Therefore, it would be necessary to consider that P_c<1 for small particles, which may be regarded a correction for of Eq. (2). Indeed, the numerical simulations carried out by Sundaram and Collins [67] showed that the Abrahamson's model is not applicable at Stokes numbers below approximately 15.

In the present work, the collision efficiency model derived by Webber and Paddock [6, 61] was used,

$$P_c = \frac{3}{2}\left(\frac{d_1}{d_2}\right)^2\left[1 + \frac{\frac{3}{16}Re}{1+0.249Re^{0.56}}\right] \tag{27}$$

in which Re is the Reynolds number of the bubble. One problem in using Eq. (25) is that P_c becomes larger than 1 at $d_1/d_2 > 0.1$ and $0 < Re \leq 300$. Therefore, Eq. (27) has been modified as follows,

$$P_c = \tanh^2\left(\sqrt{\frac{3}{2}\left(1 + \frac{\frac{3}{16}Re}{1+0.249Re^{0.56}}\right)}\left(\frac{d_1}{d_2}\right)\right) \tag{28}$$

so that the condition of $P_c < 1$ can be met. Despite the different functional forms involved, Eqs. (27) and (28) give essentially the same values of P_c for smaller particles, as shown in Figure 2.

2.9 Probability of Aggregates Transferring to Froth

As a bubble-particle aggregate is formed, it rises in the pulp phase with a velocity of U_0 and hit the pulp-froth interface. The bubble laden with hydrophobic particles can bounce back to the pulp phase due the elasticity of the bubble. Many investigators observed the phenomenon as free bubbles rise to the air-water or solid-water interfaces [68-73]. Also, the bubble-particle aggregate may break up and lose particles depending on the kinetic energy imparted by the interface onto the aggregate. It is, therefore, necessary to consider the probability (P_f) for the aggregate to successfully enter the froth phase without losing hydrophobic particles, which may be described as follows,

$$P_f = P_i(1 - P_r) \tag{29}$$

where P_i is the probability of the aggregate to be at the interface after bouncing n times, and P_r is the probability of rupture.

If a bubble-particle aggregate bounces n times to a halt, P_i should be $1/n$. Let us assume that the aggregate has a kinetic energy E_{ai} as it approaches the interface initially, and that it is reduced to E_{af} after n bounces. Assuming that the bubble retains its kinetic energy by a factor of

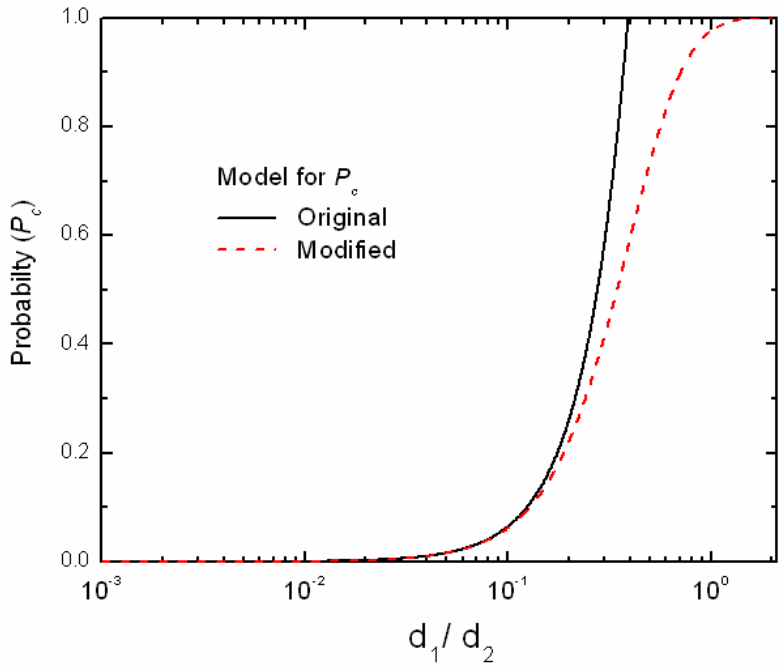

Fig.2. Comparison of Eq.(27) and Eq.(28). Both give the same values of P_c at $d_1/d_2 <$ 0.1, while the latter corrects the over-prediction of the former for larger particles.

α after each bounce, one obtains the following relation,

$$E_{a,f} = \alpha^n E_{a,i} \tag{30}$$

It has been shown that at the air-water interface U_0 decreases by approximately ten-fold after bouncing *n* time, in which case the bubble should retain only 1% of its kinetic energy when it is ready to penetrate the air-water interface [74]. Zenit and Legendre [68] derived an expression for α as follows,

$$\alpha = \exp\left(-60\sqrt{\frac{9\mu^2}{d_2\gamma_{lv}\rho_3}}\right) \tag{31}$$

From Eqs. (30) and (31), one can derive an expression for *n* and hence P_i as follows:

$$P_i = 13\sqrt{\frac{9\mu^2}{d_2\gamma_{lv}\rho_3}} \tag{32}$$

Regarding the probability of aggregate rupture (P_r) at the pulp-froth interface, it is necessary to know the kinetic energy (E_{iw}) imparted by the wave motion at the interface relative to the kinetic energy (E_{ka}) of the bubble-particle aggregate after bouncing *n* times. The former may be considered to be the square of the wave propagation velocity at the smallest wavelength η, *i.e.* the kolmogorov's length scale, while the latter can be estimated form a momentum balance. In the present work, the wave velocity has been estimated assuming fluids above and below the interfacial wave is relatively quiescent in horizontal direction. For the interface formed between two fluids of different densities, *i.e.*, water with a density of ρ_3 at the bottom and the foam with a density of $\rho_f \sim 0.33\rho_3$ on the top, one can readily obtain the following [75],

$$E_{iw} = \left(\sqrt{\frac{g\eta}{2\pi}\left(\frac{\rho_3-\rho_f}{\rho_3+\rho_f}\right)}\right)^2 = \frac{g}{4\pi}\left(\frac{\nu^3}{\varepsilon_b}\right)^{1/4} \tag{33}$$

where *g* is gravity, and ν is the kinematic viscosity of water.

For a bubble whose surface is 50% covered by hydrophobic particles, one obtains the following relation from a momentum balance:

$$E_{ka} = \frac{\left(m_2\sqrt{\overline{u}_2{}^2} - 2\left(\frac{d_2}{d_1}\right)^2 m_1\sqrt{\overline{u}_1{}^2}\right)^2}{10^2\left(m_2+2\left(\frac{d_2}{d_1}\right)^2 m_1\right)^2} \tag{34}$$

where m_2 is the bubble mass, m_1 is particle mass. In the present work, the RMS velocities have been determined using the energy dissipation rates in the collection zone. Also, it has been assumed that a bubble-particle aggregate loses its kinetic energy by a factor 10^2 after *n* bounces at the froth-pulp interface. Note here that the $2(d_2/d_1)^2$ term of Eq. (34) represents the number

of particles adhering on the surface of the bubble of diameter d_2. Note also that E_{iw} and E_{ka} have been normalized by mass.

Conceptually, the probability of bubble-particle aggregate penetrating the pulp-froth interface (P_r) should increase as the ratio between E_{iw} and E_{ka} decreases. Thus, it is assumed that,

$$P_r = exp\left(-\frac{E_{iw}}{E_{ka}}\right) \tag{35}$$

Substituting Eqs. (32) and (35) into Eq. (29), one can determine the probability of bubble-particle aggregates entering the froth phase without losing particles.

3. NUMERICAL SIMULATION

Simulations were run to show the effect of different variables on the flotation rate constant. The variables studied were: the particle diameter (d_1), bubble diameter (d_2), surface tension (γ_{lv}), contact angle (θ), zeta potentials of particles (ζ_1) and of bubbles (ζ_2), and mean energy dissipation rate ($\bar{\varepsilon}$).

Unless otherwise stated, the values of the different parameters used for the simulations were as follows: $\bar{\varepsilon}$ = 2.0 W/kg (=2.5kW/m^3 as the specific energy input), ζ_1 = -15 mV, ζ_2 = -30 mV, γ_{lv} = 68.0 mN/m. The specific gravity (SG) of the particle was 4.1 (chalcopyrite). The pulp density of the flotation pulp was 20% by weight, and the air hold-up was 20% by volume. It was assumed also that the water contact angle (θ) of the floatable particles is 60^o, from which one obtains the value of K_{131} = 3.27x10^{-20} J using Eq. (19).

The Hamaker constants used in the present work were 3.0x10^{-19} J for chalcopyrite, 0 for air, and 4.38x10^{-20} J for water, from which the value of A_{132} = -7.13x10^{-20} J was obtained using the geometric mean combining law. Substituting the value of A_{132} obtained in this manner to Eq. (16), one can calculate the repulsive dispersion interaction energy (V_D) for bubble-particle interaction. The electrostatic interaction energy (V_E) was calculated using Eq. (15) using different values of Ψ_1 and Ψ_2 (or ζ_1 and ζ_2) and κ^{-1} = 96 nm. The hydrophobic interaction energy (V_H) was calculated using Eq. (17) with the value of K_{132} = 3.65x10^{-19} J, which was obtained using Eq. (18) from the values of K_{131} = 3.27x10^{-20} J and K_{232} = 4.07x10^{-18} J.

It should be noted here that the flotation rate constants (k_p) predicted from Eq. (8) represent the results of the events occurring in the pulp phase only. On the other hand, the rate constants obtained from experiment include the events occurring both in the pulp and froth phases. One can relate the k predicted from Eq. (8) to flotation recovery from the fraction froth recovery. If the fractional recovery in the pulp and froth phases are R_p and R_f, respectively, the overall fractional recovery (R) should be the product of the two, *i.e.*, $R = R_pR_f$. The recovery for a bank of n flotation cells, the recovery becomes [7, 76],

$$R = 1 - \left(1 - \frac{R_pR_f}{R_pR_f + 1 - R_p}\right)^n \tag{36}$$

For a single flotation cell or a batch flotation cell, R_c is given by[7, 77, 78],

$$R_p = 1 - \left(1 + k_p t\right)^{-1} \tag{37}$$

where t is the retention of the particles in the cell. R_f, on the other hand, has been given by the following relation [79, 80].

$$R_f = \frac{d_{2-0}}{d_{2-f}} exp\left(-N\frac{6h_f}{d_{2-0}}\left(1 - \frac{d_{2-0}}{d_{2-f}}\right)\left(\frac{d_1}{d_{2-0}}\right)^2\right) + R_W exp\left(-0.0325(\frac{\rho_3}{\rho_1} - 1) - 6.3 \times 10^4 d_1\right) \tag{38}$$

where $d_{2\text{-}0}$ and $d_{2\text{-}f}$ are bubble diameters at the bottom and top of a froth phase, respectively, h_f is the height of the froth phase under consideration, N is an adjustable constant, and R_w is the fractional water recovery. Most of the variables in Eq. (38) are input parameters, R_w and $d_{2\text{-}f}$ are obtained *a posteriori* from bubble coarsening and drainage models [79, 80].

Fig. 3-A shows a typical plot of flotation rate constant (k_p) versus particle diameter (d_1) as predicted by Eq. (8). The values of the various model parameters used in the simulation are given in the inset. As shown, k_p reaches a maximum at d_1 of approximately 200 μm, and the plot shows difficulties in floating ultrafine and coarse particles. Note here that the k_p values given in this plot are for pulp phase recovery. Therefore, the k_p values should be higher than those reported from experimental data. Nevertheless, the simulation results are generally in the same range as those reported in the literature. Trahar and Warren[81] reported, for example, the k_p values in the range of 0.2 to 5 min^{-1} for copper flotation, while Ahmed and Jameson [82] reported the k_p in the range of 0.01 to 3 min^{-1} for the flotation of quartz.

Fig. 3-B shows the recovery (R) as a function of particle size with t = 2 minutes and n = 15 and 30. Also shown for comparison are the plant operation data reported by Gaudin *et al*. [83], and Lynch *el al.* [77]. The shapes of the R *vs*. d_1 curves are typical of what has been observed in many flotation plants worldwide. The solid and dashed lines represent model predictions from Eq. (36) using appropriate fitting parameters. As the references from which the experimental data have been extracted do not give information on operational details, the predictions were made for 15-cell bank (dashed line) and 30-cell banks (solid line) with a 4-minute retention time in each cell. The fractional froth recovery (R_f) was adjusted to fit the experimental data. In estimating R_f using Eq. (38), the values of $d_{2\text{-}0}/d_{2\text{-}f}$ = 0.25, R_w = 0.51, N = 2 were used at a superficial gas rate of 2.3cm/s. Both the simulation and experimental data presented in Figure 3-B demonstrate difficulties in floating mineral particles below 10 μm and above 200 μm.

While Figure 3-B shows the recovery data converted from the flotation rate constants, the direct comparison between the data of the flotation rate constants along particle size change and the model is given in Fig.4. Duan *et al*.[84] obtined the overall flotation rate constant of chalcopyrite particles using the size- to-recovery data. Realizing that the data were obtained from

a lab-scale batch cell test, the overall flotation rate constant, k, for this comparison was obtained using the following expression [7],

$$k = k_p R_f \tag{39}$$

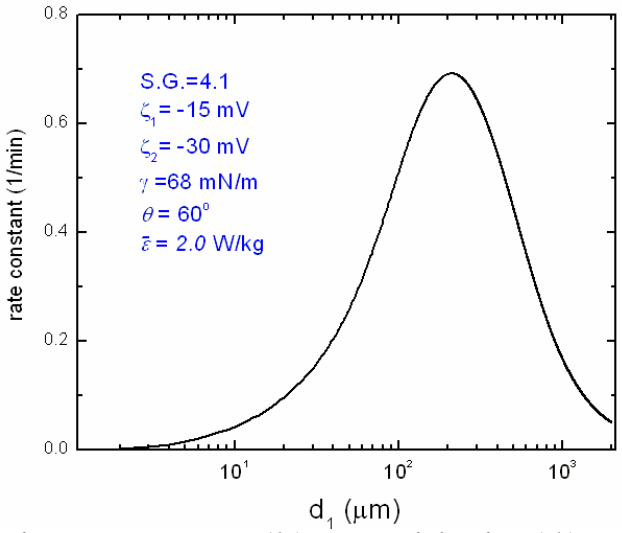

Fig. 3-A. The flotation rate constants (k_p) *vs.* particle size (d_1) as predicted from Eq. (8). It was assumed that the energy dissipation rate in the collection zone was 50% of the mean energy dissipation ($\bar{\varepsilon}$), and the one in the bubble generation zone was 15 times higher than $\bar{\varepsilon}$.

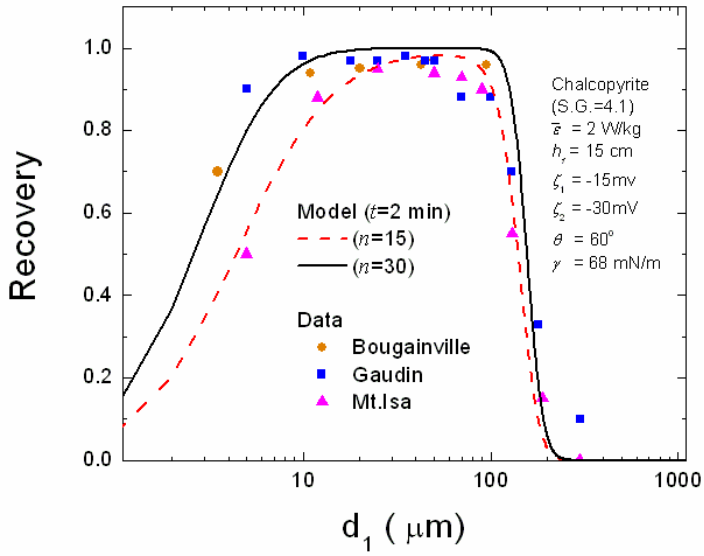

Fig. 3-B. Fractional recovery of chalcopyrite as predicted from Eq. (36) on the basis of the k_p values given in Figure 3-A. The data points represent the size-by-size recoveries obtained at operating plants as reported by Gaudin (1931) and Lynch *et al*. (1981). As these references did not specify the operational details, the predictions were made for fifteen-cell bank (n=15) and thirty-cell banks (n=30) with a 2-minute retention time in each cell.

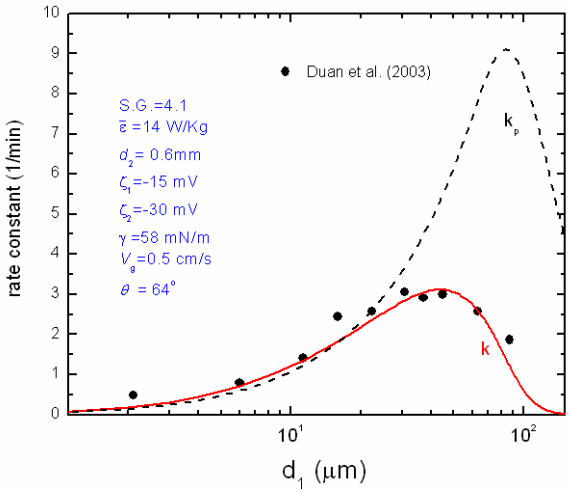

Fig. 4. Comparison of the rate constants predicted using Eq.(8) and Eq.(39) and the experimental data obtained by Duan *et al*.[84] for the flotation of chalcopyrite using a laboratory-scale Rushton flotation cell at the superficial gas rate of 0.5 cm/s.

where k_p and R_f were defined in Eqs.(8) and (38) respectively. In the simulation, all the components were evaluated using the information given in the experimental work, while several unknown parameters had to be assumed. Therefore, the following were used for estimating k : $\bar{\varepsilon}$=14 W/kg, ζ_1=-15mV, ζ_2=-30 mV, γ=58 mN/m, V_g=0.5 cm/s, θ =65°, h_f=2cm, $d_{2\text{-}0}/d_{2\text{-}f}$ = 0.9, R_w = 0.5, N = 3.5. The difference between k and k_p in Fig.4, especially in the range of coarse particle sizes, indicates that coarse particles recovery is hindered in the presence of froth phase.

Fig. 5 shows the effects of the various parameters on the k and R values presented in Figs.

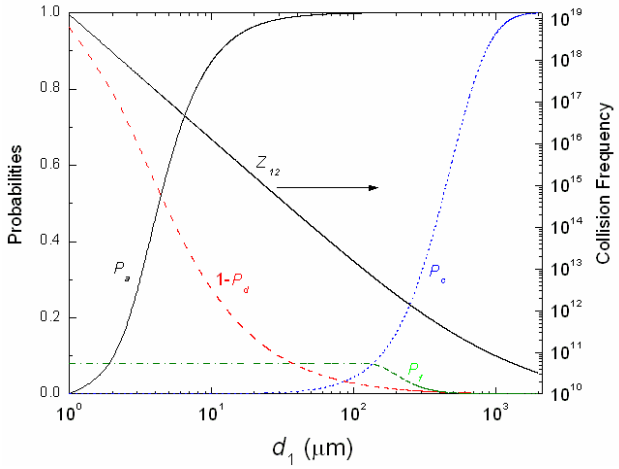

Fig.5. Effect of particle size on collision frequency (Z_{12}), collision efficiency (P_c), probability of adhesion (P_a), probability of detachment (P_d), and probability of particles transferring to froth. The hydrodynamic and surface chemistry parameters are the same as shown in Figure 3.

3-A and -B, respectively. It is shown that collision probability (Z_{12}) which is represented by Eq. (2), increases with decreasing particle size. This is due to the increase in the number density of particles (N_1) with decreasing particle size. Therefore, the changes in Z_{12} alone do not explain the difficulty in floating fine particles. On the other hand, the probability of collision (P_c) decreases sharply with decreasing particle size. Thus, the difficulty in floating fine particles can be attributed to the changes in the product of Z_{12} and P_c, which means that the hard-core collision model of Abrahamson [19] alone is not adequate for modeling flotation. His model is based on the random collision at high Stokes numbers, and ignores the likelyhood that smaller particles follow fluid flow or the stream lines around bubbles. Ralston *et al*, [11, 17] calculated the trajectories of particles around bubbles using the Basset-Boussinesq-Ossen (BBO) equation, and calculated the collision efficiencies. They showed that P_c was less than unity even under potential flow conditions. However, the values of P_c obtained in the present work are much smaller than predicted by Ralston *et al*.

It is shown also that the probability of adhesion (P_a) decreases with decreasing particle size. This can be attributed to the decrease in the kinetic energy (E_k) of the particles colliding with air bubbles. At low E_k, particles would have difficulties in overcoming the energy barriers created by the repulsive double-layer force. Fig. 3 shows also that the probability of the particles not being detached, *i.e.*, (1-P_d), decreases as particle size increases, which is the main reason that coarse particles are difficult to float. At the larger particle sizes, the RMS velocity increases (Eq.

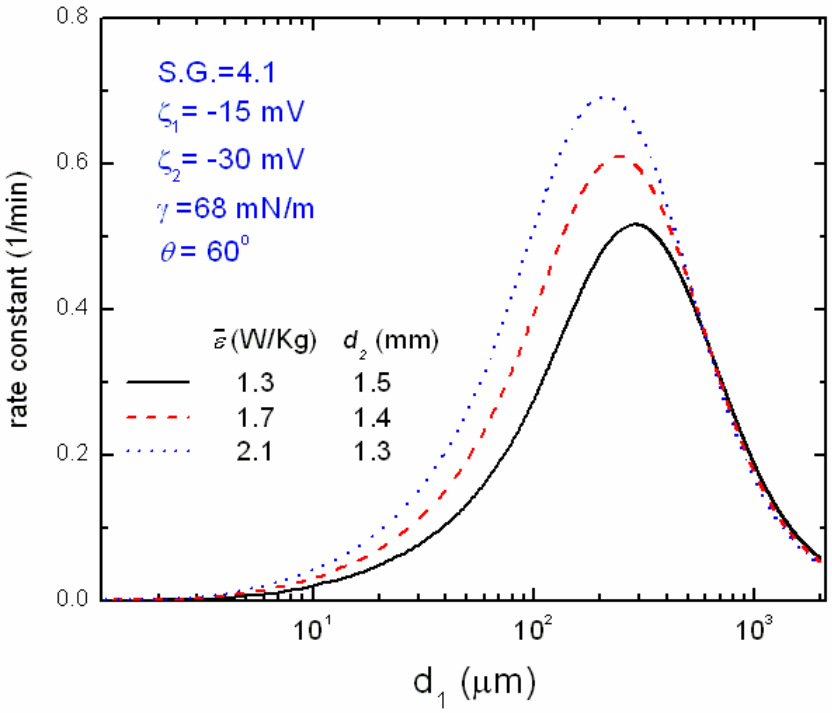

Fig.6. Effect of energy dissipation rate ($\bar{\varepsilon}$) and bubble size (d_2) on flotation rate constant (k). Higher energy dissipations generate smaller bubbles, and they give higher rates at a given particle size (d_1). The optimum particle size for flotation shifts to smaller sizes, indicating that smaller bubbles are beneficial for fine particle flotation.

(9)) and the kinetic energies of detachment (E'_k) increases as square of particle velocity, causing an increase in the probability of detachment (P_d). Also shown in Fig. 5 is the probability (P_f) of aggregates transferring bubble-particle aggregates to froth phase.

As shown in Figure 5, the probabilities of transferring bubble-particle aggregates to froth phase (P_f) are much smaller than those of other sub-processes. They do not change much at particle sizes below approximately 100 μm, but decreases significantly for coarser particles. This finding suggests that the difficulty in floating coarse particles is partly due to the sharp decrease in P_f with increasing particle size above 100 μm. It should be noted, however, that in predicting P_f it was assumed that the velocity of bubble-particle aggregate is reduced by approximately tenfold after n bounces at the pulp-froth interface, which entails a hundredfold decrease in kinetic energy. This assumption was based on the experimental result reported in the literature for free air bubbles with no particles attached [74]. For bubbles coated with hydrophobic particles, however, could have higher inertia and hence higher P_f . Unfortunately, there are no experimental results reported in the literature for bubble-particle aggregates bouncing at the pulp-froth interface. Further work is, therefore, necessary to gather additional information.

Fig. 6 shows the effects of changing the mean energy dissipation rate ($\bar{\varepsilon}$) on flotation rate constant (k) in the pulp phase. The simulation results are plotted versus particle size (d_1). As $\bar{\varepsilon}$ increases, bubble size (d_2) decreases according to Eq. (26) as shown in the inset. The results

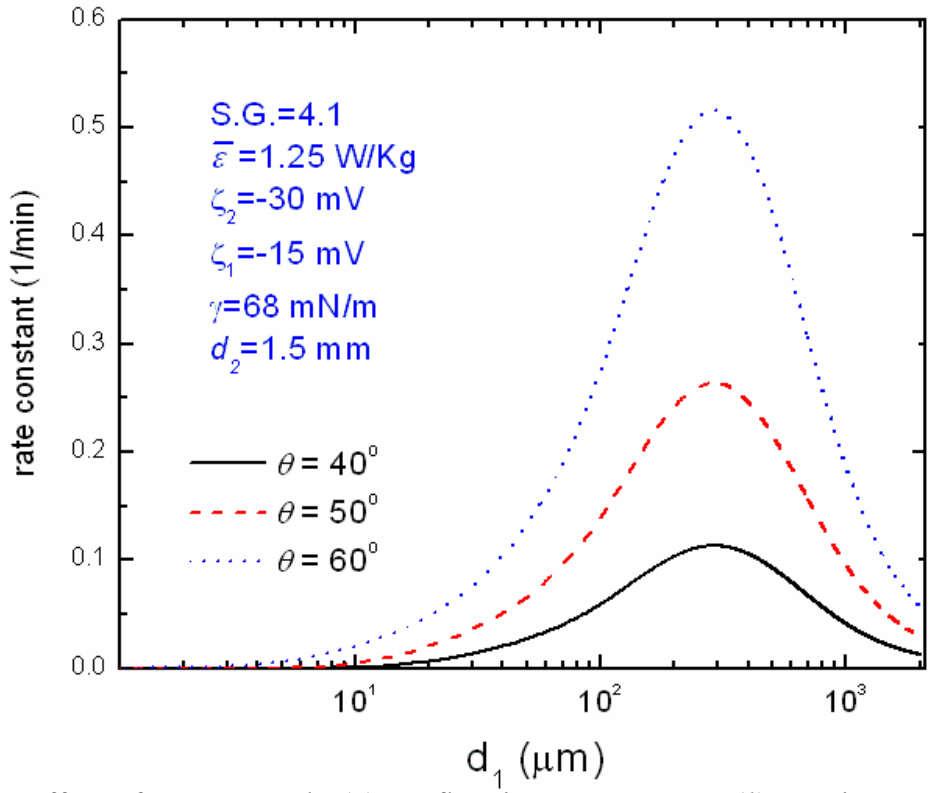

Fig.7. Effect of contact angle (θ) on flotation rate constant (k). An increase in contact angle causes the energy barrier (E_1) to decrease and the work of adhesion (W_a) to increase, both contributing to increased rate constant.

show that as $\bar{\varepsilon}$ increases k increases in general, which can be attributed to the increase in the kinetic energy for attachment (E_k). This finding is in agreement with the work of Ahmed and Jameson [82], who showed that an increase in agitation caused an increase in the rate of flotation of latex particles. Note here that an increase in energy input shifts the k vs. d_1 curves toward the finer particle sizes, which suggests that a higher energy input is helpful for the flotation of finer particles. This observation can be explained by the fact that fine particles do not have sufficient kinetic energies to overcome the energy barrier (E_1), which is one of the main causes for the difficulty in floating fine particles. This problem can be overcome by increasing the specific energy input for flotation. The increase in k with increasing $\bar{\varepsilon}$ may also be attributed to the corresponding decrease in bubble size. However, the changes in bubble size are too small to account for the large decrease in k.

Figs. 7 and 8 show the effects of various surface chemical parameters. The results of varying the contact angle (θ), along with particle size (d_1), have been plotted *vs.* the latter in Fig. 7. As shown, the flotation rate constant (k) increases with increasing particle hydrophobicity. An increase in hydrophobicity should have triple benefits. First, it causes an increase in the work of adhesion (W_a) and, hence, a decrease in the probability of detachment (P_d) as suggested by Eqs. (13) and (12), respectively. Second, an increase in hydrophobicity should increase the hydrophobic force constant (K_{131}), which should in turn reduce the energy barrier (E_1) and, hence, the probability of adhesion (P_a) as suggested by Eq. (11). Third, an increase in hydrophobicity should increase the critical rupture thickness (H_c), which should decrease the

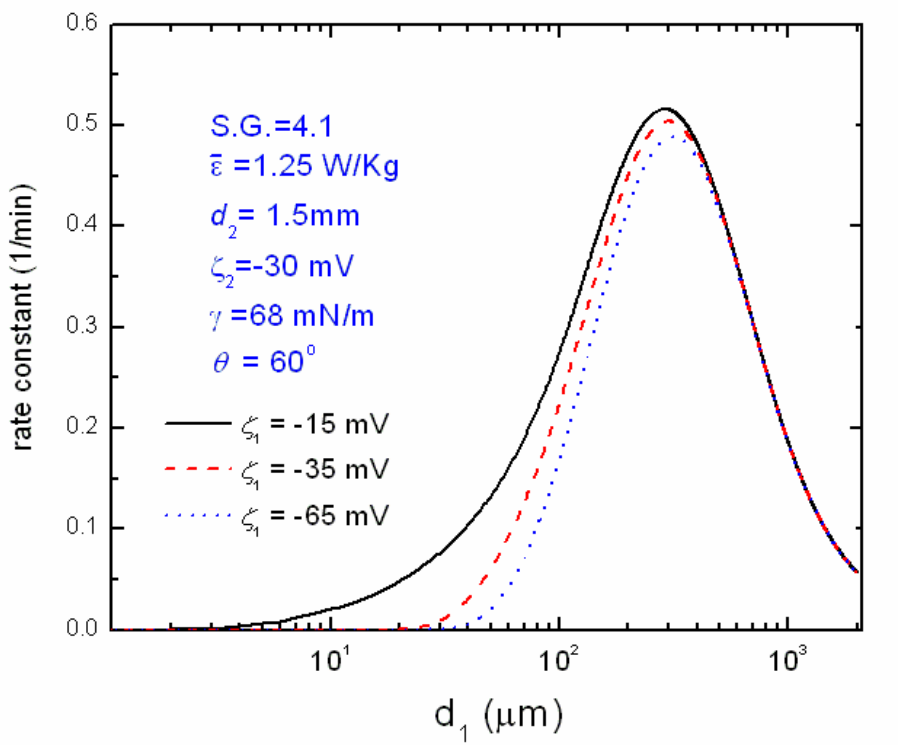

Fig.8. Effect of particle zeta potential (ζ_1) on flotation rate constant (k). k increases with a decrease in the negative zeta-potential of the particles due to a decrease in energy barrier (E_1).

extent of decrease in the particle velocity due the hydrodynamic resistance. This should in turn increase the kinetic energy of attachment (E_k) and, hence, the probability of attachment (P_a) as suggested by Eq. (11).

Fig. 8 shows the simulation results obtained by varying the zeta-potentials (ζ_1) of particles at different particle sizes. The results show that k increases substantially as ζ_1 becomes less negative. Since the zeta-potential of air bubbles is negative, a decrease in the magnitude of the negative zeta-potential of particles should result in a decrease in the electrostatic repulsion between bubble and particle, which should in turn decrease the energy barrier (E_1) and, hence, increase k. This finding is in agreement with the work of many investigators, who showed that flotation recovery is maximum when the magnitude of zeta-potential is minimum [5, 85-89]. A decrease in the negative zeta-potential should also increase in the critical rupture thickness (H_c). At a larger H_c, the velocity of the particle approaching an air bubble becomes larger due to a decrease in the hydrodynamic resistance as discussed in the foregoing paragraph. This should also increase the kinetic energy of attachment (E_k) and, hence, the flotation rate. Thus, some of the beneficial effects of controlling zeta-potentials of bubbles and particles are the same as those obtainable by control of particle hydrophobicity. The benefits of controlling zeta-potentials are more readily discernable at smaller particle sizes. With larger particles, the beneficial effects are overcome by the larger detachment probabilities (P_d) and lower probabilities of pulp-to-froth

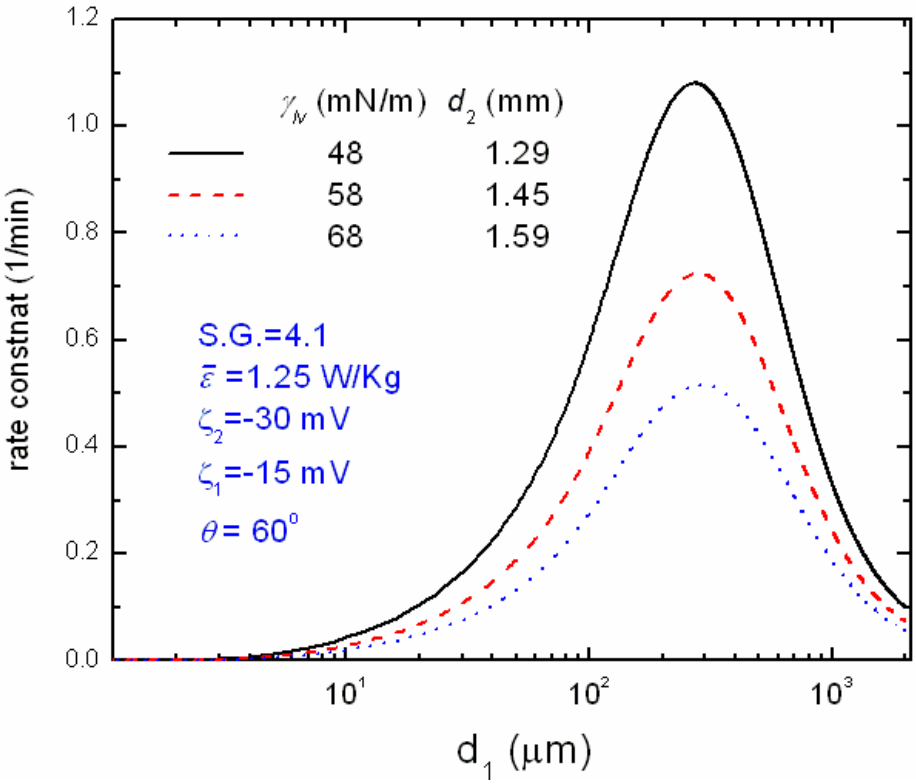

Fig.9. Effect of surface tension (γ_{lv}) on flotation rate constant (k). A higher surface tension causes larger bubble sizes and deteriorated flotation rate.

transfer probability (P_f).

Fig. 9 shows the simulation results obtained by changing the surface tension of water (γ_{lv}) and particle size (d_1). The results show that as surface tension is decreased flotation rate is increased at the entire particle size range investigated. This finding can be explained by the decrease in bubble size (d_2) with decreasing surface tension (γ_{lv}) in accordance to the bubble generation model represented by Eq. (26) and as shown in the inset. On the other hand, a decrease in γ_{lv} should cause a decrease in work of adhesion (W_a) according to Eq.(13) and hence cause an increase in the probability of detachment (Eq.(12)). Obviously, change in γ_{lv} affects d_2 more than W_a in terms of flotation recovery.

4. DISCUSSION

The model developed in the present work is by no means complete, as flotation is a complex three-phase phenomenon, and much is still unknown. The most difficult part of modeling flotation under turbulent flow conditions is to accurately determine the kinetic energies involved in the sub-processes of bubble-particle attachment and detachment sub-processes, both of which are related to energy dissipation rates. In the present work, a flotation cell was subdivided into two compartments, *i.e.*, high and low energy dissipation zones. It may be necessary, however, to use a multi-compartment model for energy dissipation. Better still may be to use the local energy dissipation rates that can be readily determined from CFD simulation.

Many investigators studied the kinetics of thinning of the wetting films of water formed on flat and well-defined surfaces of solids [27, 90, 91]. The changes in film thickness can be monitored accurately using the optical interference technique. The results showed that as an air bubble is pressed against a flat solid surface in a horizontal orientation, the air bubble deforms to produce a plane-parallel wetting film. The change in curvature associated with this process creates a pressure difference between the liquid in the film and the bulk solution, causing the film to thin spontaneously. As the film thinning continues to a thickness of approximately 200 nm, the process is controlled by the disjoining pressure (Π), which is created by the forces acting between the two surfaces, *i.e.*, solid and air bubble, facing each other in the wetting film. If Π is positive (repulsive), the film thinning stops at an equilibrium thickness (H_e), and the film does not rupture. If the Π is negative (attractive), then the film ruptures at a critical rupture thickness (H_c), creating an air/solid interface. In general, both H_c and the kinetics of film thinning increases with increasing hydrophobicity (contact angle) of the solid [26].

In flotation, air bubbles collide with mineral particles and create wetting films between them. For a successful flotation, the films must rupture during the short contact times allowed under highly dynamic conditions. Thus, the basic mechanisms involved in bubble-particle attachment should be the same as those of the wetting films discussed above. To model the attachment process, one must consider all of the forces involved, including the hydrodynamic, capillary, and surface forces. During the initial stages of film thinning, the first two forces are important, while the surface forces become important during the latter stages. Whether a film ruptures or not and how fast it thins are determined mainly by the surface forces. As has already

been discussed, the DLVO forces, *i.e.*, the van der Waals-dispersion force and the double-layer force are often repulsive under most flotation conditions. Thus, it is necessary to consider the presence of hydrophobic force, as in Eq. (14). Figure 1 shows a plot of the extended DLVO theory for a hypothetical case. It gives a value of the energy barrier (E_1) to be $5\text{x}10^{-17}$ J, which needs to be overcome by the hydrodynamic forces available in a cell for a successful flotation. It would, therefore, be of interest to determine E_1 experimentally and compare the results with that obtainable by an extended DLVO plot.

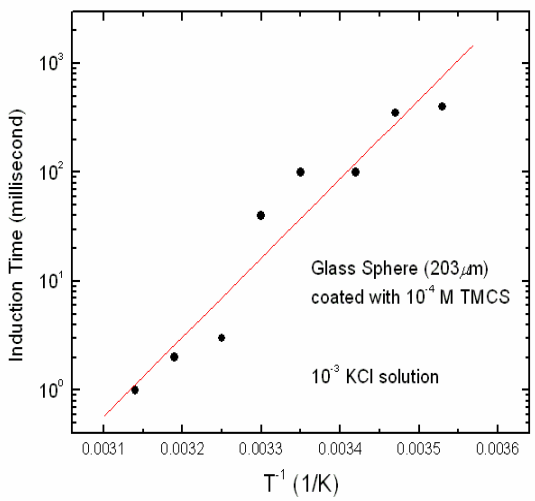

Fig. 10-A. Temperature effect on induction time. The slope of the plot yields $E_1 = 3\times10^{-17}$ J at 25°C from Eq.(39).

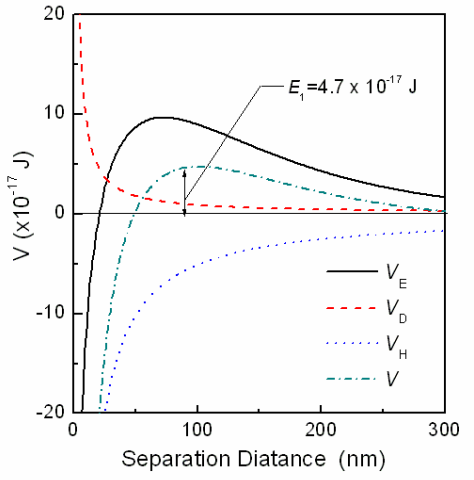

Fig. 10-B. The potential energy curves showing the extended DLVO theory in the corresponding system with Fig.9-A. The parameters used in the theoretical predictions were as follows: Ψ_1= -60 mV, Ψ_1= -15mV, A_{132}= -7.08 $\text{x}10^{-20}$ J, K_{132}= $2.3\text{x}10^{-19}$J, r_1=0.1mm, r_2=1 mm.

In the present work, E_1 has been determined from the induction time measurements conducted at different temperatures. Figure 10-A shows the results obtained with the glass spheres (d_1 = 203 μm) hydrophobized with TMCS (10^{-4} M) to obtain $\theta = 50^o$. The measurements were conducted in a 10^{-3} M KCl solution at fixed speeds for bubbles approaching and retreating to and from a bed of particle. The results have been plotted according to the Arrhenius equation [92, 93],

$$t = t_0 \exp\left(\frac{E_1}{k_b T}\right) \tag{39}$$

where t is the induction time, t_0 a constant, k_b the Boltzmann's constant, and T is the absolute temperature. The induction time is found to decrease substantially with increasing temperature. From the slope, one obtains $E_1 = 3\times10^{-17}$ J at 25°C, which agrees well with that (= 4.7×10^{-17} J) obtained from an extended DLVO plot given in Figure 9-B. The plot was made with the following parameters: ζ_1 = -60 mV [94], ζ_2 = -15 mV [95], and $K_{132} = 2.3\times10^{-19}$ J. The hydrophobic force constant was obtained using the combining rule (Eq. (18)) with $K_{131} = 2.16\times10^{-20}$ J and $K_{232} = 2.5\times10^{-18}$ J. The former was obtained using Eq. (19) from $\theta = 50^o$ for the glass spheres used in the induction time measurement. The value of the bubble zeta-potential (ζ_2) may appear lower than those (-30 to -15 mV) reported in the literature [9, 40, 96]. In the present work, the lowest limit of -15 mV was chosen in view of the relatively large bubble size (2 mm) used in the induction time measurements. It has been shown that bubble zeta-potentials decrease considerably with increasing bubble size [95]. The agreement between the calculated and experimental values of E_1 justifies the approach taken in the present work in modeling flotation.

It has been found that the pulp-phase flotation rate constant, k, predicted from Eq. (8) are considerably higher than those reported in the literature from batch flotation experiments. This is particularly the case for coarse particles, which can be attributed to the fact that froth phase recovery drops off sharply with increasing particle size. Another reason for the discrepancy between the predicted and laboratory experimental results is that the energy dissipation rates employed in the model calculations are substantially lower than those used in laboratory flotation experiments.

5. SUMMARY AND CONCLUSION

A flotation model has been derived to predict flotation recovery under turbulent flow conditions from both hydrodynamic and surface chemistry parameters. The model can predict the flotation rate constants in the pulp phase of a flotation cell, which will allow predicting the corresponding flotation recovery. By combining such information with those in the froth phase, it is possible to predict the overall flotation recovery. It has been found that the model can be used to successfully simulate the industrial flotation results reported in the literature.

The simulation results obtained under typical operating conditions employed for the flotation of chalcopyrite show that flotation becomes difficult at particle sizes below 10 μm and above approximately 200 μm, which are consistent with the upper and lower particle size limits reported in the literature. The difficulty in floating fine particles is due to the low collision

efficiency (P_c) rather than collision frequency (Z_{12}). In fact, the latter increases with decreasing particle size. That fine particles have low kinetic energies also contribute to the low P_a and hence low flotation recovery. This problem can be overcome by increasing the specific energy input to a flotation cell. On the other hand, the difficulty in floating coarse particles is due to the high probability of detachment under turbulent flow conditions and the low probability of bubble-particle aggregates entering froth phase.

The simulation results show also that flotation rate is critically dependent on contact angle, ζ-potential, and surface tension, as demonstrated amply in the literature and in flotation practice. In general, flotation rate increases with increasing contact angle at all particle sizes. When the ζ-potentials of air bubbles are negative, flotation rate increases with a decrease in the negative ζ-potentials of particles. The simulation results suggest that proper control of ζ-potentials helps the flotation of finer particles rather than that of coarser particles. Simulation results obtained by changing the surface tension of water show that flotation rare increases with decreasing surface tension, which in turm causes a decrease in bubble size. The induction time measurements were conducted at different temperatures to determine the energy barrier for bubble-particle attachment. The result is similar to that obtained using the extended DLVO theory.

6. REFERENCES

1. Sutherland, K.L., *Physical Chemistry of Flotation. XI. Kinetics of the Flotation Process.* The Journal of Physical and Colloid Chemistry, 1948. **52**(2): p. 394-425.
2. Schuhmann, R., *Flotation Kinetics. I. Methods for steady-state study of flotation problems.* The Journal of Physical Chemistry, 1942. **46**(8): p. 891-902.
3. Gaudin, A.M., *Flotation*. 1932, New York: McGraw Hill.
4. Derjaguin, B.V. and S.S. Dukhin, *Theory of flotation of small and medium-size particles.* Transactions of Institutions of Mining and Metallurgy, 1961. **70**: p. 221-246.
5. Reay, D. and G.A. Radcliff, *Removal of fine particles from water by dispersed air flotation: effects of bubble size and particle size on collection efficiency.* Canadian Journal of chemical engineering, 1973. **51**: p. 178-185.
6. Weber, M.E. and D. Paddock, *Interceptional and gravitational collision efficiencies for single collectors at intermediate Reynolds numbers.* Journal of Colloid and Interface Science, 1983. **94**(2): p. 328-335.
7. Finch, J.A. and G.S. Dobby, *Column flotation*. 1990: Pergamon press.
8. Yoon, R.H. and G.H. Luttrell, *The effect of bubble size on fine particle flotation.* Mineral Processing and Extractive Metallurgy Review, 1989. **5**: p. 101-122.
9. Yoon, R.-H. and L. Mao, *Application of Extended DLVO Theory, IV: Derivation of Flotation Rate Equation from First Principles.* Journal of Colloid and Interface Science, 1996. **181**(2): p. 613-626.
10. Pyke, B., D. Fornasiero, and J. Ralston, *Bubble particle heterocoagulation under turbulent conditions.* Journal of Colloid and Interface Science, 2003. **265**(1): p. 141-151.
11. Ralston, J., S.S. Dukhin, and N.A. Mishchuk, *Inertial hydrodynamic particle-bubble interaction in flotation.* International Journal of Mineral Processing, 1999. **56**(1-4): p. 207-256.

12. Sherrell, I. and R.-H. Yoon. *Development of a turbulent flotation model*. in *Centenary of flotation symposium*. 2005. Barisbane, Australia.
13. Sherrell, I., *Development of a flotation rate equation from first principles under turbulent flow conditions*, in *Mining and Minerals Engineering*. 2004, Virginia Tech: Blacksburg.
14. Koh, P.T.L. and M.P. Schwarz, *CFD modelling of bubble-particle collision rates and efficiencies in a flotation cell.* Minerals Engineering, 2003. **16**(11): p. 1055-1059.
15. Koh, P.T.L. and M.P. Schwarz, *CFD modelling of bubble-particle attachments in flotation cells.* Minerals Engineering, 2006. **19**(6-8): p. 619-626.
16. Bloom, F. and T.J. Heindel, *On the structure of collision and detachment frequencies in flotation models.* Chemical Engineering Science, 2002. **57**(13): p. 2467-2473.
17. Ralston, J., et al. *Flotation rate constant prediction for metal sulfide particles*. in *Centenay of flotation symposium*. 2005. Brisbane, Australia.
18. Schubert, H., *On the turbulence-controlled microprocesses in flotation machines.* International Journal of Mineral Processing, 1999. **56**(1-4): p. 257-276.
19. Abrahamson, J., *Collision rates of small particles in a vigorously turbulent fluid.* Chemical Engineering Science, 1975. **30**(11): p. 1371-1379.
20. Derjaguin, B.V. and S.S. Dukhin. in *13th international mineral processing congress*. 1969.
21. Mika, T.S. and D.W. Fuerstenau. *A microscopic model of the flotation process*. in *8th international mineral processing congressqLeningrad, U.S.S.R.* 1968. Leningrad.
22. Hunter, R.J., *Fundamentals of colloid science*. 1986: Oxford science publications.
23. Overbeek, J.T.G., *Colloid science*. 1952: Elsevier.
24. Smoluchowski, M., *Mathematical theory of the kinetics of the coagulation of colloidal particle.* Z. phys. Chem, 1917. **92**: p. 129.
25. Jowett, A. and S.M.M. Safvi, *Refinements in methods of determining flotation rates.* Trans. AIME, Metallurgical and petroleum engineers, 1960. **217**: p. 351-357.
26. Yoon, R.H. and J.L. Yordan, *The critical rupture thickness of thin water films on hydrophobic surfaces.* Journal of Colloid and Interface Science, 1991. **146**(2): p. 565-572.
27. Israelachvili, J. and R. Pashley, *The hydrophobic interaction is long range, decaying exponentially with distance.* Nature, 1982. **300**(5890): p. 341-342.
28. Christenson, H.K. and P.M. Claesson, *Direct measurements of the force between hydrophobic surfaces in water.* Advances in Colloid and Interface Science, 2001. **91**(3): p. 391-436.
29. Pazhianur, R. and R.H. Yoon, *Model for the origin of hydrophobi force.* Minerals and Metallurgical processing, 2003. **20**(4): p. 178-184.
30. Yoon, R.-H. and S.A. Ravishankar, *Long-Range Hydrophobic Forces between Mica Surfaces in Dodecylammonium Chloride Solutions in the Presence of Dodecanol.* Journal of Colloid and Interface Science, 1996. **179**(2): p. 391-402.
31. Considine, R.F., R.A. Hayes, and R.G. Horn, *Forces Measured between Latex Spheres in Aqueous Electrolyte:??Non-DLVO Behavior and Sensitivity to Dissolved Gas.* Langmuir, 1999. **15**(5): p. 1657-1659.
32. Meagher, L. and V.S.J. Craig, *Effect of Dissolved Gas and Salt on the Hydrophobic Force between Polypropylene Surfaces.* Langmuir, 1994. **10**(8): p. 2736-2742.

33. Tyrrell, J.W.G. and P. Attard, *Atomic Force Microscope Images of Nanobubbles on a Hydrophobic Surface and Corresponding Force? 昂 eparation Data.* Langmuir, 2002. **18**(1): p. 160-167.
34. Ishida, N., et al., *Nano Bubbles on a Hydrophobic Surface in Water Observed by Tapping-Mode Atomic Force Microscopy.* Langmuir, 2000. **16**(16): p. 6377-6380.
35. Mao, M., et al., *Is There a Thin Film of Air at the Interface between Water and Smooth Hydrophobic Solids?* Langmuir, 2004. **20**(5): p. 1843-1849.
36. Sakamoto, M., et al., *Origin of Long-Range Attractive Force between Surfaces Hydrophobized by Surfactant Adsorption.* Langmuir, 2002. **18**(15): p. 5713-5719.
37. Zhang, J., et al., *Effects of Degassing and Ionic Strength on AFM Force Measurements in Octadecyltrimethylammonium Chloride Solutions.* Langmuir, 2005. **21**(13): p. 5831-5841.
38. Meyer, E.E., Q. Lin, and J.N. Israelachvili, *Effects of Dissolved Gas on the Hydrophobic Attraction between Surfactant-Coated Surfaces.* Langmuir, 2005. **21**(1): p. 256-259.
39. Xu, Z. and R.-H. Yoon, *The role of hydrophobia interactions in coagulation.* Journal of Colloid and Interface Science, 1989. **132**(2): p. 532-541.
40. Xu, Z. and R.-H. Yoon, *A study of hydrophobic coagulation.* Journal of Colloid and Interface Science, 1990. **134**(2): p. 427-434.
41. Chia, Y.H. and P. Somasundaran, *A theoretical approach to flocculation in carrier flotation for beneficiation of clay.* Colloids and Surfaces, 1983. **8**(2): p. 187-202.
42. Schimmoller, B.K., G.H. Luttrell, and R.H. Yoon. *A combined hydrodynamic-surface force model for bubble-particle collection*. in *18th international mineral processing congress*. 1993. Sydney, Australia.
43. Mao, L. and R.-H. Yoon, *Predicting flotation rates using a rate equation derived from first principles.* International Journal of Mineral Processing, 1997. **51**(1-4): p. 171-181.
44. Camp, P.R. and P.C. Stein, *Velocity gradients and internal work in fluid motion.* Journal of the Boston Society of Civil Engineers, 1943. **30**(4): p. 219-237.
45. Saffman, P.G.a.T., J.S., *On the collision of drops in turbulent coluds.* Journal of Fluid Mechanics, 1956. **1**: p. 16-30.
46. Schumann, R., *Flotation kinetics: I. Moethods for steady state study of flotation problems.* Journal of physical chemistry, 1942. **46**: p. 891-902.
47. Tomlinson, H.S. and M.B. Flemming, *Flotation rate studies*, in *6th International Mineral Processing Congress*. 1963. p. 563.
48. Liepe, F. and H.O. Moeckel, *Untersuchungen zum Stoffvereinigen in Flüssiger Phase.* Chemical Technology, 1976. **28**.
49. Brady, M.R., et al., *Evaluation of multiphase flotation models in grid turbulence via Particle Image Velocimetry.* International Journal of Mineral Processing, 2006. **80**(2-4): p. 133-143.
50. Lee, C.A. and L.E. Erickson, *Bubble breakup and coalescence in turbulent gas-liquid dispersions.* Chemical Engineering Communications, 1987. **59**: p. 65-84.
51. Derjaguin, B.V., N.V. Churaev, and V.M. Muller, *Surface Forces*. 1987, New York: Consultatn Bureau-Plenum.
52. Ralston, J., S.S. Dukhin, and N.A. Mishchuk, *Wetting film stability and flotation kinetics.* Advances in Colloid and Interface Science, 2002. **95**(2-3): p. 145-236.

53. Luttrell, G.H. and R.H. Yoon. *Determination of the probability of bubble-particle adhesion using induction time measurements*. in *International symposium on the production and processing of fine particles*. 1988. Montreal, Canada.
54. Dobby, G.S. and J.A. Finch. in *114th annual AIME meeting*. 1985. New York.
55. Hogg, R., T.W. Healy, and D.W. Fuerstenau, *Mutual coagulation of colloidal dispersions.* Transactions of Faraday Society, 1966. **62**: p. 1638-1651.
56. Rabinovich, Y.I. and N.V. Churaev, *Effect of electromagnetic delay on the forces of molecular attraction.* Kolloidnyi Zhurnal, 1979. **41**(3): p. 468-474.
57. Yoon, R.-H., D.H. Flinn, and Y.I. Rabinovich, *Hydrophobic Interactions between Dissimilar Surfaces.* Journal of Colloid and Interface Science, 1997. **185**(2): p. 363-370.
58. Yoon, R.-H. and B.S. Aksoy, *Hydrophobic Forces in Thin Water Films Stabilized by Dodecylammonium Chloride.* Journal of Colloid and Interface Science, 1999. **211**(1): p. 1-10.
59. Wang, L. and R.-H. Yoon, *Hydrophobic Forces in the Foam Films Stabilized by Sodium Dodecyl Sulfate:Effect of Electrolyte.* Langmuir, 2004. **20**(26): p. 11457-11464.
60. Goren, S.L. and M.E. O'Neill, *On the hydrodynamic resistance to a particle of a dilute suspension when in the neighbourhood of a large obstacle.* Chemical Engineering Science, 1971. **26**(3): p. 325-338.
61. Luttrell, G.H. and R.-H. Yoon, *A hydrodynamic model for bubble-particle attachment.* Journal of Colloid and Interface Science, 1992. **154**(1): p. 129-137.
62. Luttrell, G.H., *Hydrodynamic studies and mathematical modeling of fine coal flotation*, in *Mining and Minerals Engineering*. 1986, Virginia Polytechnic Institute and State University: Blacksburg, Virginia.
63. Jowett, A. *Formation and disruption of particle-bubble aggregates in flotation*. in *Fine particle processing: Proceedings of International symposium on fine particles*. 1980: SME.
64. Schulze, H.J., *Physicochemical elementary processes in flotation*. 1983: Elsevier.
65. Lu, S., Y. Ding, and J. Guo, *Kinetics of fine particle aggregation in turbulence.* Advances in Colloid and Interface Science, 1998. **78**(3): p. 197-235.
66. Okamoto, Y., M. Nishikawa, and K. Hashimoto, *Energy dissipation rate distribution in mixing vessels and its effects on liquid-liquid dispersion and solid-liquid mass transfer.* International Chemical Engineering, 1981. **21**(1): p. 88-94.
67. Sundaram, S. and L.R. Collins, *Collision statistics in an isotropic particle-laden turbulent suspension. Part 1. Direct numerical simulations.* Journal of Fluid Mechanics, 1997. **335**(-1): p. 75-109.
68. Zenit, R. and D. Legendre, *The coefficient of restitution for air bubbles colliding against solid walls in viscous liquids.* Physics of Fluids, 2009. **21**(8): p. 083306-12.
69. Sanada, T., M. Watanabe, and T. Fukano, *Effects of viscosity on coalescence of a bubble upon impact with a free surface.* Chemical Engineering Science, 2005. **60**(19): p. 5372-5384.
70. Sunol, F. and R. Gonzalez-Cinca, *Rise, bouncing and coalescence of bubbles impacting at a free surface.* Colloids and Surfaces A: Physicochemical and Engineering Aspects, 2010. **In Press, Corrected Proof**.
71. Krzan, M., K. Lunkenheimer, and K. Malysa, *Pulsation and Bouncing of a Bubble Prior to Rupture and/or Foam Film Formation.* Langmuir, 2003. **19**(17): p. 6586-6589.

72. Malysa, K., M. Krasowska, and M. Krzan, *Influence of surface active substances on bubble motion and collision with various interfaces.* Advances in Colloid and Interface Science, 2005. **114-115**: p. 205-225.
73. Boulton-Stone, J.M. and J.R. Blake, *Gas bubbles bursting at a free surface.* Journal of Fluid Mechanics Digital Archive, 1993. **254**(-1): p. 437-466.
74. Barnocky, G. and R.H. Davis, *The lubrication force between spherical drops, bubbles and rigid particles in a viscous fluid.* International Journal of Multiphase Flow, 1989. **15**(4): p. 627-638.
75. Currie, I.G., *Fundamental mechanis of fluids*. 2nd ed. 1993: McGraw Hill.
76. Harris, C.C., *Flotation machines*, in *Flotation-A.M. Gaduin Memorial volume*, M.C. Fuerstenau, Editor. 1976, AIME. p. 753-815.
77. Lynch, A.J., M.W. Johnson, and E.V. Manlapig, eds. *Mineral and coal flotation circuits: their simulation and control*. Developments in mineral processing 3. 1981, elsevier.
78. MacMullin, P.B. and M. Weber, *The theory of short-circuiting in continuous flow mixing vessels in series and the kinetics of chemical reactions in such systems.* Transactions of Americal Isntitute of Chemical Engineeris, 1935. **31**: p. 409-458.
79. Do, H., *Development of a turbulent flotation model from first principles*, in *Engineering Science and Mechanics*. 2010, Virginia Polytechnic Institute and State University: Blacksburg.
80. Do, H. and R.H. Yoon, *A model for froth-phase recovery in a flotation cell.* International Journal of Mineral Processing, 2010. **to be submitted**.
81. Trahar, W.J. and L.J. Warren, *The flotability of very fine particles -- A review.* International Journal of Mineral Processing, 1976. **3**(2): p. 103-131.
82. Ahmed, N. and G.J. Jameson, *The effect of bubble size on the rate of flotation of fine particles.* International Journal of Mineral Processing, 1985. **14**(3): p. 195-215.
83. Gaudin, A.M., J.O. Groh, and H.B. Henderson, AIME Eng. Tech. Pub, 1931. **414**.
84. Duan, J., D. Fornasiero, and J. Ralston, *Calculation of the flotation rate constant of chalcopyrite particles in an ore.* International Journal of Mineral Processing, 2003. **72**(1-4): p. 227-237.
85. Devivo, D.G. and B.L. Karger, *Studies in the Flotation of Colloidal Particulates: Effects of Aggregation in the Flotation Process.* Separation Science and Technology, 1970. **5**(2): p. 145 - 167.
86. Baker, H.F. and K.J. Miller, *Zeta poetntial contro: its application in coal preparation.* Mining congress journal, 1968. **55**: p. 43-44.
87. Chander, S. and D.W. Fuerstenau, Trans. AIME, 1972. **252**.
88. Fuerstenau, D.W., Trans. AIME, 1957. **208**: p. 1365.
89. Jacock, M.J. and R.H. Ottewill, Trans. Inst. Min. & Metall., 1963. **72**: p. 497.
90. Laskowski, J. and J.A. Kitchener, *The hydrophilic--hydrophobic transition on silica.* Journal of Colloid and Interface Science, 1969. **29**(4): p. 670-679.
91. Blake, J.R. and J.A. Kitchener, *Stability of aqueous films on hydrophobic methylated silica.* Journal of Chemical Society, Faraday Transactions 1: Physical chemistry in condensed phases, 1972. **68**: p. 1435-1442.
92. Eigeles, M.A. and M.L. Volova. *Kinetic investigation of effect of contact time, temperature and surface condition on the adhesion of bubble to mineral surfaces*. in *5th International Mineral Processing Congress*. 1960. London: Inst. Min. Metall.

93. Yoon, R.-H. and J.L. Yordan, *Induction time measurements for the quartz--amine flotation system.* Journal of Colloid and Interface Science, 1991. **141**(2): p. 374-383.
94. Ducker, W.A., Z. Xu, and J.N. Israelachvili, *Measurements of Hydrophobic and DLVO Forces in Bubble-Surface Interactions in Aqueous Solutions.* Langmuir, 1994. **10**(9): p. 3279-3289.
95. Usui, S., H. Sasaki, and H. Matsukawa, *The dependence of zeta potential on bubble size as determined by the dorn effect.* Journal of Colloid and Interface Science, 1981. **81**(1): p. 80-84.
96. Blake, P. and J. Ralston, *Controlled methylation of quartz particles.* Colloids and Surfaces, 1985. **15**: p. 101-118.

CHAPTER 3

INDUCTION TIME MEASUREMENT FOR SINGLE-PARTICLE FLOTATION

Abstract

Bubble and particle attachment plays the most important role in flotation because it is the prerequisite for successful flotation. With regard to the bubble-particle attachment, the effect of various parameters on floatability has been studied in this report by measuring the time required for completing the attachment. The time, called induction time, showed significant changes with changing parameters such as bubble size, particle size, moving speed of bubble, surface tension, and electrolyte concentration of the solution. The overall experimental results agreed with the prediction by the flotation model which was developed in another work by the present authors. The effect of temperature on induction time was also studied, and the corresponding results could verify the extended DLVO theory which was used in the flotation model.

1. Introduction

Flotation is a separation technique which has been used in the mining industry for more than a century for the recovery of valuable minerals. Of the various subprocesses of flotation, attachment of hydrophobic mineral particles to air bubbles is the most important. For the attachment to be accomplished, the liquid film intervening between bubble and particle surfaces should rupture. The time required for this rupture process is referred to as induction time in flotation research, and it has been considered as a good indicator for the floatability of minerals under a given chemical condition. Floatability is also evaluated by contact angle of particles. Of the two, evaluating floatability by induction time is more reliable because the measurement is conducted in a dynamic environment while contact angle represents only the property of equilibrium state. Generally, the shorter the induction time is, the higher the floatability [1].

The first experiment on induction time may date back to Sven-Nilson [2]'s work in which a method was devised for estimating relatively short induction time. In this report, a captive bubble was vibrated with varying frequencies against a submerged mineral surface. The time it took for the interfacial film to rupture at a sufficiently low frequency was considered as the induction time, and it was found to be 0.01~0.1 seconds for typical minerals. Since then, many investigators used different techniques to determine induction time [3-7]. Nevertheless, the number of references on induction time measurement does not correspond to its significance in flotation research. It seems due to the limitations of experimental techniques used, as well as the ambiguity concerning the definition of actual induction time. Several researchers considered induction time as the resultant time of three discrete steps to complete attachment: drainage of liquid film between particle and air bubble surfaces followed by the rupture time of the film, and the spreading of contact area after the rupture [2, 8, 9]. Those three steps may be distinguishable for the case when particles are large relative to bubble because the attachment commences in a relatively long timescale due to large contact area. However, the steps may have less meaning in actual flotation systems where attachment timescale is generally very short due to smaller particle sizes than bubbles. Therefore, the term 'induction time' may well be used interchangeably with 'attachment time' in the experiment that simulates bubble-particle attachment of actual flotation [3].

Regarding the timescales, the work by Ye *et al*. [10] may indicate the particular difference of timescale between the induction time measured on a polished mineral surface and the one on a particle bed of the same material. They found that induction time measured on a polished surface is orders of magnitude greater than that measured on a particle bed. However, there is a blemish in their comparison that the authors compared two systems that are dynamically dissimilar. The data on polished mineral surfaces were obtained by analyzing the images at the interface between the mineral surface and a bubble kept underneath the surface by its buoyant force. On the other hand, the bubble's motion and contact time with a particle bed was well controlled by an electromechanical driver.

Eigeles and Volova [11] were the first who conducted induction time experiments at a particle bed. Induction time was measured by moving a bed of small mineral particles in a solution toward and then away from a fixed captive bubble. The same approach was adopted by other researchers with modified and improved induction timer apparatus [1, 10, 12]. Using

similar apparatus, Ye *et al*.[10] measured induction time in coal flotation systems while Yoon and Yordan [1] did in quartz-Amine flotation systems especially with extensive investigation on the effects of flotation chemistry. Hewitt *et al*. [13] also measured induction time in an environment more dynamically similar to actual flotation. In their experiments, a video camera was used to record hydrophobic particles settling onto a rising bubble. However, their induction time was not measured directly but inferred from the analysis of the collection efficiency data determined by measuring the number of attached particles per bubble. Recently, Wang *et al*.[3] measured induction time between a hydrophobic solid sphere and a bubble using the same technique as Gu *et al*. [12]. However, the radius of sphere was exaggerated to the extent as large as the bubble radius in order to detect the attachment more clearly.

In the present work, induction time measurements have been carried out for several systems: quartz-amine, and quartz-silane systems. The effects of different physical parameters such as bubble size, particle size, and bubble's approaching speed have been investigated as well as the effect of chemical properties such as surface tension, contact angle, and electrolyte concentrations.

2. Experimental

The methodology for measuring induction time was originally adopted from other literature that had successfully proved its validity for assessing floatability in certain systems [1].

2.1 Sample preparation

Particles of various hydrophobicties were obtained using two different methods. First, different sizes of glass spheres obtained from Potters Industries Inc. were hydrophobized by submerging them in solutions of trimethylchlorosilane (TMCS) in cyclohexane by following the method descrined in literature [14-16]. Samples of desired sizes were first preheated in a convection oven at 80^{o}C for 24 hours, and kept immersed in designated TMCS solutions at ambient temperature for another 24 hours. After supposedly complete reaction, particles were removed from the solution to be washed twice with pure cyclohexane, and then dried in a convection oven at 100^{0}C. At the same time with the particle preparation, glass plates of 1.5x1.0 cm^2 were also immersed in the same solution so that the contact angles of the plate and sphere were the same.

In addition to the glass-TMCS system, another system was considered as well. Spherical glass particles of various sizes obtained from Potters Industries Inc. were hydrophobized by submerging in solutions of 5×10^{-6}M C_{18}TACl. This particular concentration was found to yield the strongest hydrophobicity of silica surface according to Zhang *et al.* [17]. Samples had to be immersed for at least 2 hours for the adsorption to reach equilibrium. At the same time, glass plates of 1.5x1.0 cm^2 were also prepared under the same conditions, representing particles of infinite size. The plate samples were prepared in case the particle samples would be too small beyond the equipment's 1 millisecond sensitivity. It should be also noted here that cleaning sample surfaces was a crucial factor in the experiment as dirty surfaces caused inhomogeneous adsorptions on them and hence poor reproducibility. The cleaning process is well described elsewhere [17].

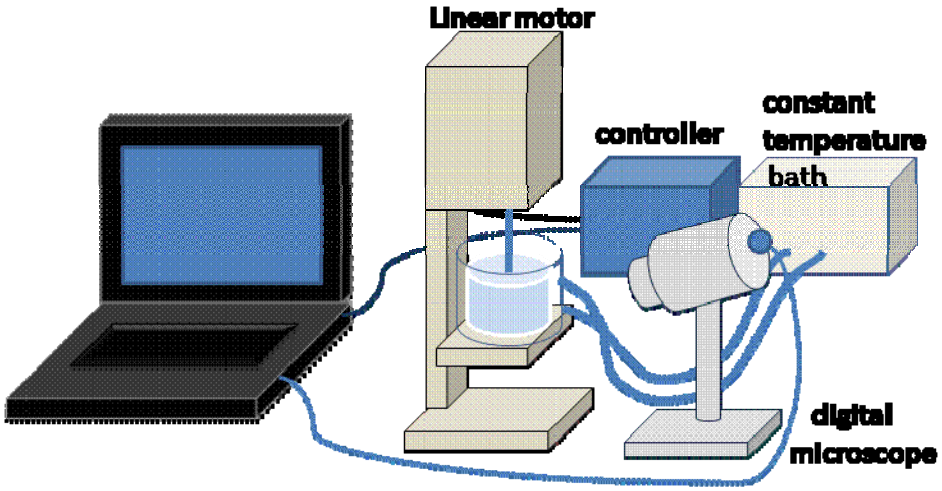

Figure.1. Experimental setup for induction time measurement

2.2 Equipment and procedure

The experimental setup is shown in Fig.1. A programmable linear D.C. motor was assembled atop a glass capillary tube. Then single air bubble of approximately 1,1.5 or 2 mm diameter was generated in each test by injecting constant volume of air through a syringe connected to the inlet of the tube. The motor mount was designed such that the tube tip can be dipped in a small solution container placed on a rack where the bubble motion was observed more closely by a digital microscope. A glass titration vessel with thermostatic jacket was chosen as the container, so that the solution could be kept in constant temperature of certain degrees by circulating water into the jacket from a constant temperature bath.

The tube tip's moving speed, distance, and the contact time were programmable. The contact time was adjusted in several trials, from which the minimum was sought. The minimum contact time at which the bubble successfully picked up more than one particle with reproducibility of at least 5 out of 10 trials was defined as the induction time, as has been in the original experiments by Yoon and Yordan [1].

3. Experimental Results

Previously, a flotation model was developed by considering both the hydrodynamic and chemical properties [18, 19]. The following experimental results agreed with some of what the model predicted when those properties were changed.

3.1 Effect of particle size

Figure 2 shows the effect of particle sizes on induction time. The results obtained with two different samples are plotted in one figure. Bubble diameter in both experiments was 2mm. For the glass-TMCS samples, the glass spheres were hydrophobized in 10^{-4} % by volume TMCS-in-

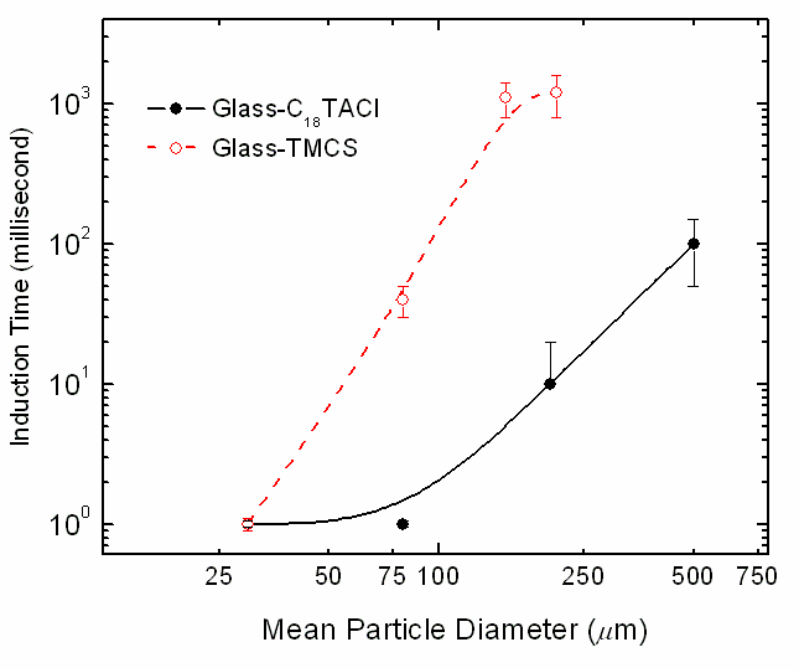

Figure.2. Effect of particle sizes on induction time

cyclohexane solutions, and immersed in pure water with 0.1 M NaCl. Approaching and retracting speed of the bubble were both 7.8 cm/s. For the glass-C_{18}TACl samples, glass spheres were immersed in 5×10^{-6} M C_{18}TACl solutions with 0.01 M NaCl, and bubble moved at 315 cm/s in both approaching and retracting directions. The results show higher induction times for larger particle sizes. This agrees with the general observation that large particles are difficult to float.

3.2 Effect of bubble size

In figure 3, the effects of bubble size on induction time are shown. Bubble size control was possible by injecting different air volume. Approximately 1.0 mm, 1.5 mm, and 2.0 mm diameter bubbles were made to compare. Particle samples were the same as those used in the experiment for Figure 2, but the diameter was fixed at 203 μm. The moving speed of bubble was 315 cm/s in both approaching and retracting directions. Electrolyte concentration was 10^{-3} M of NaCl.

As Figure 3 indicates, particles attach more quickly to smaller bubbles than to larger bubbles. This result agrees with the predictions of the flotation model by Do and Yoon [18-20] that small bubbles are beneficial to flotation. This result also corresponds to the theoretical prediction by the Reynolds equation that is commonly used to estimate the thinning rate of wetting films [21]. The thinning rate is proportional to the pressure difference between the liquid and gas phase. Therefore, small bubbles should induce faster film thinning because the pressure difference is inversely proportional to the radius of air drop, according to the Laplace equation.

3.3 Effect of bubble speed

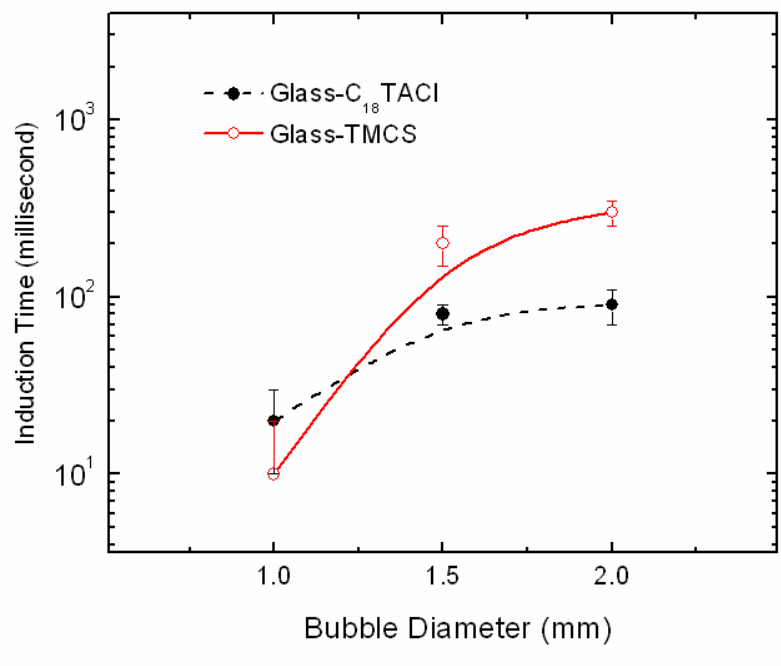

Figure.3. Effect of bubble sizes on induction time

In figure 4, the effects of the approaching speed of a bubble are shown. The retracting speed may be of interest as well. However, only the approaching speed is studied because the present work focuses on bubble-particle attachment only. In fact, the effect of retracting speed was not observable because its change did not cause any difference in induction time. It may be because

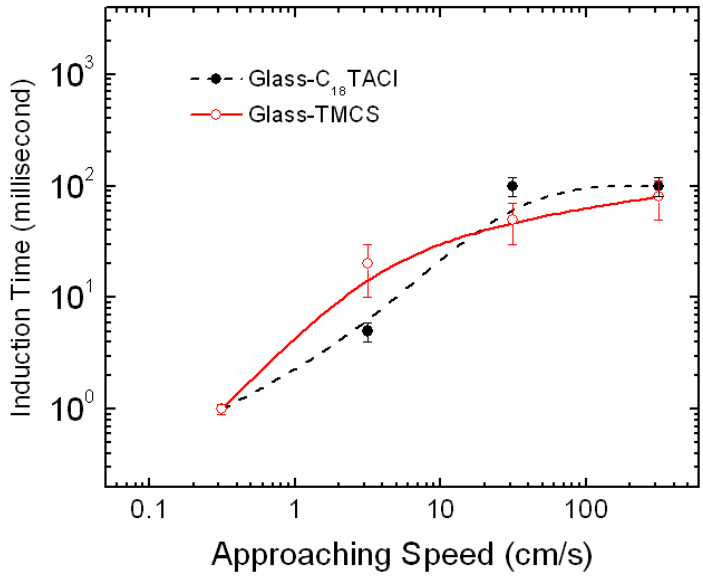

Figure.4. Effect of the approaching speed of the bubble on induction time

particles require much higher energy to be detached from bubble surfaces, and the present experimental setup could not reach up to the necessary speed.

For the particles of glass-C_{18}TACl system, the particle diameter was 500 μm, and the retracting speed was 315 cm/s. The particles of glass-TMCS system were hydrophobized in solutions of 80% Cyclohexane and 20% TMCS by volume, and the experiments were conducted in the presence of 1 M NaCl. The diameter was 156 μm, and the retracting speed was 315 cm/s as well.

The results in figure 4 show that induction time gets longer as the approaching speed of a bubble increases. This was contrary to the intuition that the intervening liquid film between air bubble and particle might drain faster at high approaching speed. However, the results conform to physical insight in that bubble surfaces are deformable. Bubbles are more likely to deform at high moving speed. Therefore, the contact area between air bubble and particle bed is large at high approaching speed of a bubble, and the liquid film should take a long time to drain off. The results also agree with Arbiter and Harris's statement that induction time generally decreases as the relative velocity between bubble and particles become smaller [9].

3.4 Effect of surface tension

Figure 5 shows that induction time decreases with increasing surface tension. The surface tension was controlled by adding a surfactant, MIBC. The results can be understood with the help of the Reynolds equation as well. The thinning rate of liquid film between air bubble and particle is proportional to the pressure difference. In turn, the pressure difference is proportional to surface tension as the Laplace equation suggests. Therefore, thinning rate is faster at higher

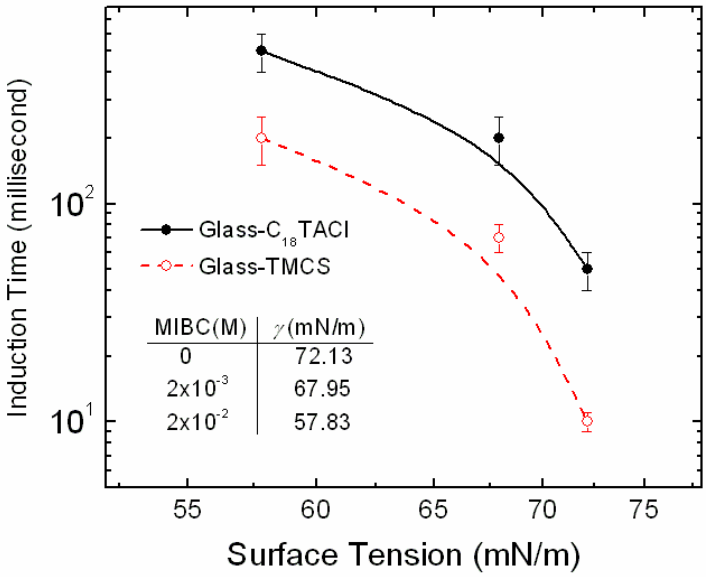

Figure.5. Effect of surface tension on induction time

surface tension. Finch and Smith [22] measured the time-dependent surface tension and observed similar results that particles attach better at higher surface tensions.

Nevertheless, the results are contrary to the prediction made in Chapter 2 that high surface tension deteriorates flotation performance. The discrepancy is because the flotation model developed in Chapter 2 considered the interdependency between bubble size and surface tension, while in the present experiment surface tension was controlled independently.

3.5 Effect of electrolyte concentration

Figures 6 and 7 show the change of induction time with the increase of NaCl concentration. Higher electrolyte concentration has an effect of compressing electrical double layers, which should diminish the repulsion force between bubble and particles. In that case, the induction time has to get shorter with higher NaCl concentrations. Figure 6 shows this effect for relatively low contact angles of particles (less than 50 degrees) hydrophobized in the glass-TMCS system. On the other hand, for relatively higher contact angles (above 50 degrees), it shows the opposite. This indicates that the change in hydrophobic force due to electrolyte concentration change is more dominant than the other effect, *i.e.*, double-layer compression. This agrees with the observation in other literature that hydrophobic force decreases significantly with increasing NaCl concentrations [17, 23].

For the case of glass-C_{18}TACl system, the results indicate this conclusion more clearly, as shown in figure 7. The samples were hydrophobized in $5x10^{-6}$ M C_{18}TACl, which yielded the contact angle above 60 degrees. In the plot, each line represents two different particle sizes and the results are in very different time scales. While particles attached in the timescale of milliseconds,

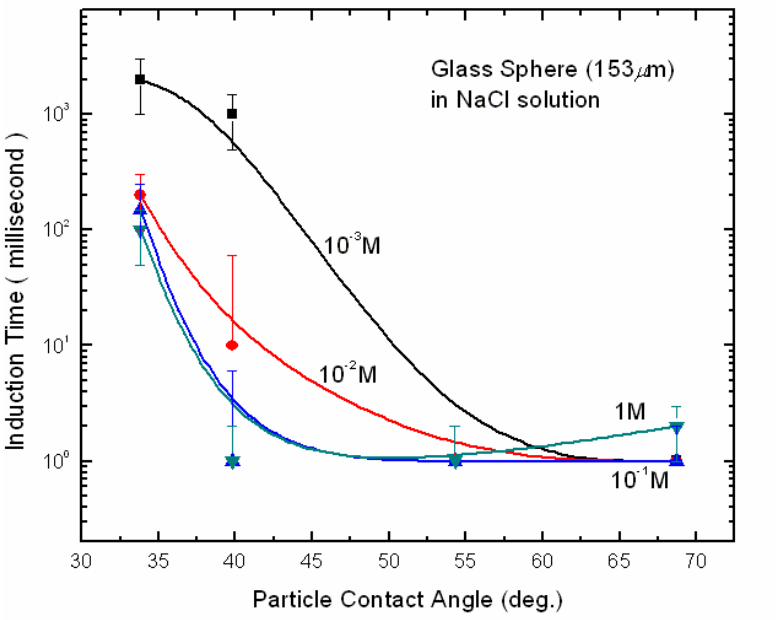

Figure. 6. The change of induction time with NaCl concentration for particles of various contact angles.

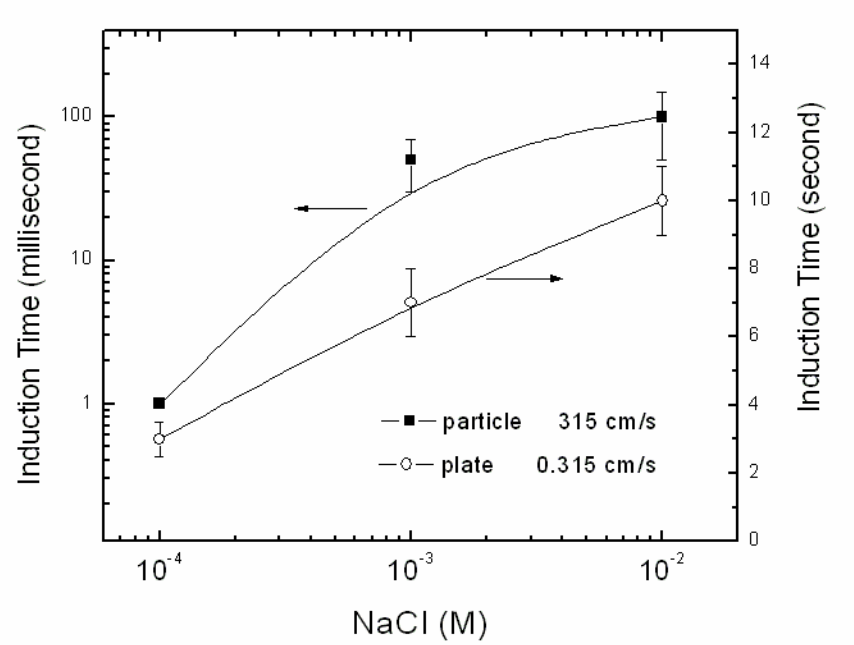

Figure.7. Effect of electrolyte concentration on induction time for glass particles (■) and glass plate (○). Moving speed of bubbles for each case was 315cm/s and 0.315 cm/s, respectively.

plates did in seconds. This result agrees with the recent observation in the same condition that putting more electrolyte in the solution reduces hydrophobic force [17], hence longer induction time.

3.6 Effect of temperature

The temperature effect on induction time is shown in Figure 8. The samples of glass-C_{18}TACl system were 500 μm in diameter and hydrophobized in the solution of 10^{-5}M C_{18}TACl. The bubbles moved at 315 cm/s. On the other hand, the samples of glass-TMCS sytem were 203 μm in diameter, and immersed in 10^{-3} M KCl solution during the measurement. Bubble moving speed was 315cm/s and the particles were hydrophobized by 10^{-4} M TMCS solution.

As shown in figure 8, induction time decreases as temperature increases. This result can be interpreted in several different aspects. For example, unless the results are attributed to surface forces present between bubble and particles, they may be due to surface tension and viscosity changes with temperature. However, for the temperature range of this experiment (10~40 ^{o}C), surface tension of pure water decreases only by 6.2% while viscosity decreases by 50%. Therefore, the induction time change of this experiment can be attributed partly to the decrease of viscosity, while the surface tension effect regarding the temperature change is minimal. The Reynolds equation also helps understanding this interpretation in that the film intervening bubble and particle thins in an inverse proportion to viscosity.

On the other hand, if the surface forces are responsible, the result can be interpreted by the aspect of the critical rupture thickness. Critical rupture thickness is defined as the thickness at which thin liquid film breaks down and the two surfaces separated by the film make a contact. There are several models for critical rupture thickness [24-26], and they assume there is instability at the air-water interface due to interfacial forces. The rupture model by Ivanov and Dimitrov [24] describes this thickness as proportional to the square root of the absolute temperature if all other properties are set equal. At higher temperature, the critical thickness is higher and accordingly induction time is shorter because particles attach to bubble at earlier stage.

4. Discussion

In the flotation model developed by Do and Yoon [18-20], the activation energy of bubble-particle attachment was the key parameter in determining floatability. The activation energy was estimated by the extended DLVO theory that describes the combined effect of the interfacial energies due to van der Waals-dispersion force, the double-layer force, and the hydrophobic force. In other words,

$$V = V_E + V_D + V_H \tag{1}$$

where V is the free energy of interaction between bubble and particle, V_E the electrostatic interaction energy, V_D the van der Waals-dispersion interaction energy, and V_H is the hydrophobic interaction energy.

The electrostatic interaction energy (V_E) between a particle of radius r_1 and a bubble of radius r_2 can be calculated using the model derived by Hogg, Healey and Fuerstenau [27]

$$V_E = \frac{\pi\epsilon_0\epsilon r_1 r_2(\Psi_1^2+\Psi_2^2)}{(r_1+r_2)}\left[\frac{\Psi_1^2\Psi_2^2}{\Psi_1^2+\Psi_2^2}\ln\left(\frac{1+e^{-\kappa H}}{1-e^{-\kappa H}}\right)+\ln(1+e^{-2\kappa H})\right] \tag{2}$$

where ϵ_0 is the permittivity in vacuum, ϵ the dielectric constant of the medium, Ψ_1 and Ψ_2 are the double layer potentials for particle and bubble, respectively, κ the inverse Debye length, and H is the closest separation distance between particle and bubble. As an approximation, Ψ_1 and Ψ_2 may be substituted by ζ–potentials.

The dispersion interaction energy can be calculated using the following relation [28],

$$V_D = -\frac{A_{132}r_1r_2}{6H(r_1+r_2)}\left[1-\frac{1+2bl}{1+bc/H}\right] \tag{3}$$

where A_{132} is the Hamaker constant for the interaction between particle **1** and bubble **2** in a medium **3**. The second term of Eq. (3) is a correction factor for the retardation effect, where b (=3x10^{-17} s for most materials) is a parameter characterizing materials of interacting particles, l (=3.3x10^{15} s^{-1} for water) is a parameter characterizing the medium, and c is the speed of light [29].

The hydrophobic interaction energy (V_H) between bubble and particle may be calculated using the following equation [29]

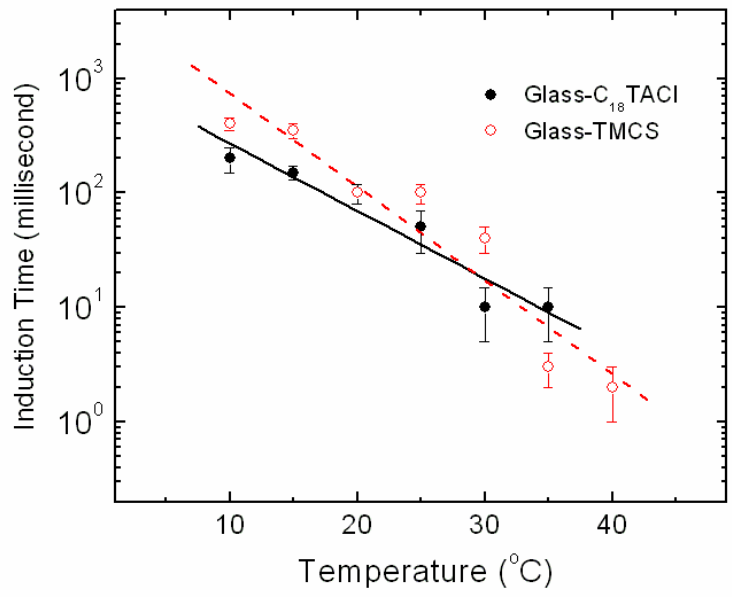

Figure.8. Effect of temperature on induction time

$$V_H = -\frac{r_1 r_2 K_{132}}{6(r_1+r_2)H} \quad (4)$$

where K_{132} is the hydrophobic force constant with the subscript 132 meaning the same as A_{132}.

Although the theory was used in Do and Yoon [18-20]'s the flotation model, it has not been validated yet. The validation may be possible in the following sense.

It has been shown in other literature that the activation energy can be obtained by analyzing the experimental data of induction time change with temperature, which may be described by an Arrhenius type equation as follows [1, 11].

$$t = t_0 \exp\left(\frac{E_1}{k_b T}\right) \quad (5)$$

where t is the induction time, t_0 a constant, k_b the Boltzmann's constant, and T is the absolute temperature of the solution. Manipulating Eq.(5), it is found that the slope of the log t *vs.* T^{-1} plot corresponds to E_1/k_b. The data obtained with glass-TMCS system in figure 8 was rearranged in this way. Then the log t vs. T^{-1} plot yielded E_1=2.99×10^{-17} J at 25°C. This value represents the experimentally obtained activation energy, which can be compared with the calculated value of E_1 to validate the extended DLVO theory.

Figure 9 shows the potential energy vs. distance curve described by the extended DLVO theory, using input parameters as follows: r_1 = 100 μm, r_2 = 1 mm, ζ_1 = -60 mV [30], ζ_2 = -15 mV [31], and K_{132} = 2.3×10^{-19} J. The hydrophobic force constant (K_{132}) was obtained using the

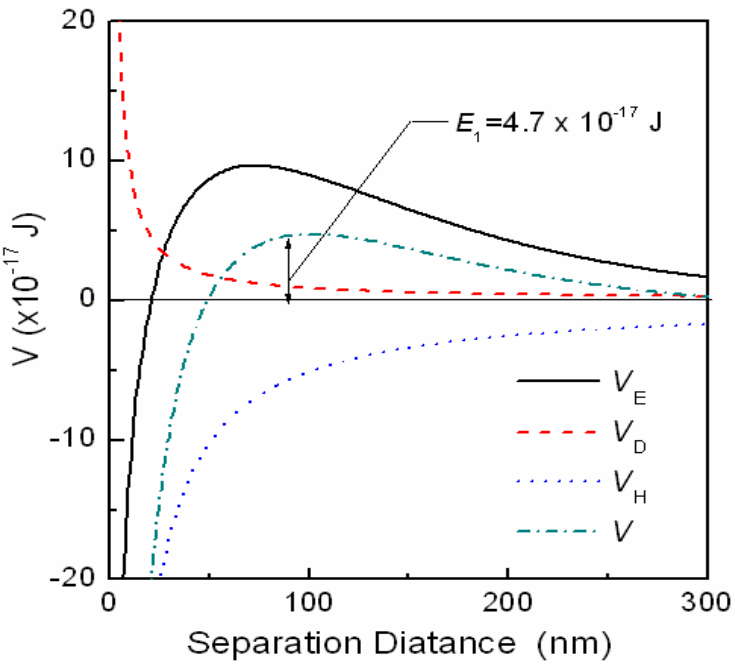

Figure. 9. The potential energy curves showing the extended DLVO theory in the corresponding samples of glass-TMCS system in Figure 8. The parameters used in the theoretical predictions were as follows: Ψ_1= -60 mV, Ψ_1= -15mV, A_{132}= -7.08 x10^{-20} J, K_{132}= 2.3x10^{-19}J, r_1=0.1mm, r_2=1 mm.

combining rule proposed by Yoon *et al*. [32]. The value of the bubble zeta-potential (ζ_2) used for the curve was somewhat lower than those (-30 to -15 mV) reported in the literature [14, 29, 33]. The lowest limit of -15 mV was chosen in view of the relatively large bubble size (2 mm) used in the induction time measurements. It has been shown that bubble zeta-potentials decrease considerably with increasing bubble size [31].

In figure 9, the curve shows the maximum potential energy, the activation energy, of 4.7×10^{-17} J. This agrees well with the one experimentally obtained (= 2.99 ×10^{-17} J). Therefore, this agreement between the two justifies the extended DLVO theory used in the flotation model by Do and Yoon.

5. Summary and conclusions

Induction times of glass-TMCS and glass-C_{18}TACl systems have been measured using an apparatus that simulates the single-bubble flotation. Some measurements were conducted to see the effect of physical parameters on induction time. As a result, it was found that induction time increases when particle or bubble sizes are large, and also when the approaching speed of bubble is high. Induction time measurements were also conducted under different chemical conditions in terms of surface tension and electrolyte concentration. The results showed that induction time decreases as surface tension increases, while the effects of electrolyte concentration varied

depending on the hydrphobicity of particles. Finally, it was also shown that the activation energy of the bubble-particle attachment can be assessed by analyzing the induction time change with temperature. The value of activation energy obtained from the data analysis agreed well with the value predicted by the extended DLVO theory. This agreement suggests that that hydrophobic force is the driving force for bubble-particle attachment, and that asymmetric hydrophobic force can be predicted using the geometric mean combining rule.

6. References

1. Yoon, R.-H. and J.L. Yordan, *Induction time measurements for the quartz--amine flotation system.* Journal of Colloid and Interface Science, 1991. **141**(2): p. 374-383.
2. Sven-Nilsson, I., *Einfluß der Berührungszeit zwischen Mineral und Luftblase bei der Flotation.* Colloid & Polymer Science, 1934. **69**(2): p. 230-232.
3. Wang, W., et al., *An induction time model for the attachment of an air bubble to a hydrophobic sphere in aqueous solutions.* International Journal of Mineral Processing, 2005. **75**(1-2): p. 69-82.
4. Eigeles, M.A., *Selective flotation and the effect of flotation reagents on it*. 1950, Moscow: Science Press.
5. Glembotsky, V.A., *The time of attachment of air bubble to minerals in flotation and ints measurement.* Izv, Akad, Naukk USSR, Otd. Teh. Nauk., 1953. **11**: p. 1524-1531.
6. Evans, L.F., *Bubble-mineral attachment in flotation.* Ind. Eng. Chem., 1954. **46**: p. 2420-2431.
7. Leja, J., *Surface chemistry in froth flotation*. 1982, New York: Plenum press.
8. Nguyen, A.V., H.J. Schulze, and J. Ralston, *Elementary steps in particle--bubble attachment.* International Journal of Mineral Processing, 1997. **51**(1-4): p. 183-195.
9. Arbiter, N. and C.C. Harris, *Flotation kinetics*, in *Froth Flotation 50th Anniversary Volume*, D.W. Fuerstenau, Editor. 1962, AIME. p. 215-246.
10. Ye, Y., S.M. Khandrika, and J.D. Miller, *Induction-time measurements at a particle bed.* International Journal of Mineral Processing, 1989. **25**(3-4): p. 221-240.
11. Eigeles, M.A. and M.L. Volova. *Kinetic investigation of effect of contact time, temperature and surface condition on the adhesion of bubble to mineral surfaces*. in *5th International Mineral Processing Congress*. 1960. London: Inst. Min. Metall.
12. Gu, G., et al., *Effects of physical environment on induction time of air-bitumen attachment.* International Journal of Mineral Processing, 2003. **69**(1-4): p. 235-250.
13. Hewitt, D., D. Fornasiero, and J. Ralston, *Bubble-particle attachment.* Journal of Chemical Society, Faraday Transactions, 1995. **91**: p. 1997-2001.
14. Blake, P. and J. Ralston, *Controlled methylation of quartz particles.* Colloids and Surfaces, 1985. **15**: p. 101-118.
15. Xu, Z. and R.-H. Yoon, *The role of hydrophobia interactions in coagulation.* Journal of Colloid and Interface Science, 1989. **132**(2): p. 532-541.
16. Mao, L. and R.-H. Yoon, *Predicting flotation rates using a rate equation derived from first principles.* International Journal of Mineral Processing, 1997. **51**(1-4): p. 171-181.
17. Zhang, J., et al., *Effects of Degassing and Ionic Strength on AFM Force Measurements in Octadecyltrimethylammonium Chloride Solutions.* Langmuir, 2005. **21**(13): p. 5831-5841.

18. Do, H., *Development of a turbulent flotation model from first principles*, in *Engineering Science and Mechanics*. 2010, Virginia Polytechnic Institute and State University: Blacksburg.
19. Do, H. and R.H. Yoon, *A flotation model under turbulent flow conditions.* Journal of Colloid and Interface Science, 2010. **submitted**.
20. Do, H. and R.H. Yoon, *A turbulent flotation model derived from first principles*, in *23rd International Mineral Processing Congress*. 2006: Istanbul, Turkey.
21. Pan, L. and R.H. Yoon, *Hydrophobic forces in wetting films of water formed on Xanthate-coated gold surfaces.* Faraday discussion, 2010. **146**: p. xxx-xxx.
22. Finch, J.A. and G.W. Smith, *Bubble-solid attachment as a function of bubble surface tension.* Canadian Metallurgical Quarterly, 1975. **14**(1): p. 47-51.
23. Wang, J. and R.H. Yoon. *Surface forces measured between Xanthate-coated gold surfaces*. in *ECS meeting*. 2010. Vancouber, Canada.
24. Ivanov, I.B. and D.S. Dimitrov, *Hydrodynamics of thin liquid films.* Colloid & Polymer Science, 1974. **252**(11): p. 982-990.
25. Ruckenstein, E. and R.K. Jain, *Spontaneous rupture of thin liquid films.* Journal of Chemical Society, Faraday Transactions 2, 1974. **70**: p. 132-147.
26. Vrij, A. and J.T.G. Overbeek, *Rupture of thin liquid films due to spontaneous fluctuations in thickness.* Journal of the American Chemical Society, 1968. **90**(12): p. 3074-3078.
27. Hogg, R., T.W. Healy, and D.W. Fuerstenau, *Mutual coagulation of colloidal dispersions.* Transactions of Faraday Society, 1966. **62**: p. 1638-1651.
28. Rabinovich, Y.I. and N.V. Churaev, *Effect of electromagnetic delay on the forces of molecular attraction.* Kolloidnyi Zhurnal, 1979. **41**(3): p. 468-474.
29. Yoon, R.-H. and L. Mao, *Application of Extended DLVO Theory, IV: Derivation of Flotation Rate Equation from First Principles.* Journal of Colloid and Interface Science, 1996. **181**(2): p. 613-626.
30. Ducker, W.A., Z. Xu, and J.N. Israelachvili, *Measurements of Hydrophobic and DLVO Forces in Bubble-Surface Interactions in Aqueous Solutions.* Langmuir, 1994. **10**(9): p. 3279-3289.
31. Usui, S., H. Sasaki, and H. Matsukawa, *The dependence of zeta potential on bubble size as determined by the dorn effect.* Journal of Colloid and Interface Science, 1981. **81**(1): p. 80-84.
32. Yoon, R.-H., D.H. Flinn, and Y.I. Rabinovich, *Hydrophobic Interactions between Dissimilar Surfaces.* Journal of Colloid and Interface Science, 1997. **185**(2): p. 363-370.
33. Xu, Z. and R.-H. Yoon, *A study of hydrophobic coagulation.* Journal of Colloid and Interface Science, 1990. **134**(2): p. 427-434.

CHAPTER 4

DEVELOPING A DRAINAGE MODEL IN FOAMS INCORPORATING HYDROPHOBIC FORCE

Abstract

A foam drainage model that can predict bubble coarsening has been derived by considering that drainage rate increases with increasing the hydrophobic force. Hydrophobic force is the force that attracts two surfaces of air bubbles and reduces the interstitial liquid amount to a critical value for bubble coalescence. Therefore, hydrophobic force should be considered in the modeling of foam drainage, but no model in the literature addresses its significance. In the present report, however, the flow rates with and without hydrophobic force considerations have been compared to derive the relation between the flow increase and hydrophobic force. As a result, it was found that the average flow velocity increases by the relative significance of the hydrophobic force to Van der Waals force. The change of the number of bubbles due to coalescence was coupled to the drainage model by assuming that the number decreases exponentially with the local changes of liquid fraction.

1. Introduction

1.1 Foam Drainage Equation

Foam is a colloidal system where gas bubbles are separated by thin liquid films. It has a wide range of applications such as food processing, sanitary systems, chemical reactors, froth flotation and so forth. Despite a wide applicability, the mechanisms for controlling foam stability are not fully understood due to complexities involved. A theoretical model is required to understand spatial and temporal kinematics of gas-liquid distributions and to describe the instability, which would be of great advantage to some industrial applications. For example, mining industries will benefit especially from such advancement because the properties of foam are critical controlling parameters that determine the rate of froth flotation, the industry's most important separation process.

The fluid in a foam flows through the network of channels, known as *plateau borders* (PB), which serves as the predominant channels of fluid flow. The PBs are randomly oriented and inter-connected through nodes where the segments of PBs meet. The bubble films osculated to the PBs are called the *lamellae*, but they are not considered to play important role in most of drainage models developed to date. It is assumed that channel (or PB) flow is dominant [1-4].

The flow through the channels is described by the continuity equation,

$$\frac{\partial \varepsilon}{\partial t} + \frac{\partial (\varepsilon U)}{\partial x} = 0 \quad , \tag{1}$$

where ε is the local liquid fraction defined as the ratio of area occupied by liquid to total cross-sectional area, U is the average velocity of flow through PBs, and x is the draining direction. Equation (1) basically states that the rate of change of the liquid mass flow inside a PB is balanced by the changes induced by the flow velocity through the surface area. Typically, U is derived assuming the Poiseuille flow in a pipe, *i.e*. no slip at the interfacial wall [1-6] while some, but not many, derived U assuming plug flow inside PBs [7, 8]. In either case, the assumptions are valid depending on the characteristics of foam. For example, no-slip at the plateau border wall is valid when the foam is made from high concentration surfactant solutions [9]. On the other hand, no-slip boundary condition is not strict valid. Flexible boundary conditions may also be useful, depending on the amounts of liquids held and the chemicals used [10].

Following the definition of ε, Eq.(1) can be expressed in terms of the total number of PBs (N_{PB}) and the average cross-sectional area of a single PB (A).

$$\frac{\partial N_{PB} A}{\partial t} + \frac{\partial (N_{PB} A U)}{\partial x} = 0 \tag{2}$$

In foams, thin fluid film breakage causes bubble coarsening and change in N_{PB}. However, the dynamics of coarsening bubbles has not been fully understood, but it is necessary to

incorporate bubble coarsening in modeling foam drainage. Most of the drainage models developed to date assume that N_{PB} is constant, which has been shown to be the case for dry and stable mono-dispersed foams of polyhedral bubbles. However, foam drainage models developed without considering dynamics of coarsening are not useful in a sense that drainage rates of industrial foams are much faster than predicted by the models. An attempt has been made recently to relate foam drainage equation with the dynamics of N_{PB} by Cox *et al*.[11]. The authors explained qualitatively how drainage is affected by changing bubble sizes by considering N_{PB} as a random distribution function. Using a similar approach, one can obtains the following equation.

$$\frac{\partial A}{\partial t} + \frac{\partial (AU)}{\partial x} + A\left(\frac{\partial \ln N_{PB}}{\partial t} + U\frac{\partial \ln N_{PB}}{\partial x}\right) = 0 \qquad (3)$$

Using Eq.(3), foam drainage is generalized by taking into account the dynamics of coarsening. Details are discussed in the following sections.

1.2 Film and node contribution in foam drainage

The role of lamellae films in foam drainage has not been fully understood yet, but it is obvious that drainage is generally disturbed due to film drainage and ruptures. Many models of film drainage and film rupture have been introduced [12-14], but none of them can be considered generic or sufficiently verified in experiment. It is partly because so many variables are involved in film dynamics under various conditions, and also because the present understandings are based on many controversial evidences. Because those models mostly consider horizontal films, employing them to foam drainage is inappropriate in that foam films have various orientations. In addition, let alone the film dynamics modeling, incorporating the drainage and rupture inside films with drainage model is another challenge.

Of those few who took this challenge, some succeeded in the modeling, only with boundary conditions that liquids flow from films into PBs [15-17]. However, these conditions may betray the real phenomena according to the observation by Carrier *et al.*[18]. The authors found liquids in vertical films flow across from the upper node to the lower, and left the possibility of liquid flowing through films.

In addition to the interpretation of the film's role in foams, the role of PB nodes is also intriguing. The importance of nodes in foam drainage was first posed by Koehler *et al*. [19] who studied both experimentally [10, 19] and numerically [11, 18]. Koehler *et al*. [19] observed the significant change of the correlation between liquid influx rate and the flow's front wave velocity in foams under certain conditions. The authors then attributed the change to the transition of flow characteristics between the PB-dominated flow and the node-dominated flow. In fact, the latter was devised to explain the unexpected flow enhancement by relaxing the no-slip boundary condition at the plateau border walls.

The two, films and nodes in foam, play significant roles in changing the flow characteristics because films, nodes, and plateau borders dynamically interplay with each other. However, the present work regard films and nodes simply as extra fluid volume, hence, substitute the term N_{PB} with N^* which is newly defined as the *effective* number of PBs comprising film's and node's contribution. Eq.(3) may then be rewritten as follows.

$$\frac{\partial A}{\partial t} + \frac{\partial (AU)}{\partial x} + A\left(\frac{\partial \ln N^*}{\partial t} + U\frac{\partial \ln N^*}{\partial x}\right) = 0 \qquad (4)$$

1.3 Various views on foam drainage

The average draining velocity U in Eq. (4) can be expressed analytically by integrating the axial flow profiles in a single plateau border [3, 20-22], or by an analogy with Darcy's law for flows in porous media [2, 7, 23]. Since Darcy's law does not describe the details of flows but indicates only the effective permeability as the coefficient of the correlation between flow velocity and pressure gradient, *U*'s in the corresponding references are based on the semi-empirical relation for the coefficient of Darcy's equation. The coefficient is hard to obtain analytically since foam permeability interplays with so many variables [24]. As a matter of fact, there is no report that verified the theoretical value of U in an isolated plateau border. The closest may be the work by Pitios *et al.* [25] in which PB channels had to be exaggerated for experimental convenience. On the other hand, some researchers measured flow rates in a volume of foam and later showed the validity of theoretically estimated U [2, 7, 23]. In both cases, it was found that the theoretical value of U is lower than the experimentally obtained value in certain systems.

The discrepancy is explained in several different aspects. One prevalent aspect is that foam's rheological property, i.e., surface viscosity, is responsible for the difference. Surface viscosity was originally postulated by Boussinesq [26] to explain the unexpected retardation in fluid droplet's settling velocity, and it had invoked many researchers for many decades into the controversy over its real identity. In fact, the surface viscosity may be phenomenally identical to the Marangoni effect but simply observed in different aspects, as it was stated in the historical review of interfacial rheology by Edwards *et al* [27]. Under the premise that surface viscosity is a unique physical property of a fluid interface, some models for the average flow velocity introduced a mobility parameter [3, 22, 28] or its inverse, the Boussinesque number [20], to fit the model to the actual experimental data. However, the parameter can be considered an adjustable constant because there is not a good method yet to measure the surface viscosity of practical foams [29]. In addition, the surface viscosity measurement may be erroneous due to the intimate coupling of bulk and interfacial viscous effects [27].

With a more general aspect on the problem, Durand and Langevin [23] analyzed the average flow velocity in a way that the mobility parameter can be related to the interfaces' diffusivity, surfactant solubility, elasticity, and so on. As a result, their drainage model coupled

with the average PB flow velocity conformed to the drainage model of Koehler *et al.* [7] when the parameter was large, and to the model by Verbist *et al*. [1] when the parameter was small. The model, however, did not provide good verification.

For all the different aspects, solving drainage equation in consideration of such various parameters may not be a good approach because it requires too many independent variables to be estimated, as well as precise experimental technique. Therefore, the current work will simplify the problem after ignoring the dynamical change of fluids in films and nodes by lumping them into N^* as seen in Eq.(4). On the other hand, the foam drainage is incorporated with bubble coalescence and the *slip* velocity inside PBs. *Slip* is defined as any situation in dynamics of fluids where the value of tangential component of the velocity appears to be different from that of the solid surface immediately in contact with it [30]. Slip velocity is a controversial topic also, especially in foam.

However, the relationship between the slip and wetting property of interface, the contact angle, is relatively well known even though the origin of slip velocity is ambiguous. According to various experimental data, slip is more apparent in the flows on the surface that induces high contact angle [30]. This observation may be interpreted such that the same relationship exists between slip and the hydrophobicity, because contact angle is commonly regarded as an indicator for the degree of *hydrophobic* force. Hydrophobic force is an attractive interfacial force that is known to enhance the flow between two hydrophobic surfaces immersed in water [31]. The air-water interface is also a hydrophobic surface [32-35], but no good theory on the origin of hydrophobic force is yet to emerge. Nevertheless, the force should be considered in the modeling of foam drainage so that one can have more practical approach. Regarding this, the present work will show that slip is in fact a reasonable way to account the role of hydrophobic force in foam drainage. In conjunction with the hydrophobic force, the change in PB numbers due to coarsening and the slip velocity will be derived in the following as well, so that they can be combined with the drainage model.

2. Model Development

To incorporate the hydrophobic force in foam drainage model, it is first necessary to introduce the disjoining pressure in foams. By definition, disjoining pressure is the difference between the pressure in the bulk of one phase and the pressure at the intervening phase between two surfaces. It is a common concept in colloid science and can be predicted by the DLVO theory [36]. DLVO theory accounts for the total surface interaction energy as the combined effect of well-known surface forces: electrostatic force and Van der Waals dispersion force. However, this theory is not applicable for the thin water films confined between two hydrophobic surfaces as in foams [37, 38]. Therefore, additional attraction force between hydrophobic surfaces needs to be considered. In this regard, the disjoining pressure in a foam film may be given as [38, 39],

$$\Pi = \Pi_E + \Pi_W + \Pi_H \tag{5}$$

where Π_E is the pressure due to electrostatic repulsion force, Π_W is the pressure due to the Van der Waals force, and Π_H is the same due to hydrophobic force. Given H as the separation distance between two surfaces, Π_E is expressed by the following equation for simplicity [40].

$$\Pi_E = \alpha \exp(-\kappa \cdot H), \tag{6}$$

where κ is the inverse Debye length, and α is a constant determined by the system properties.

The disjoining pressure due to Van der Waals force is also given by [40]

$$\Pi_W = -\frac{A_{232}}{6\pi(H)^3}, \tag{7}$$

where A_{232} is the Hamaker constant with the subscript 232 meaning that two air bubbles **2** interact across an aqueous media **3** (water).

It is assumed here that the magnitude of disjoining pressure due to hydrophobic force decays with the separation distance H by the same power law as in Π_W, *i.e.*

$$\Pi_H = -\frac{K_{232}}{6\pi(H)^3}, \tag{8}$$

where K_{232} is the hydrophobic force constant with the subscript meaning the same as in Eq. (7). At present, no one knows the origin of the hydrophobic force. Under this situation, it may be acceptable to represent Π_H in the same form as with Π_W [41].

2.1 Average velocity of flow inside PBs

The model represented by Eq. (4) can be simplified if the average velocity of flow through PBs (U) is expressed in terms of PB area (A). U has been analytically modeled by many investigators [2, 3, 5, 6, 20, 22, 42]. The various models converge to the following fundamental expression,

$$U = \frac{A}{3\varphi\mu}\frac{dP}{dx} \tag{9}$$

where the PB cross sectional area, A, is a variable that changes with the position and time in a foam, μ is viscosity, and φ is a factor determined solely by the cross-sectional shape [43]. For example, the factor is 8π for a circular section, 34.6 for a triangular section [4, 22], and 49.1 for the cross section of PBs [3]. The factor, 1/3, in Eq. (9) used because U is an average of all possible PB orientations [4, 23]. P is the pressure inside PB, and typically it consists of gravitational and capillary forces. In addition, disjoining pressure is also taken into consideration. Thus,

$$P = \rho g x + \frac{\gamma}{r_{PB}} - \Pi \tag{10}$$

where ρ is liquid density, g is gravity, A is the PB cross-sectional area, γ is surface tension, r_{PB} is the radius of curvature of PB. The PB cross-sectional area can be as $A = C^2 r_{PB}^2$, where C is approximately 0.4 for a tricuspid-shaped PB cross-section and r_{PB} is the PB radius Π is the disjoining pressure represented by Eq. (5). Assuming for simplicity that hydrophobic force component is the most dominant term in Π and the unit length of the separation distance between two PB walls is $2r_{PB}$, one obtains,

$$\Pi \approx \beta \frac{K_{232}}{(2r_{PB})^3} \tag{11}$$

where β is the coefficient taking into account the geometry of PB. Differentiating the disjoining pressure with respect to x,

$$-\frac{d\Pi}{dx} = \beta K_{232} \frac{3}{(2r_{PB})^4} \frac{d2r_{PB}}{dx} = \frac{3\beta K_{232} C^{3/2}}{16} \frac{1}{A^2\sqrt{A}} \frac{dA}{dx} \tag{12}$$

Therefore, from Eqs. (9), (10) and (12), the average flow velocity is obtained as follows.

$$U = \frac{1}{3\varphi\mu}\left[\rho g A - \left(\frac{C\gamma}{2} - \frac{3\beta K_{232} C^3}{16A}\right)\sqrt{A}\frac{\partial A}{\partial x}\right] \tag{13}$$

Although Eq. (13) is the correct expression incorporating the effect of hydrophobic force component of disjoining pressure, it is necessary to compare the order of magnitude of each term. Noting that K_{232}/A is typically in the order of 10^{-11}~10^{-12} N/m^2 while γ is in 10^{-3} N/m$_2$, the disjoining pressure term is negligible and Eq. (9) reduces to:

$$U = \frac{1}{3\varphi\mu}\left[\rho g A - \frac{C\gamma}{2}\sqrt{A}\frac{\partial A}{\partial x}\right] \tag{14}$$

A contribution from the surface tension gradient may have to be added to Eq. (10), as authors like Stein and Laven [9] criticized, but it is excluded for this research because there is yet no good analytical formula describing surface tension gradient in foam systems. In fact, Eq.(10) corresponds to the model for U that was derived under no-slip boundary condition without considering the disjoining pressure terms [43, 44]. This may indicate that hydrophobic force or disjoining pressure has no significant effect on the flows through PB channels. However, this conclusion is contrary to the observation that hydrophobized porous media reveal enhanced flow rate [45-47]. Therefore, the discrepancy may be compensated by introducing slip velocity at PB walls.

2.2 Slip velocity on hydrophobic interfaces

Flows in foam PBs are analogous to the one through micro channels of solid walls. The slip velocity in micro channels of solid walls has been well reviewed in other literature, and the

controversy on various possible origins of slip has been numerated [30]. For example, surface roughness is suspected as one of possibilities because rough surfaces produce the regions where gas molecules are trapped, and the regions are regarded responsible for the slip of liquids flowing over the gas layer [30, 48]. In the same context, the slip is also presumed coming from the nanobubbles present near hydrophobic surfaces [30, 49].

On the contrary, if there is no gas trapped between the wall troughs or dissolved in the liquid, surface roughness should suppress the slip because rough surface induces resistance of the fluid at the interface. On the other hand, many experimentalists observed slip on solid surfaces with special treatment even after degassing the liquid [45, 50, 51]. This suggests that the slip may not result from gas layers on the surface, but from special surface treatment. The surface treatment mentioned here indicates controlling the wetting property of the surface. The wetting property is typically estimated by measuring contact angles, which is a criterion for evaluating the degree of hydrophobicity. Therefore, hydrophobicity of the surface seems to have strong correlations with the slip velocity in micro channels. The effect of hydrophobic interaction related to slip phenomena has been reviewed [52].

According to the data on solid surfaces of various contact angles, the average flow velocity in micro channels should be augmented by slip velocities by means of a factor f,

$$f = 1 + \frac{4\lambda}{a} \tag{15}$$

where λ is the slip length and a is the radius of the flow channel [30]. The slip length is defined as the extrapolation of channel radius at which zero fluid velocity is imposed. The value of λ is usually measured from experiments either directly or indirectly, but the ratio λ/a may be approximated once the surface interaction forces in the channel are known.

The factor, f, given by Eq. (15) is applicable to solid hydrophobic surfaces. However, it is assumed that the foam PB walls also follow the same relationship between the hydrophobicity and slip. Given that the contact angle or hydrophobic force parameter of the channel wall is an indicator for slip velocity [30], this assumption is valid because liquid-air interface is highly hydrophobic [32-35]. Based on this assumption, λ/a in Eq. (15) may be estimated as described below.

Suppose a PB in a foam. For simplicity's sake, consider an axis-symmetric Poiseulle flow problem for a circular pipe of radius a as shown in Fig.1. Solving the Navier-Stokes equations with no-slip conditions at the pipe walls, one obtains the velocity profile as follows (profile 1),

$$u_1(R) = -\frac{1}{4\mu}\frac{\partial P_1}{\partial x}(a^2 - R^2) \tag{16}$$

where μ is the viscosity of the fluid, R is the distance from the pipe center in vertical direction, and P_1 is the driving pressure.

One obtains another velocity profile for the case of slip by applying the boundary condition that u is zero at the imaginary position outside the channel perimeter as described in Fig. 1 (profile 2). One can find in this case that

$$u_2(R) = -\frac{1}{4\mu}\frac{\partial P_2}{\partial x}((a+\lambda)^2 - R^2)\ , \tag{17}$$

where λ is again the slip length defined as the fictitious distance outside the surface where the no-slip boundary condition is satisfied.

The heads of the flow profiles, u_1 and u_2, are considered equal because the disjoining pressure in PB channel is considered negligible in deriving Eq. (14). Therefore, the profile of $u_2(R)$ is simply a translation of $u_1(R)$ in x direction by the value u_2 at $R = a$ [53]. On this ground, λ can be approximated by comparing the integrands of the two velocity profiles, *i.e.*,

$$\int_{-a-\lambda}^{a+\lambda} u_2(R)dR - \int_{-a}^{a} u_1(R)\,dR = (\lambda + 2a)u_2(a) \tag{18.1}$$

$$\therefore \lambda = \sqrt[3]{-4 + 4\frac{\partial P_1}{\partial P_2}}\,a \tag{18.2}$$

The driving pressures P_1 and P_2 have the following expressiond considering both the capillary pressure and interfacial forces [21].

$$P_1 = -\frac{\gamma}{r_{PB}} + P_g + \Pi_{\mathrm{W,E,H}} \tag{19.1}$$

$$P_2 = -\frac{\gamma}{r_{PB}} + P_g + \Pi_{\mathrm{W,E}} \tag{19.2}$$

Here, γ is the surface tension, r_{PB} the radius of curvature of PBs, P_g the gas pressure, and Π is the

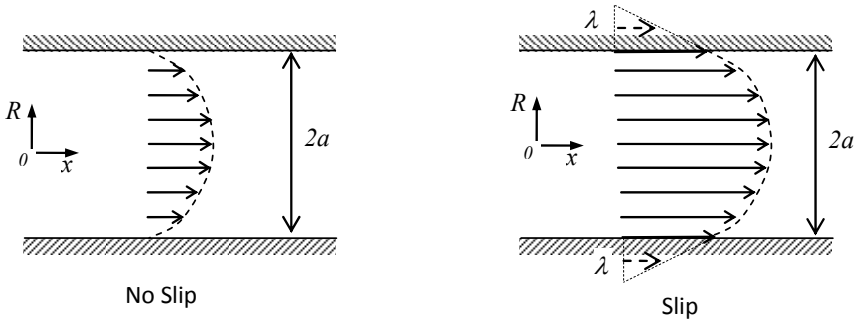

Figure. 1. Poiseulle flow in a cylindrical pipe. Velocity profile 1 with no slip boundary condition (left) and profile 2 with slip (right).

disjoining pressures. Π is th sum of the pressures due to the attractive van der Waals force (W), repulsive electrostatic force (E), and attractive hydrophobic force (H). The van der Waals and hydrophobic components of Π are given as follows:

$$\Pi_{\mathrm{W}} = -\frac{A_{232}}{6\pi(2a)^3} \tag{20}$$

$$\Pi_{\mathrm{H}} = -\frac{K_{232}}{6\pi(2a)^3} \tag{21}$$

The values of A_{232} and K_{232} are easily available in the literature, including those of Wang and Yoon [54-56].

Assuming P_g to be constant, and taking the partial derivatives of P_1 and P_2 with respect to the separation distance $2a$,

$$\frac{\partial P_1}{\partial P_2} = \frac{\partial P_1/\partial 2a}{\partial P_2/\partial 2a} = \frac{\frac{\gamma}{r_{PB}{}^2}\frac{\partial r_{PB}}{\partial 2a} - \kappa\alpha\exp(-\kappa\cdot 2a) + \frac{A_{232}}{2\pi(2a)^4} + \frac{K_{232}}{2\pi(2a)^4}}{\frac{\gamma}{r_{PB}{}^2}\frac{\partial r_{PB}}{\partial 2a} - \kappa\alpha\exp(-\kappa\cdot 2a) + \frac{A_{232}}{18\pi(2a)^4}} \tag{22}$$

Here, the value for $A_{232} = 2.95\times10^{-21}$J is considered to be constant, although there is a degree of variations for different systems [37, 57]. Since the double layer force term and $\partial r_{PB}/\partial 2a$ are negligible, Eq.(22) may be simplified further as,

$$\frac{\partial P_1}{\partial P_2} \approx 1 + \frac{K_{232}}{A_{232}} \tag{23}$$

After substituting Eq. (23) into Eq. (18.2), one finds the ratio between λ and a to be,

$$\frac{\lambda}{a} = \sqrt[3]{\frac{4K_{232}}{A_{232}}} \tag{24}$$

Eq. (24) indicates that PB wall's no slip condition is valid when there is no hydrophobic interaction in PB or much less than the Van der Waals force, and hydrophobic surfaces induce faster drainage due to slip.

2.3 Bubble coalescence in foam

Although the present drainage model represented by Eq.(4) does not show any parameter representing film rupture process, it certainly describes the effect due to flows in lamella films and film rupture by introducing additional term, *i.e.*, effective number of PBs (N*). Knowing that N* is simply a modification of N_{PB}, the relation between N_{PB} and the number of bubbles, N_{B}, should be the first concern. There are no functional relations between N_{B}, and N_{PB}. Nevertheless, it is general known that N_{PB} is proportional to N_{B} by a factor n_{pb}, which is defined as the average number of PBs per a bubble. n_{pb} should actually be a variable for topological properties. For example, n_{pb} = 2 if foam is packed with spherical bubbles, and n_{pb} = 10 for pentagonal

dodecahedra cells [42]. However, in the present model, it is considered to be a constant for simplicity. It will eventually be shown that the value of $n_{pb}$is trivial in the final form of drainage model.

Aside from the argument for actual numbers of N_{PB}, n_{pb}, and N_{B}s, one useful form describing the bubble population change may be the exponential decay in time [58]. On this basis, the following is suggested for predicting N^* in Eq.(4).

$$N^* = n_{pb}^* N_b = n_{pb}^* \times N_{B,0} \exp\left(-C\sqrt{\frac{A_{crit}}{A}}\right) \tag{25}$$

where n_{pb}^* is the effective number of PBs per cell, $N_{B,0}$ is the initial number of bubbles, and the term in the bracket is devised to incorporate the instability of the bubble. Again, n_{pb}^* should end up trivial in the final drainage model. A_{crit}, is the critical PB area, a threshold value for A at which bubbles are more likely to rupture due to instability. C is an adjustable parameter. Although arbitrary value is given in the present report, A_{crit} may be determined by chemical characteristics such as surfactant concentration. This will be addressed in the discussion section. By Eq.(25), local values of the average bubble size can be predicted as well, using the resultant liquid holdup profile. Examples will be given in the later sections of this report.

2.4 Foam drainage equation

Substituting Eq.(25) into Eq.(4) and rearranging, the following is obtained.

$$\frac{\partial A}{\partial t} + \frac{1}{1+C\sqrt{\frac{A_{crit}}{A}}}\frac{\partial}{\partial x}(AfU) + \left(\frac{C\sqrt{\frac{A_{crit}}{A}}}{1+C\sqrt{\frac{A_{crit}}{A}}}\right) fU\frac{\partial A}{\partial x} = 0 \tag{26}$$

Eq. (26) can be solved numerically, along with U in Eq. (14). Note that this equation is reduced to the classical foam drainage equation widely cited and reviewed in the literature [1], when there is no-slip at the PB walls (f=1), and bubbles are stable in size (C=0).

It is necessary to non-dimensionalize the governing equations for numerical accuracy and also for obtaining generality in comparing with any data available in various systems. Given $x_0 = \sqrt{0.4\gamma/\rho g}$ and $t_0 = 3\mu_{eff}/\sqrt{0.4\gamma\rho g}$, Eqs.(14) and (26) are nondimensionalized using the following variables.

$$A = \alpha {x_0}^2 \qquad x = \xi x_0 \qquad t = \tau t_0 \qquad u = v(t_0/x_0) \tag{27}$$

Therefore, the final non-dimensional forms of Eqs. (14) and (26) are,

$$\frac{\partial \alpha}{\partial \tau} + \frac{1}{1+C\sqrt{\frac{\alpha_{crit}}{\alpha}}} \frac{\partial}{\partial \xi}(\alpha f v) + \left(\frac{C\sqrt{\frac{\alpha_{crit}}{\alpha}}}{1+C\sqrt{\frac{\alpha_{crit}}{\alpha}}} \right) f v \frac{\partial \alpha}{\partial \xi} = 0 \tag{28.1}$$

$$v = \alpha - \frac{1}{2\sqrt{\alpha}} \frac{\partial \alpha}{\partial \xi} \tag{28.2}$$

3. Simulation Results and Model Verification

The drainage model represented by Eqs. (28.1) and (28.2) was solved numerically using the finite difference method. Figure 2 shows the results of the numerical simulations of free drainage in the proposed model. The model parameters were arbitrarily chosen. Comparing the liquid profiles along the foam column at the drainage time of τ=100, figure 2A shows that hydrophobic force enhances the drainage. The bubble size changes along the foam column corresponding to the liquid drainage are plotted together, as shown in Figure 2B. Therefore, Figure 2 suggests that bubbles grow with lower liquid fraction, as it was intended in the coalescence model in Eq. (25). The conclusion is that larger bubbles induce faster drainage, which is also consitent with experimental observations in other literature [59, 60]. Figure 3 indicates this typical observation more clearly by the simulated plot of the liquid fraction and bubble size change in time. The time at which liquid fraction start diminishing corresponds approximately to the point at which bubble size starts increasing.

In addition to the numerical example, the model simulation is verified with experiment. The wetness of coarsening foam was estimated by measuring the local and temporal changes of

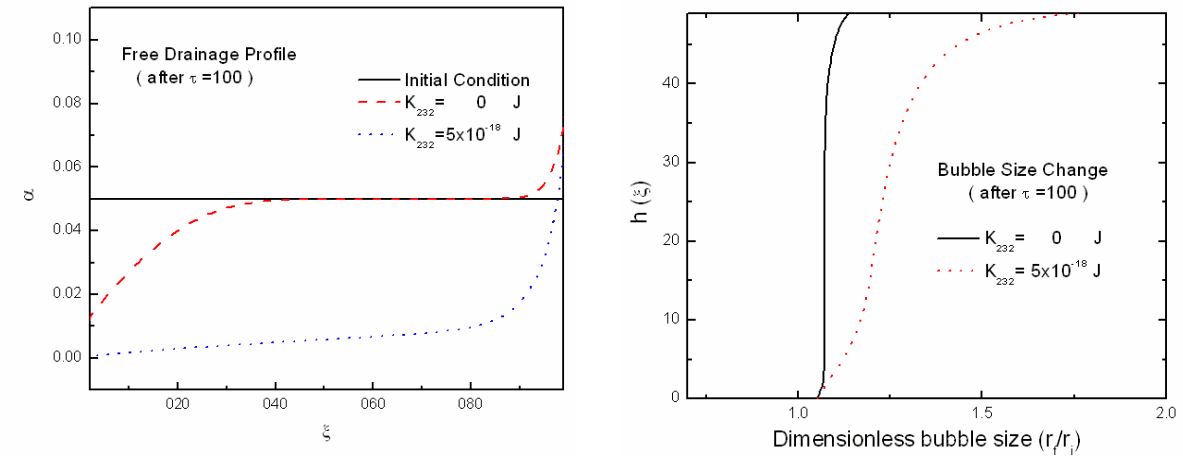

Figure. 2. A) An example of the free drainage profile (left). It indicates that hydrophobic force enhances flow rate. ξ represents the distance from the top of the foam, α represents the amount of liquids held. B) the bubble size change corresponding to the liquid fraction change along the foam column heigh *h* (right). The bubble sizes were normalized by the initial size.

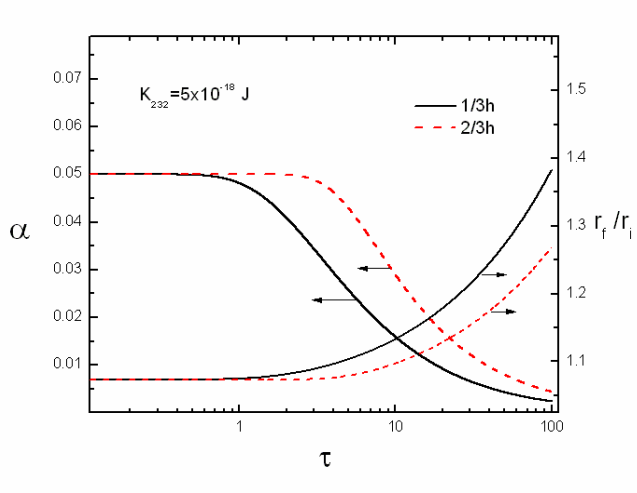

Figure. 3. Liquid fraction and bubble size change in time at the position 1/3 (solid line) and 2/3 (dashed line) of foam height. The time at which liquid fraction α starts diminishing corresponds approximately to the point at which the dimensionless bubble size (r_f/r_i) grows. Input parameters are the same with those used for Fig. 2.

capacitance in a foam column. The details of the methodology are described in the work by Do *et al*. [60]. In the present experiment, foam was made from the solution of 5×10^{-6} M Neodol 23-6.5 (molecular weight =480), allowing significant coarsening but the drainage to occur slow enough. Local changes of bubble sizes representing top, middle, and bottom of foam column were also recorded repeatedly, and averaged.

Figure 4 shows a comparison of the model with the data obtained. Given initial conditions,

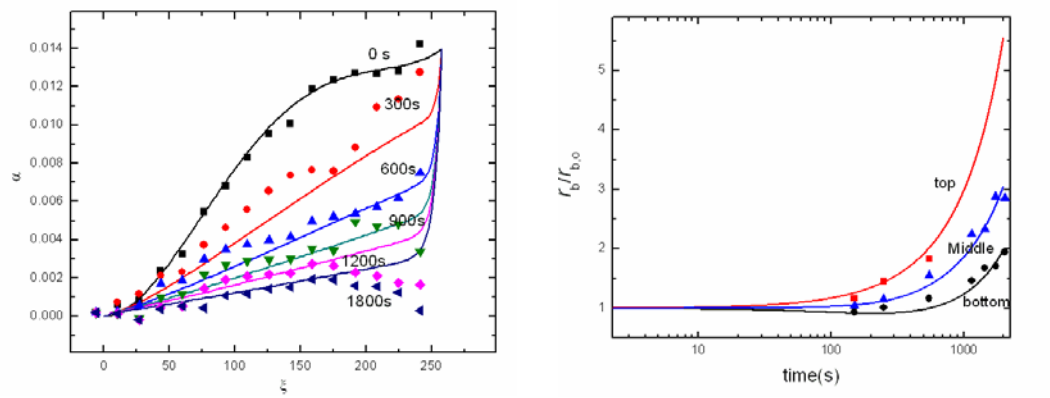

Figure. 4. Free drainage of coarsening foam compared with experimental data. The drainage profile (left), and bubble coarsening (right). The model used the following parameter values: $K_{232}=5\times10^{-19}$J. C=0.4, A_{crit}=0.1

and fitting parameters, i.e., A_{crit}=0.1 and C=0.4, the model predicted the changes in liquid profile as well as the bubble size change, which are in good agreements with experimental results. The results are also consitent with the typical observations that drier foams have higher rate of coarsening, or that large bubbles induce faster drainage [59-61].

4. Discussion

It should be noted again that A_{crit} in Eq.(26) is a parameter used in the present work as a measure of instability of foams at finite liquid fraction. The same concept has been employed for experimental studies [59]. However, critical rupture thickness (h_{cr}) is a more widely used measure for foam instability. Therefore, it may be used to derive a relation between A_{cr} and h_{cr}. The relationship between the film thickness and the radius of curvature of PB for dry, flowing foam was given by Hartland and Barber [62]. Their expression can be modified as follows,

$$\sqrt{A_{cr}} = 2.8\left(\frac{\mu R_s d_{2-max}^2}{\rho g}\right)^{1/4} h_{cr}^{1/4} \tag{29}$$

A and h have been replaced by A_{cr} and h_{cr}, respectively. Other parameters used in Eq. (29) include liquid density (ρ), dynamic viscosity (μ), and gravity (g). Also, R_s is the superficial surface area rate defined as the changes of bubble surface area per time per unit cross-sectional area, and $d_{2\text{-max}}$ is the maximum bubble size. R_s and $d_{2\text{-max}}$ may be considered adjustable parameters to correlate A_{cr} and h_{cr}, because they are not determined by the system properties. Therefore, as shown in this example, converting A_{cr} to h_{cr} does not have a particular advantage in applying to foam drainage equation as it will bring in additional parameters into the model. In fact, A_{cr} may be more convenient to use than h_{cr}, as the latter is useful for horizontal films only. Moreover, h_{cr} is especially difficult to measure if the foam is unstable and its measurement requires sophisticated instrumentation, while A_{cr} can be measured optically.

5. Summary and conclusion

A foam drainage model that can predict bubble coarsening has been developed. The model can be used to predict the changes in bubble size along the foam height. It has been a challenge to couple foam drainage and bubble coarsening. The model requires only two adjustable parameters to fit foam bubble size data, and is based on the premise that hydrophobic force is a significant factor in determining the drainage rate. The relation between hydrophobic force and slip length inside a plateau border has been derived and use to predict the changes in liquid fraction. The model shows the interdependency among hydrophobic force, liquid fraction, and bubble size and predicts that drainage rate becomes faster when bubble size becomes larger. The model predictions are in agreement with the experimental data.

6. References

1. Verbist, G., D. Weaire, and A.M. Kraynik, *The foam drainage equation.* Journal of Physics: Condensed Matter, 1996. **8**(21): p. 3715-3731.
2. Neethling, S.J., H.T. Lee, and J.J. Cilliers, *A foam drainage equation generalized for all liquid contents.* Journal of Physics: Condensed Matter, 2002. **14**(3): p. 331-342.
3. Leonard, R.A. and R. Lemlich, *A study of interstitial liquid flow in foam. Part I. Theoretical model and application to foam fractionation.* AIChE Journal, 1965. **11**(1): p. 18-25.
4. Gol'dfarb, I.I., K.B. Kann, and I.R. Shreiber, *Liquid flow in foams.* Fluid Dynamics, 1988. **23**(2): p. 244-249.
5. Haas, P.A. and H.F. Johnson, *A Model and Experimental Results for Drainage of Solution between Foam Bubbles.* Industrial & Engineering Chemistry Fundamentals, 1967. **6**(2): p. 225-233.
6. Koehler, S.A., et al., *Dynamics of foam drainage.* Physical Review E, 1998. **58**(2): p. 2097.
7. Koehler, S.A., S. Hilgenfeldt, and H.A. Stone, *A Generalized View of Foam Drainage: Experiment and Theory.* Langmuir, 2000. **16**(15): p. 6327-6341.
8. Kann, K.B., *Steady filtration through foam.* Fluid Dynamics, 1986. **21**(3): p. 420-425.
9. Stein, H.N. and J. Laven, *On the Validity of the Foam Drainage Equation.* Journal of Colloid and Interface Science, 2001. **244**(2): p. 436-438.
10. Durand, M., G. Martinoty, and D. Langevin, *Liquid flow through aqueous foams: From the plateau border-dominated regime to the node-dominated regime.* Physical Review E, 1999. **60**(6): p. R6307.
11. Cox, S.J., et al., *Applications and Generalizations of the Foam Drainage Equation.* Proceedings: Mathematical, Physical and Engineering Sciences, 2000. **456**(2002): p. 2441-2464.
12. Vrij, A. and J.T.G. Overbeek, *Rupture of thin liquid films due to spontaneous fluctuations in thickness.* Journal of the American Chemical Society, 1968. **90**(12): p. 3074-3078.
13. Ruckenstein, E. and R.K. Jain, *Spontaneous rupture of thin liquid films.* Journal of Chemical Society, Faraday Transactions 2, 1974. **70**: p. 132-147.
14. Ivanov, I.B. and D.S. Dimitrov, *Hydrodynamics of thin liquid films.* Colloid & Polymer Science, 1974. **252**(11): p. 982-990.
15. Desai, D. and R. Kumar, *Liquid holdup in semi-batch cellular foams.* Chemical Engineering Science, 1983. **38**(9): p. 1525-1534.
16. Bhakta, A. and E. Ruckenstein, *Decay of standing foams: drainage, coalescence and collapse.* Advances in Colloid and Interface Science, 1997. **70**: p. 1-124.
17. Ramani, M.V., R. Kumar, and K.S. Gandhi, *A model for static foam drainage.* Chemical Engineering Communications, 1993. **48**(3): p. 455-465.
18. Carrier, V., S. Destouesse, and A. Colin, *Foam drainage: A film contribution?* Physical Review E, 2002. **65**(6): p. 061404.
19. Koehler, S.A., S. Hilgenfeldt, and H.A. Stone, *Liquid Flow through Aqueous Foams: The Node-Dominated Foam Drainage Equation.* Physical Review Letters, 1999. **82**(21): p. 4232.
20. Nguyen, A.V., *Liquid Drainage in Single Plateau Borders of Foam.* Journal of Colloid and Interface Science, 2002. **249**(1): p. 194-199.
21. Bhakta, A. and E. Ruckenstein, *Drainage of a Standing Foam.* Langmuir, 1995. **11**(5): p. 1486-1492.

22. Desai, D. and R. Kumar, *Flow through a plateau border of cellular foam.* Chemical Engineering Science, 1982. **37**(9): p. 1361-1370.
23. Durand, M. and D. Langevin, *Physicochemical approach to the theory of foam drainage.* The European Physical Journal E: Soft Matter and Biological Physics, 2002. **7**(1): p. 35-44.
24. Stone, H.A., et al., *Perspectives on foam drainage and the influence of interfacial rheology.* Journal of Physics: Condensed Matter, 2003. **15**(1): p. S283-S290.
25. Pitois, O., C. Fritz, and M. Vignes-Adler, *Liquid drainage through aqueous foam: study of the flow on the bubble scale.* Journal of Colloid and Interface Science, 2005. **282**(2): p. 458-465.
26. Boussinesq, M.J., *Sur l'existance d'une viscosite' superficielle, dans la mince couche de transition separant un liquide d'une autre fluide contigu. .* Ann. Chim. Phys., 1913. **29**: p. 349-357.
27. Edwards, D.A., M.P. Brenner, and D.T. Wasan, *Interfacial transport process and rheology*. Butterworth-Heinemann series in chemical engineering. 1991.
28. Koehler, S.A., S. Hilgenfeldt, and H.A. Stone, *Foam drainage on the microscale: I. Modeling flow through single Plateau borders.* Journal of Colloid and Interface Science, 2004. **276**(2): p. 420-438.
29. Stevenson, P., *Dimensional analysis of foam drainage.* Chemical Engineering Science, 2006. **61**(14): p. 4503-4510.
30. Lauga, E., M.P. Brenner, and H.A. Stone, *Microfluidics: The No-Slip Boundary Condition*, in *Handbook of experimental fluid dynamics*, C. Tropea, A. Yarin, and J.F. Foss, Editors. 2007, Springer: New-York. p. 1219-1240.
31. Israelachvili, J. and R. Pashley, *The hydrophobic interaction is long range, decaying exponentially with distance.* Nature, 1982. **300**(5890): p. 341-342.
32. Craig, V.S.J., B.W. Ninham, and R.M. Pashley, *The effect of electrolytes on bubble coalescence in water.* The Journal of Physical Chemistry, 1993. **97**(39): p. 10192-10197.
33. Deschenes, L.A., et al., *Inhibition of Bubble Coalescence in Aqueous Solutions. 1. Electrolytes.* The Journal of Physical Chemistry B, 1998. **102**(26): p. 5115-5119.
34. Du, Q., E. Freysz, and Y.R. Shen, *Surface Vibrational Spectroscopic Studies of Hydrogen Bonding and Hydrophobicity.* Science, 1994. **264**(5160): p. 826-828.
35. van Oss, C.J., R.F. Giese, and A. Docoslis, *Hyperhydrophobicity of the Water-Air Interface*, in *Journal of Dispersion Science & Technology*. 2005, Taylor & Francis Ltd. p. 585-590.
36. Derjaguin, B.V. and S.S. Dukhin, *Theory of flotation of small and medium-size particles.* Transactions of Institutions of Mining and Metallurgy, 1961. **70**: p. 221-246.
37. Wang, L. and R.-H. Yoon, *Role of hydrophobic force in the thinning of foam films containing a nonionic surfactant.* Colloids and Surfaces A: Physicochemical and Engineering Aspects, 2006. **282-283**: p. 84-91.
38. Yoon, R.H. and L. Wang, *Hydrophobic forces in foam films*, in *colloids and interface science series*, Tadros, Editor. 2007, Wiley-VCH. p. 161-186.
39. Yoon, R.H., *The role of hydrodynamic and surface forces in bubble-particle interaction.* International Journal of Mineral Processing, 2000. **58**(1-4): p. 129-143.
40. Yoon, R.-H. and B.S. Aksoy, *Hydrophobic Forces in Thin Water Films Stabilized by Dodecylammonium Chloride.* Journal of Colloid and Interface Science, 1999. **211**(1): p. 1-10.

41. Wang, L., *A Response to the Comment on "Hydrophobic Forces in the Foam Films Stabilized by Sodium Dodecyl Sulfate: Effect of Electrolyte"*. Langmuir, 2008. **24**(9): p. 5194-5196.
42. Narsimhan, G. and E. Ruckenstein, *Structure, drainage and coalescence of foams and concentrated emulsions*, in *Foams: Theory, Measurments, and Applications*, R.K. Prud'homme and K.B. Kann, Editors. 1995, Marcel Dekker: New York.
43. Nguyen, A.V. and H.J. Schulze, *Colloidal Science of Flotation*. Surfactant science series. 2003: CRC Press.
44. Prud'homme, R.K. and S.A. Khan, eds. *Foams: theory, measurement, and applications*. surfactant science series. 1995, Marcel Dekker.
45. Henniker, J.C., *Retardation of flow in narrow capillaries.* Journal of Colloid Science, 1952. **7**(4): p. 443-446.
46. Pfahler, J., et al., *Liquid transport in micron and submicron channels.* Sensors and Actuators A: Physical, 1989. **22**(1-3): p. 431-434.
47. Hasegawa, T., M. Suganuma, and H. Watanabe, *Anomaly of excess pressure drops of the flow through very small orifices.* Physics of Fluids, 1997. **9**(1): p. 1-3.
48. Choi, C.-H. and C.-J. Kim, *Large Slip of Aqueous Liquid Flow over a Nanoengineered Superhydrophobic Surface.* Physical Review Letters, 2006. **96**(6): p. 066001.
49. Tretheway, D.C. and C.D. Meinhart, *A generating mechanism for apparent fluid slip in hydrophobic microchannels.* Physics of Fluids, 2004. **16**(5): p. 1509-1515.
50. HUANG, P., J.S. GUASTO, and K.S. BREUER, *Direct measurement of slip velocities using three-dimensional total internal reflection velocimetry.* Journal of Fluid Mechanics, 2006. **566**(-1): p. 447-464.
51. Huang, P. and K.S. Breuer, *Direct measurement of slip length in electrolyte solutions.* Physics of Fluids, 2007. **19**(2): p. 028104-3.
52. Meyer, E.E., K.J. Rosenberg, and J. Israelachvili, *Recent progress in understanding hydrophobic interactions.* Proceedings of the National Academy of Sciences, 2006. **103**(43): p. 15739-15746.
53. Tabeling, P., *Introduction to microfluidics*. 2005: Oxford university press.
54. Wang, L. and R.-H. Yoon, *Hydrophobic Forces in the Foam Films Stabilized by Sodium Dodecyl Sulfate:??Effect of Electrolyte.* Langmuir, 2004. **20**(26): p. 11457-11464.
55. Wang, L. and R.-H. Yoon, *Hydrophobic forces in thin aqueous films and their role in film thinning.* Colloids and Surfaces A: Physicochemical and Engineering Aspects, 2005. **263**(1-3): p. 267-274.
56. Wang, L. and R.-H. Yoon, *Effects of surface forces and film elasticity on foam stability.* International Journal of Mineral Processing, 2008. **85**(4): p. 101-110.
57. Israelachvili, J.N., *Intermolecular & surface forces*. 2nd ed. 1992: Academic press.
58. Szekrenyesy, T., K. Liktor, and N. S?dor, *Characterization of foam stability by the use of foam models 1. Models and derived lifetimes.* Colloids and Surfaces, 1992. **68**(4): p. 267-273.
59. Carrier, V. and A. Colin, *Coalescence in Draining Foams.* Langmuir, 2003. **19**(11): p. 4535-4538.
60. Do, H., et al., *Coarsening foam- Numerical modeling and experimental results*, in *Flotation 07 symposium*. 2007: Cape town, South Africa.
61. Saint-Jalmes, A. and D. Langevin, *Time evolution of aqueous foams: drainage and coarsening.* Journal of Physics: Condensed Matter, 2002. **14**(40): p. 9397-9412.

62. Hartland, S. and A.D. Barber, *A model for a cellular foam.* Trans. Instn Chem. Engrs, 1974. **52**: p. 43-52.
63. Saint-Jalmes, A., Y. Zhang, and D. Langevin, *Quantitative description of foam drainage: Transitions with surface mobility.* The European Physical Journal E: Soft Matter and Biological Physics, 2004. **15**(1): p. 53-60.
64. Saint-Jalmes, A., *Physical chemistry in foam drainage and coarsening.* Soft Matter, 2006. **2**(10): p. 836-849.

CHAPTER 5

PREDICTING THE CRITICAL RUPTURE THICKNESS OF FREE FOAM FILMS

ABSTRACT

A thin film ruptures when a fluid layer gets thinner than a critical thickness. In other literature, this critical thickness has been attempted to predict using the instability criteria for a wavy interface of the film. However, the predictions of those models deviate from experimental observations in the case of aqueous films at low surfactant concentrations. The discrepancy results from the hydrophobic force in the film, but the origin of the force has not been well understood yet. The force can be typically evaluated from film thinning kinetics data. On the other hand, there has been no model yet to incorporate it with the rupture. In this chapter, a model for predicting the critical rupture thickness has been derived by assuming that the hydrophobic force causes the instability of air-water film interfaces. As a result, the model could predict the rupture thickness and the time of rupture in the presence of the hydrophobic force.

1. Introduction

The drainage and rupture in thin liquid films have been of great interest among many researchers because understanding the subject is critical to the productivity improvement in certain industries. For example, the mining industry has been active in studying this subject because liquid film's thinning rate and rupture determine the efficiency of the flotation [1], the most widely practiced mineral separation technique in the industry.

With regard to the thinning of films in such applications, some interests remained only in the physics of film thinning due to the hydrodynamic forces between two approaching bubbles or spheres [2-4]. On the other hand, some researchers studied film thinning in the scale where interfacial forces is as significant as hydrodynamic forces, by incorporating the disjoining pressure to the Reyonolds equation [5, 6]. Disjoining pressure is practically the difference between the pressure in the bulk of liquid film and the pressure at the air-water interface. It is usually negligible in the large scale physical phenomena, but becomes significant in analyzing the colloidal scale problems such as foam films. However, in foam films, this approach was under criticism because the Reynolds equation had been derived originally for tangentially immobile surfaces while foam films may be regarded mobile. Therefore, many researchers relaxed the boundary condition of the Reynolds equation to match the theory and true experimental observations [7-9].

Even though it is still controversial whether foam film surface is mobile or immobile, the present work assumes the immobile boundary of foam films based on experimental evidences. Recently, Valkovska *et al*. [10] showed by a thinning rate model that the effect of disjoining pressure is more significant in film drainage / rupture than the effect of the interfacial mobility. Angaraska *et al*. [11] also checked the effect of surface mobility in small, thin aqueous films experimentally, but found it negligible even with the tiny amount of surfactant.

1.1 Thin film rupture models

The thinning rate of foam films may well be predictable on the premise that the Reynolds equation is valid with or without mobility considerations. On the contrary, predicting when films rupture is still a mystery. In general, film gets unstable as it thins down, but the actual thickness of rupture or the rupture time is hardly predictable because there is no universal criterion. This threshold of thickness at which films tend to break is defined as the critical rupture thickness, H_{cr}. Although the exact mechanisms of this instability are not vindicated so far, many authors [9, 12, 13] followed the criterion to reach H_{cr} suggested by Vrij [5]. Vrij's criterion is based on the idea that films fail when the waves on the air-water interfaces grow substantially, as first posed by Scheludko [14]. After observing scattered light on soap films, Vrij suggested that the reflections were possibly due to irregular corrugations of the film interface [15]. Then a theory for the rupture was made out of this hypothesis [5]. However, in finalizing the model equation for H_{cr},

he introduced an empirical correction factor to make the rupture thickness correspond with specific experimental examples [5, 16]. On the other hand, some authors took more mathematical account for the rupture with the same idea of 'fluctuating interfaces' [17-19]. In theory, their wave evolution was resulting from boundary disturbances, but no practical examples were given except for the numerical simulations based on arbitrary initial conditions.

The wave-induced instability also inspired other notable researchers like Ivanov *et al*. [9, 20]. Their rupture criterion was such that films break when the amplitude of the wave on each faces of the film is tall enough to touch each other. In their approach, the surface mobility was thought to be the most contributing factor to the rupture, but later the leading author had to contradict himself in the work with Valvoska *et al*.[10] by showing that mobility was insignificant. In addition, their own experimental data did not agree well with predictions [9]. In a similar approach, Ruckenstein and Jain [12] put in the derivation an extra potential energy term other than the energy due to Vand der Waals force. This term was regarded as perturbations of the surface potential due to fluctuating nature. In the authors' approach, all aspects such as surface viscosity, diffusion effect, and purity were implied in the model. Having a parameter subject to the surfactant's solubility and concentration, the model became identical with Vrij's model [5] when the concentration was high.

While the rupture criteria for the above-mentioned models were such that the critical thickness equals twice the amplitude of surface wave itself, Sharma and Ruckenstein [13, 21] set slightly different criterion. Assuming that rupture is caused by the relatively small 'thermal' fluctuations riding on the thinnest trough of the 'hydrodynamic' surface waves, the authors found numerically the relationship between film thickness and thermal fluctuation. Then a model was developed based on this relation [21]. The thermal fluctuation was also implemented within the model by Radoev *et al*. [8], who saw the problem as attaining the state of instability due to the Brownian motion on the surface, unlike the else who saw it as the consequence of the instability evolution.

The film rupture models introduced above are hardly universal since each model was verified only numerically or, at best, compared to data of specific conditions where interfacial forces were relatively well-understood. Moreover, for the interesting case of aqueous surfactant films, none of those models are close to practical observations because the films are much more unstable than expected due to an additional attractive force called hydrophobic force [22-25]. Hydrophobic force seems eminent in aqueous films of low surfactant concentrations in particular, and therefore it holds importance in areas like mineral processing where such a low concentration is commonly employed.

1.2 Hydrophobic force in aqueous surfactant films

The drainage rate or rupture of foam films is usually predicted by the Reynolds equation in the literature. However, many researchers had overlooked the existence of the attractive '*hydrophobic*' force in applying the disjoining pressure into the equation. Because the DLVO theory, that is used to calculate the interaction energies of colloidal scale interfaces, has been failing to conform with certain experimental data especially in the examples of hydrophobic surfaces [26], many researchers ascribed the discrepancy to this unveiled force. The force had been first observed between hydrophobic solid surfaces [27], but later, air bubbles forming liquid films were found strongly hydrophobic as well [28-31]. However, hydrophobic force in foam films has been particularly questioned by strong-believers of the DLVO theory [32]. Despite of this controversy, there are more evidences for the flaws of the obsolete theory than the unconvincing evidences of hydrophobic force [33, 34].

In the experiments on foam films by Wang and Yoon [22-25], the authors modified the DLVO theory by introducing the additional disjoining pressure induced by hydrophobic force (Π_H). The pressure term was assumed following the same power-law decay rule as the van der Waals force, such that

$$\Pi_H = -\frac{K_{232}}{6\pi H^3} \tag{1}$$

where K_{232} is the hydrophobic force constant ,and H is the film thickness. It should be noted that subscript 232 was devised for conveniently implying that the force exists in media 3 squeezed between media 2s, *i.e.* in the liquid film held between two air bubbles. Due to lack of complete theory, there is no direct measurement method of K_{232} value yet, but it can be found indirectly by analyzing the foam film thinning kinetics data [22-25]. The assumption that Π_H takes after the disjoining pressure induced by Van der Waals force has several advantages [34]. First, it is easy to compare hydrophobic force with the Van der Waals force, by simply assessing K_{232} and the Hamaker constant. In addition, as simple it is and has fewer variables, the given form in Eq.(1) may simplify the derivation of film rupture model. Therefore, Eq.(1) will be used in describing hydrophobic force in the present film rupture model. Details of model derivation shall be described in the next.

2. Modeling the rupture of thin films

It has been noted in the introduction that the film thinning velocity predicted by the Reynolds equation, V_{Re}, deviates from the practical observations in aqueous surfactant films [22-25]. This finding may be represented by the following relationship [9, 10],

$$V = f^3 V_{Re} \tag{2}$$

where V is the actual film thinning velocity, and f^3 is the coefficient that represents the difference between V and V_{Re}.

Substituting into Eq.(2) the Reynolds equation, one obtains the following.

$$\frac{2H^3}{3\mu R_f^2}\Delta P = f^3\frac{2H_{Re}^3}{3\mu R_{f_{Re}}^2}\Delta P \tag{3}$$

In Eq.(3), H is the film thickness, R_f is the film radius, μ is viscosity, and ΔP is the pressure difference. H and R_f with subscript Re indicate that they are the parameters pertaining to the ideal cases of Reynolds equation assumption: flat film, no-slip at the interface. Therefore, the actual film thickness observed at certain time can be expressed in terms of theoretical prediction after manipulating Eq.(3).

$$H = \left(R_f/R_{f_{Re}}\right)^{2/3} f H_{Re} \tag{4}$$

Based on this relationship, the actual critical rupture thickness H_{cr} may be estimated since all the terms in the right hand side of Eq.(4) at the time of rupture can be evaluated theoretically. In other words:

$$H_{cr} = \left(R_f/R_{f_{Re}}\right)^{2/3} f H_0 \tag{5}$$

where H_0 is the rupture thickness predicted from the film thinning kinetics using the Reynolds equation. In assessing H_0 theoretically, major assumption is that the film interfaces are stable and flat. However, it should be noted that, in the present work, thin liquid films are thought to be unstable due to fluctuations growing at the interfaces, and therefore their interfaces are not flat at least. Accordingly, a proper modification of the prediction theory for H_0 is necessary. This is described in the following section.

2.1 The rupture thickness predicted by the ideal theory

The major assumption in the present derivation of film rupture thickness is the film's fluctuating interfaces. The key idea was originally adopted from other researchers [5, 9, 12, 16], but more practical and statistical accounts are added.

In Figure 1, an example of a thin liquid film of median thickness H_{m} is presented with its corrugated surface profile superposed. For simplicity, the wave is assumed steady and to be represented by the following 2D profile (y).

$$y = \eta\sin\left(\frac{2\pi x}{\lambda}\right) \tag{6}$$

where η is the amplitude of the wave, λ is the wavelength, and x is the propagating direction.

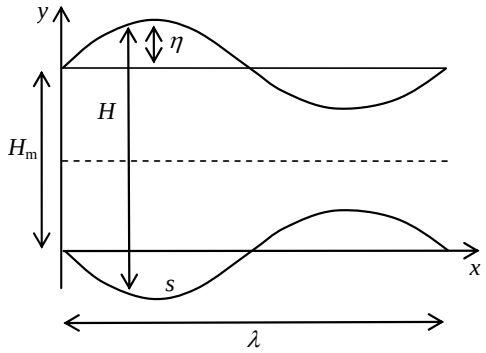

Figure.1. Waves on the film surface. H_m is the mean thickness. η is the amplitude of the wave which has the wavelength of λ.

In their approach of Vrij and Overbeek [16], the critical wavelength λ_c was defined as the representative wavelength at which the film interfaces get critically unstable causing the waves' sudden growth. Then λ_c was derived by equating the total Gibbs energy change (ΔG) to the extra energy induced by the corrugated area and other interaction energy, such that

$$\lambda_c = \sqrt{-2\pi^2\gamma\frac{dH^2}{d^2G}} \tag{7}$$

in which γ is surface tension, H is the gap between film interfaces and G is the total Gibbs energy. Eq.(7) is the wavelength criterion above which the total Gibbs energy becomes negative and fluctuation is more likely to grow [16, 20]. Vrij and Overbeek [16] took only the Van der Waals force into this account and incorporated it with the Reynolds film thinning velocity subject to capillary pressure and the extra, finally obtaining the characteristic time τ as follows where the fluctuation's most rapid growth is expected [16].

$$\tau = 96\pi^2\mu\gamma A_{232}^{-2}H_m^5 \tag{8}$$

Here, A_{232} is the Hamaker constant, again the subscript 232 meaning the same as in K_{232} (see Eq.(1)). Eq.(8) characterizes the time the film stays unstable until it fails. It should be noted here that τ gets shorter as film gets thin, meaning that the film is so unstable when it is critically thin that it can readily break.

Now one may view the total time of film thinning until the rupture as the sum of the stable 'draining' time t_d and n times the characteristic time of 'unstable fluctuating' τ [16]. Then the rate of change in H_m at the time of rupture should be infinite, and equivalently the inverse should be zero. From this, one obtains the following.

$$\frac{dt_d}{dH_m} = -n\frac{d\tau}{dH_m} \tag{9}$$

The inverse of the thinning rate on the left hand side can be substituted by the Reynolds equation with film radius R_f and pressure difference as P_c, the capillary pressure. Manipulating Eqs.(8) and (9), the final expression for H_m at the time of rupture can be derived as the following.

$$H_m = \sqrt[7]{\frac{A_{232}^2 R_f^2}{n320\pi^2\gamma P_c}} \tag{10}$$

In Vrij and Overbeek's work [16], the authors arbitrarily set n =6 based on empirical data. However, it is interesting to note that its effective is in fact comparable to the case when one takes the r.m.s. value of H_m of n=1. Since $\sqrt[7]{6} \approx \sqrt{2}$, their empirically chosen value (n=6) agrees interestingly well with the statistical account. This indicates that H_m without considering n (or with n=1) is the upper limit of the predicted rupture thickness, and H_m with n=6 is the statistical average at the particular state. In addition to this, several authors on the vibrations and waves in liquid films discuss that there are two major modes of film thinning, namely the bending mode and the squeezing mode [35-37]. The bending mode is when the wave profiles on the upper and lower interfaces of film are symmetric each other, while the squeezing mode is anti-symmetric. This may work as an additional aspect to be considered other than taking the root-squared-mean only of H_m. Considering the two modes, one half of the r.m.s value of the upper-limit H_m is the most probable value of mean film thickness, namely H_0. Therefore, one may substitute into Eq.(5) the following expression.

$$H_0 = \frac{1}{2\sqrt{2}} \sqrt[7]{\frac{A_{232}^2 R_f^2}{320\pi^2\gamma P_c}} \tag{11}$$

2.2 The role of hydrophobic force

In the next, one needs to revisit Eq.(1) to find the yet-unknown factor f related to the critical rupture thickness of aqueous surfactant films. It has been derived earlier by the same authors [1] that the increase of flow velocity in a micro channel with hydrophobic walls can be evaluated based on the relative dominance of hydrophobic force over the Van der Waals force *i.e.*, K_{232}/A_{232}. In the derivation, an assumption was made that hydrophobic force is responsible for the slip at the air-water interface [38]. The drainage inside a foam film may have an analogy with this, because the flow resembles the channel flow in 2 dimensional view if the mean film thickness is considered as channel diameter. Therefore, f can be expressed as follows.

$$f = \left(1 + 8\sqrt[3]{4K_{232}/A_{232}}\right)^{1/3} \tag{12}$$

It is assumed in the literature that film radius between two small air drops does not change while thinning [6, 11, 22-25], and at least it is not of any concern for the case of high-concentration surfactant films [7]. However, there may exist any difference between the initial film radius and the resultant radius one really observes, especially when the instability is so virulent. To account for this, the ratio between R_f and $R_{f\,\mathrm{Re}}$ was introduced in Eq.(3).

As shown in Figure 1, suppose that the ratio (R_f / $R_{f\,\mathrm{Re}}$) equals to the ratio of the wave arc length, *s*, to the corresponding wavelength, $\lambda/2$, *i.e.*

$$\frac{R_f}{R_{f_{Re}}} = \frac{s}{\lambda/2} \tag{13}$$

Then the curve length *s* is given the expression:

$$s = \int_0^{\lambda/2} \sqrt{1 + \eta^2 \left(\frac{2\pi}{\lambda}\right)^2 \cos^2\left(\frac{2\pi x}{\lambda}\right)}\, dx \tag{14}$$

Substituting Eq.(14) into Eq.(13), one obtains the following.

$$\frac{R_f}{R_{f_{Re}}} = \frac{1}{\pi}\sqrt{4\pi^2(\eta/\lambda)^2 + 1} \cdot E(\pi|\kappa) \tag{15.1}$$

$$\kappa = \frac{4\pi^2(\eta/\lambda)^2}{4\pi^2(\eta/\lambda)^2+1} \tag{15.2}$$

Here, $E(\phi|\kappa)$ is the incomplete elliptic integral of the second kind defined as [39]

$$E(\phi|\kappa) = \int_0^{\phi} \sqrt{1 - \kappa^2 \sin^2\theta}\, d\theta \tag{16}$$

where the parameter κ is in the range of 0 ~1. To determine κ from Eq.(15.2), the following relationship is required in the evaluation.

$$\frac{\eta}{\lambda} = C_1 \frac{K_{232}}{A_{232}} / C_2 \tag{17}$$

In Eq.(17), C_1 is a constant that varies with surfactant type or the system and C_2 is the reference value of K_{232}/A_{232}. C_2 was found 40~50 from the typical experimental data, and this indicates the consideration of film radius variation is particularly meaningful when the hydrophobic force is 40~50 times or more larger than the Van der Waals force. Assume high concentration of surfactants such that the film interfaces behave like immobile flat surface, *i.e.,* η/λ=0. Then the value for R_f / R_{fRe} = $E(\pi|\,0)$ /π = 1. This is also interesting to note because it indicates the assumption of invariable film radius for high surfactant concentration is valid as cited in many other works [22-25].

2.3 Prediction of critical rupture thickness and coalescence time

From Eqs. (4), (10), (11), and (14), one can derive an expression of critical rupture thickness as follows.

$$H_{cr} = \left(\frac{1}{\pi}\sqrt{4\pi^2(\eta/\lambda)^2 + 1} \cdot E(\pi|\kappa)\right)^{2/3} \left(1 + 8\sqrt[3]{4K_{232}/A_{232}}\right)^{1/3} \frac{1}{2\sqrt{2}} \sqrt[7]{\frac{A_{232}^2 R_f^2}{320\pi^2\gamma P_c}} \tag{18}$$

where the elliptic integral of the second kind E, and the parameter κ was defined in Eqs.(16) and (17), respectively. Eq. (18) reduces to Eq. (11) when K_{232} becomes much smaller that A_{232} or negligibly small.

In addition to the thickness of film rupture, one can also find the film rupture time or bubble coalescence time by integrating the Reynolds equation over the thickness variation. In other words,

$$t_c = -\frac{3\mu R_f^2}{2}\int_{H_i}^{H_{cr}} \frac{1}{H^3 \Delta P}\, dH \tag{19}$$

where H_i is the initial thickness of film. Conducting the integration for the case of high electrolyte solutions, for example, the electrostatic disjoining pressure term is negligible and the coalescence time may be predictable by the following.

$$t_c = \frac{\mu R_f^2}{4\sqrt[3]{P_c}\left(\frac{A_{232}+K_{232}}{6\pi}\right)^{\frac{2}{3}}}\left[2\sqrt{3}\tan^{-1}\left(\frac{1}{\sqrt{3}} - \frac{2}{\sqrt{3}}\sqrt[3]{\frac{6\pi P_c}{A_{232}+K_{232}}}H_i\right) - 2\sqrt{3}\tan^{-1}\left(\frac{1}{\sqrt{3}} - \frac{2}{\sqrt{3}}\sqrt[3]{\frac{6\pi P_c}{A_{232}+K_{232}}}H_{cr}\right) - \log\left(\frac{\sqrt[3]{P_c}H_{cr}+\sqrt[3]{\frac{A_{232}+K_{232}}{6\pi}}}{\sqrt[3]{P_c}H_i+\sqrt[3]{\frac{A_{232}+K_{232}}{6\pi}}}\right) + \log\left(\frac{P_c^{\frac{2}{3}}H_{cr}^2 - \sqrt[3]{P_c\left(\frac{A_{232}+K_{232}}{6\pi}\right)}H_{cr} + \left(\frac{A_{232}+K_{232}}{6\pi}\right)^{\frac{2}{3}}}{P_c^{\frac{2}{3}}H_i^2 - \sqrt[3]{P_c\left(\frac{A_{232}+K_{232}}{6\pi}\right)}H_i + \left(\frac{A_{232}+K_{232}}{6\pi}\right)^{\frac{2}{3}}}\right)\right] \tag{20}$$

3. Model verification

In the following, various experimental works are compared with the critical rupture thickness and coalescence time predicted by the model. The present model incorporated hydrophobic force with the film rupture by introducing the hydrophobic force constant K_{232}. Wang and Yoon [22-25] were the first to implement this idea, and their work may be the only reference where the values of K_{232} for certain foam films can be found directly. However, the value of K_{232} can be assessed also from other references that have film thinning kinetics or coalescence time data. For example, the predicted coalescence time shown in Figure 2 was obtained using the K_{232} values inferred from the data presented by Li [40]. Li suggested an analytical model to predict the coalescence time by studying the dynamics of film thinning in recognition of Van der Waals force and electrostatic double layer force. Then the coalescence time (t_c) model can be simplified as the following [41],

$$t_c = 0.729\left(\frac{k}{A_{232}{}^{0.46}}\right) \tag{20}$$

where A_{232} is the Hamaker constant, and k is a constant determined by the system properties such as viscosity, surface tension, and bubble diameter. The details for estimating constant k is given in Li's work where the information for all necessary parameters is available [40].

Even though it was concluded in Li's work that there was a good agreement between the theoretical calculation of t_c by Eq.(20) and the experimental results, his conclusion seems unconvincing in that the two show discrepancy in the range of 8 to 13 seconds. This range is considerably larger than the coalescence time of bubbles measured in pure water at low surfactant concentrations. Therefore, the data are necessary to be reevaluated by introducing the hydrophobic force. Assuming the coalescence between two bubble drops of equal size, Eq.(20) for this purpose can be rewritten as [41]

$$t_c = 0.729\left(\frac{k}{(A_{232}+K_{232})^{0.46}}\right) \tag{21}$$

where the hydrophobic force constant K_{232} is simply added to A_{232} since surface forces are additive. As a consequence, K_{232} can be back-calculated from the difference in t_c between theory and experiment. First, the values of k are determined following the details presented by Li's model [40]. Then the k values are substituted into Eq.(21) to calculate K_{232} by fitting the values of t_c calculated by Eq.(21) to the experimental data. K_{232} values obtained in this way are presented in Table 1.

The values have been used in the calculation of t_c by the present model (Eq.(19)), and the results are shown in Figure 2. The present model is in much better agreement with data than Li's model is.

While the values of K_{232} had to be back-calculated in the present model, values of K_{232}

Antifoam EA 146 (g/l)	K_{232} (J) BSA 0.0 g/l	BSA 0.2 g/l	BSA 1.0 g/l
1.0×10^{-2}	6.0×10^{-18}	5.0×10^{-18}	5.5×10^{-18}
2.5×10^{-2}	2.2×10^{-18}	5.0×10^{-18}	4.0×10^{-18}
8.0×10^{-2}	1.5×10^{-18}	6.5×10^{-19}	2.9×10^{-19}
1.0×10^{-1}	6.2×10^{-19}	5.0×10^{-19}	3.6×10^{-19}
2.5×10^{-1}	5.3×10^{-19}	4.4×10^{-19}	4.0×10^{-19}

Table 1. K_{232} values obtained from the data presented by Li (1994) for foam films stabilized with Bovine Serum Albumin (BSA) solutions with commercial antifoam EA142 of the polypropylene glycol type.

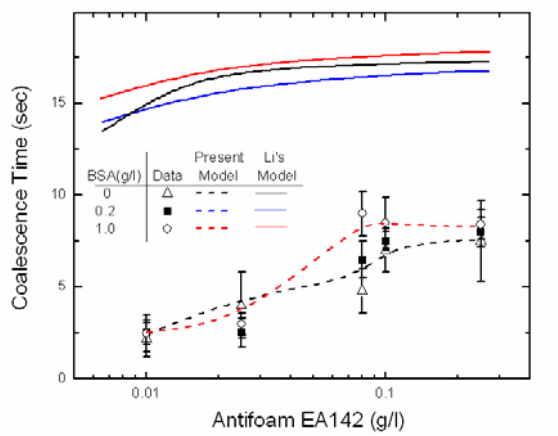

Figure. 2. Coalescence time (t_c) of a foam film made of Bovine Serum Albumin (BSA) solutions with commercial antifoam EA142 of the polypropylene glycol type. Model calculations were conducted using the K_{232} values presented in Table1. Other input parameters were: C_1=1, C_2=40, A_{232} =1×10^{-19} J, H_i=200 nm. The effects of electrostatic forces were ignored because the data were given in the presence of high electrolyte concentration (0.1 M NaCl).

obtained using different methods are also available. Wang and Yoon have reported the values of K_{232} and A_{232} for several surfactant systems [23, 24]. Using their values, the critical rupture thickness and coalescence time of the same system can be predicted by the model developed. The comparisons between the model and the experiment by Wang and Yoon are made in figures 3 and 4. As one can see, the present model is in good agreement with experimental data, even

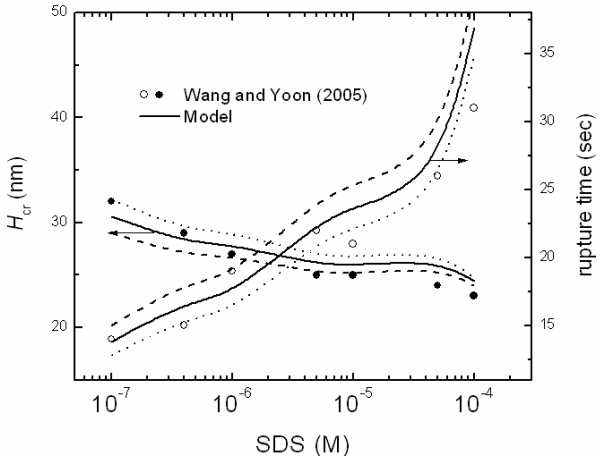

Figure. 3. Critical rupture thickness (H_{cr}) and corresponding rupture time (t_c) with surfactant SDS concentration change, in the presence of 0.3M NaCl. Input parameters were: C_1=0.07, C_2=40, H_i=250 nm. Dashed line represents the model prediction with 10% higher value of K_{232} reported by Wang and Yoon (2005), and dotted line represents the one with 10% lower value.

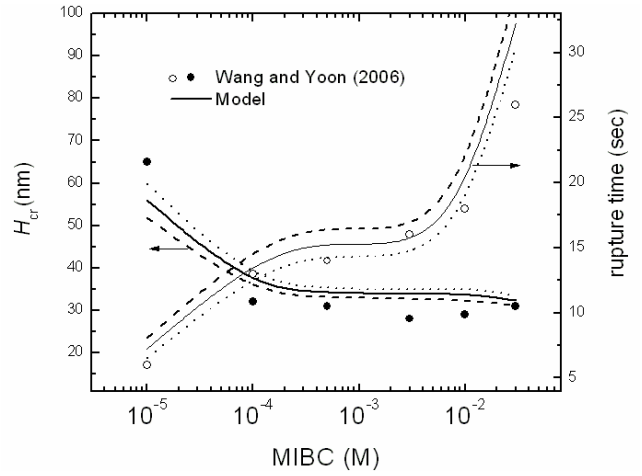

Figure. 4. Critical rupture thickness (H_{cr}) and corresponding rupture time (t_c) with surfactant MIBC concentration change, in the presence of 0.1M NaCl. Input parameters were: C_1=0.125, C_2=40, H_i=250 nm. Dashed line represents the model prediction with 10% higher value of K_{232} reported by Wang and Yoon (2006), and dotted line represents the one with 10% lower value.

with changes of K_{232} value 10% higher and lower.

Another comparison between the model and experimental data by Manev *et al.* [42] is presented in Figure 5. The authors studied the stability of emulsion and foam films. The critical rupture thickness was obtained for several different systems, but the corresponding coalescence time was not presented. Instead, they measured the drainage time for a constant range of

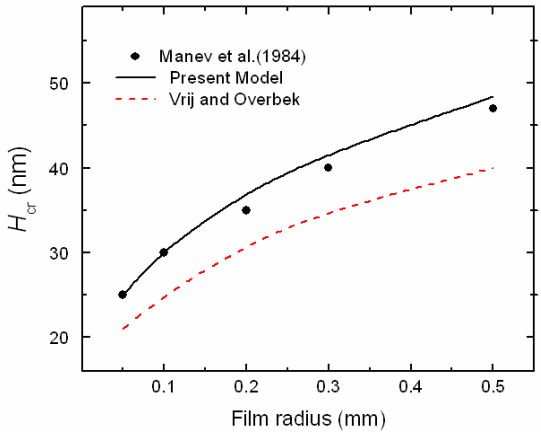

Figure. 5. Critical rupture thickness (H_{cr}) change according to the film radius change. Model calculations were conducted for the same system as Figure 3. Input parameters were same as Figure 3. : C_1=0.07, and C_2=40. The value of K_{232} was chosen 2×10^{-20} J, by extrapolating Wang and Yoon (2005)'s K_{232} vs. SDS concentration data. Dashed line represents the prediction by Vrij and Overbeek's model.

thickness, and observed slower drainage at higher surfactant concentrations in which electrostatic force was suppressed. Although their experimental conditions given by Manev et *al*.[42] are insufficient for the purpose of the present model comparison, all the necessary properties such as K_{232} and surface tension were referenced from the experimental work by Wang and Yoon [23] in which experiments were conducted in the similar environment on SDS foam films. As shown in Figure 5, the present model prediction agrees better with the experimental data than the model by Vrij and Overbeek [16]. It also agrees with the general observation that small films are much more stable than large films in a similar system [11].

4. Summary and conclusion

A model for predicting the critical rupture thickness of thin liquid film and corresponding rupture time has been derived. In the literature, no other model incorporated the hydrophobic force with the phenomena, but the present model has succeeded by applying the hydrophobic force constant in film, K_{232}. The basic assumption of the model was that thin liquid film has interfaces fluctuating due to interfacial forces, as many other models in the literature have assumed. Unlike others, the present model does not necessarily imply that the critical rupture thickness is equal to twice the amplitude of the critical interfacial wave. This was possible because the velocity increase factor and film radius change ratio were introduced to correct the rupture thickness to real practice. The model was verified by experimental data reported in other literature. Although not many presented the value of K_{232} as a direct value, K_{232} could be inferred from the given data. As a result, the model was in good agreement with experimental data reported in various references.

5. References

1. Do, H., *Development of a turbulent flotation model from first principles*, in *Engineering Science and Mechanics*. 2010, Virginia Polytechnic Institute and State University: Blacksburg.
2. Davis, R.H., J.A. Schonberg, and J.M. Rallison, *The lubrication force between two viscous drops.* Physics of Fluids A: Fluid Dynamics, 1989. **1**(1): p. 77-81.
3. Barnocky, G. and R.H. Davis, *The lubrication force between spherical drops, bubbles and rigid particles in a viscous fluid.* International Journal of Multiphase Flow, 1989. **15**(4): p. 627-638.
4. Fuentes, Y.O., S. Kim, and D.J. Jeffrey, *Mobility functions for two unequal viscous drops in Stokes flow. I. Axisymmetric motions.* Physics of Fluids, 1988. **31**(9): p. 2445-2455.
5. Vrij, A., *Possible mechanism for the spontaneous rupture of thin, free liquid films.* Discussions of Faraday Society, 1966. **42**: p. 23-33.
6. Sheludko, A., *Thin liquid films.* Advances in Colloid and Interface Science, 1967. **1**(4): p. 391-464.
7. Karakashev, S.I. and A.V. Nguyen, *Effect of sodium dodecyl sulphate and dodecanol mixtures on foam film drainage: Examining influence of surface rheology and*

intermolecular forces. Colloids and Surfaces A: Physicochemical and Engineering Aspects, 2007. **293**(1-3): p. 229-240.
8. Radoev, B.P., A.D. Scheludko, and E.D. Manev, *Critical thickness of thin liquid films: Theory and experiment.* Journal of Colloid and Interface Science, 1983. **95**(1): p. 254-265.
9. Ivanov, I.B. and D.S. Dimitrov, *Hydrodynamics of thin liquid films.* Colloid & Polymer Science, 1974. **252**(11): p. 982-990.
10. Valkovska, D.S., K.D. Danov, and I.B. Ivanov, *Stability of draining plane-parallel films containing surfactants.* Advances in Colloid and Interface Science, 2002. **96**(1-3): p. 101-129.
11. Angarska, J.K., et al., *Detection of the Hydrophobic Surface Force in Foam Films by Measurements of the Critical Thickness of the Film Rupture.* Langmuir, 2004. **20**(5): p. 1799-1806.
12. Ruckenstein, E. and R.K. Jain, *Spontaneous rupture of thin liquid films.* Journal of Chemical Society, Faraday Transactions 2, 1974. **70**: p. 132-147.
13. Sharma, A. and E. Ruckenstein, *Critical thickness and lifetimes of foams and emulsions: Role of surface wave-induced thinning.* Journal of Colloid and Interface Science, 1987. **119**(1): p. 14-29.
14. Scheludko, A., Proc. K. Akad. Wetensch, B, 1962. **65**: p. 76.
15. Vrij, A., *Light scattering by soap films.* Journal of Colloid Science, 1964. **19**(1): p. 1-27.
16. Vrij, A. and J.T.G. Overbeek, *Rupture of thin liquid films due to spontaneous fluctuations in thickness.* Journal of the American Chemical Society, 1968. **90**(12): p. 3074-3078.
17. Williams, M.B. and S.H. Davis, *Nonlinear theory of film rupture.* Journal of Colloid and Interface Science, 1982. **90**(1): p. 220-228.
18. Erneux, T. and S.H. Davis, *Nonlinear rupture of free films.* Physics of Fluids A: Fluid Dynamics, 1993. **5**(5): p. 1117-1122.
19. Ida, M.P. and M.J. Miksis, *Thin Film Rupture.* Applied Mathematics Letters, 1996. **9**: p. 35-40.
20. Ivanov, I.B., et al., *Theory of the critical thickness of rupture of thin liquid films.* Transactions of Faraday Society, 1970. **66**: p. 1262-1273.
21. Sharma, A. and E. Ruckenstein, *Stability, critical thickness, and the time of rupture of thinning foam and emulsion films.* Langmuir, 1987. **3**(5): p. 760-768.
22. Wang, L. and R.-H. Yoon, *Hydrophobic Forces in the Foam Films Stabilized by Sodium Dodecyl Sulfate:Effect of Electrolyte.* Langmuir, 2004. **20**(26): p. 11457-11464.
23. Wang, L. and R.-H. Yoon, *Hydrophobic forces in thin aqueous films and their role in film thinning.* Colloids and Surfaces A: Physicochemical and Engineering Aspects, 2005. **263**(1-3): p. 267-274.
24. Wang, L. and R.-H. Yoon, *Role of hydrophobic force in the thinning of foam films containing a nonionic surfactant.* Colloids and Surfaces A: Physicochemical and Engineering Aspects, 2006. **282-283**: p. 84-91.
25. Wang, L. and R.-H. Yoon, *Effects of surface forces and film elasticity on foam stability.* International Journal of Mineral Processing, 2008. **85**(4): p. 101-110.
26. Yoon, R.H., *The role of hydrodynamic and surface forces in bubble-particle interaction.* International Journal of Mineral Processing, 2000. **58**(1-4): p. 129-143.
27. Israelachvili, J.N. and R.M. Pashley, *The hydrophobic interaction is long range, decaying and exponentially with distance*, in *Nature*. 1988: London. p. 341-342.

28. Craig, V.S.J., B.W. Ninham, and R.M. Pashley, *The effect of electrolytes on bubble coalescence in water.* The Journal of Physical Chemistry, 1993. **97**(39): p. 10192-10197.
29. Deschenes, L.A., et al., *Inhibition of Bubble Coalescence in Aqueous Solutions. 1. Electrolytes.* The Journal of Physical Chemistry B, 1998. **102**(26): p. 5115-5119.
30. Du, Q., E. Freysz, and Y.R. Shen, *Surface Vibrational Spectroscopic Studies of Hydrogen Bonding and Hydrophobicity.* Science, 1994. **264**(5160): p. 826-828.
31. van Oss, C.J., R.F. Giese, and A. Docoslis, *Hyperhydrophobicity of the Water-Air Interface*, in *Journal of Dispersion Science & Technology*. 2005, Taylor & Francis Ltd. p. 585-590.
32. Stubenrauch, C., et al., *Comment on 'Hdrophobic Forces in the Foam Films Stabilized by Sodium Dodecyl Sulfate:Effect of Electrolyte' and Subsequent Criticism.* Langmuir, 2007. **23**(24): p. 12457-12460.
33. Ninham, B., *The Present State of Molecular Forces*, in *Smart Colloidal Materials*. 2006. p. 65-73.
34. Wang, L., *A Response to the Comment on "Hydrophobic Forces in the Foam Films Stabilized by Sodium Dodecyl Sulfate: Effect of Electrolyte".* Langmuir, 2008. **24**(9): p. 5194-5196.
35. Feather, N., *An introduction to the physics of vibrations and waves*. 1962: Edinburgh university press.
36. Hansen, R.H. and E.J. Derderian. *Plenary lecture-Problems in foam origin, drainage and rupture*. in *Symopsium on foams*. 1975. Brunel University: Academic press London.
37. Joosten, J.G.H., *Light scattering from thin liquid films*, in *Thin liquid films- fundamentals and applications*, I.B. Ivanov, Editor. 1988, Marcel Dekker.
38. Tabeling, P., *Introduction to microfluidics*. 2005: Oxford university press.
39. Abramowitz, M. and I.A. Stegun, in *Handbook of mathematical functions with formulas, graphs, and mathematical tables*. 1972, Dover: New York. p. 587-607.
40. Li, D., *Coalescence between Two Small Bubbles or Drops.* Journal of Colloid and Interface Science, 1994. **163**(1): p. 108-119.
41. Aksoy, B.S., *personal note*. 1998.
42. Manev, E.D., S.V. Sazdanova, and D.T. Wasan, *Emulsion and foam stability--The effect of film size on film drainage.* Journal of Colloid and Interface Science, 1984. **97**(2): p. 591-594.

CHAPTER 6

DEVELOPING A FROTH-PHASE RECOVERY MODEL FROM FIRST PRINCIPLES

ABSTRACT

In flotation, hydrophobic particles are selectively collected by air bubbles, and the bubble-particle aggregates enter the froth phase. However, less hydrophobic particles drop off from the froth phase, while more hydrophobic particles are recovered. The latter is referred to as true flotation in a sense that the recovery is achieved *via* bubble-particle attachment. The froth recovery model incorporating this mechanism has been developed by considering particle drop rate and the carrying capacities of bubbles. On the other hand, non-hydrophobic particles are also recovered, being carried by water entrained among bubbles. The particle recovery due to the entrainment mechanism water has also been incorporated in the model by considering water recovery as functions of bubble coarsening and the stability of bubble-particle aggregates during lateral transport to overflow lip. In addition, the entrainment model incorporates empirical parameters for particle size and density effects. The model predictions are in good agreement with experiments.

1. Introduction

Flotation is the most widely used separation process used in the mining industry. In this process, air bubbles are used to selectively collect hydrophobic particles and rise to the surface of a pulp, forming a froth phase. The bubbles laden with hydrophobic particles are removed from the top of a flotation cell, while hydrophilic particle are removed at the bottom. It has been shown recently that some of the bubble-particle aggregates break up upon encountering the pulp-froth interface, causing the particles return to the pulp phase [1] Thus, the pulp-froth interface behaves like a barrier. It has also been shown that much of the particles that have successfully entered the froth phase drop back to the pulp phase, as bubbles coalesce while rising in the froth phase and thereby cause a decrease in bubble surface area on which particle can be attached. A particle tracking method based on positron emission spectroscopy [2] clearly showed that drop back is an important sub-processes of flotation. It may appear, therefore, that both the pulp-froth interface and froth phase hinder the recovery process. On the other hand, they serve as important basis for achieving high degree of selectivity.

The stability of froth plays an important role in flotation, as it determines the final grade, recovery and throughput. Despite its importance, there are no models that can comprehensively account for all of the subprocesses occurring in the froth phase. It has been suggested that nearly twenty different physical and chemical factors influencing the froth recovery process [3]. However, the fractional recovery in the froth may be modeled in a broader sense by the following aspects. It was reported that hydrophobic force plays the most important role in determining the flotation recovery [4]. Since air bubbles are hydrophobic as well as mineral particles are [5], the froth recovery mechanisms can be grouped by two, largely. One is the recovery due to attachment [6, 7]. This is called true froth recovery because only hydrophobic particles are recovered along with the aggregates entering the froth. Through this mechanism, the collection of minerals was shown to have strong correlations with the hydrophobicity of particles and bubble surface area available for attachment. Some researchers modeled the recovery in empirical ways only, because froth bubbles are in the complicated 3 phases (solid-gas-liquid) [3, 7]. On the other hand, non-hydrophobic particles are also recovered from froth, being carried without attachment by the water in the froth [6, 7]. This is called the recovery due to entrainment [8, 9]. It is not directly related to the chemistry but is well known to play significant roles in the fine mineral particles recovery [10, 11]. Some empirical models for this recovery are also available [8, 9, 12], and generally the models include water recovery and particle size as parameters. The froth recovery models stated above have shortcomings in that their empirical parameters have complex relationship with each other and no governing criterion was given. The criterion may be found if a froth recovery model is developed in analytical way. This is possible by investigating both the drainage and bubble coarsening, because liquids drain and bubbles coalesce consistently in the froth.

The recovery mechanisms in relation to froth structure may be further simplified by regarding froth as foam. *Foam* is the term used to distinguish the liquid-gas dispersions from the liquid-gas-solid dispersions (*froths*) [13]. A foam is a two-phase system where gas cells are enclosed by liquid, and accordingly the structure looks like a network of pipe-like channels (called plateau border) and thin film walls (called lamellae) [14]. The drainage along this

structure has been a prevalent research topic for a long time because foams are commonly observed in many practical applications. Most of foam drainage models in the literature assume that liquids in foams flow mainly through the channels, and set the mass balance as the basis for the model [15-19]. The models in the literature were derived only for stable foams. In reality, foam bubbles grow, break and coalesce into larger sizes. Those models do not include the coalescence of bubbles. Relating coalescence with drainage model is challenging because the factors destabilizing foams are all interplaying with each other. For all that, the modeling effort to incorporate bubble size change has been tried recently [20].

The most convincing factor for coalescence in foam, so far, is the hydrophobic force [21]. Thin water films tend to rupture at different thicknesses for different surfactant concentrations or certain chemical conditions. In many experiments on foam film drainage, it has been shown that foam films thin faster than the prediction by the Reynolds lubrication equation and it was ascribed to hydrophobic force [21, 22]. Despite the findings, a good theory to predict the approximate time of rupture or corresponding rupture thickness is still missing. Many of the film rupture models available in the literature were good enough to predict the rupture of stable foams [23-25]. The models were derived by assuming that the rupture results from capillary waves due to the forces at the water-air interface but hydrophobic force was not considered. Therefore, the models were valid only for foam films of high surfactant concentrations at which hydrophobic force is significantly diminished [22, 26]. On this ground, the models are inappropriate for predicting the coalescence of practical foam films in such applications as mining industry, where hydrophobic force is apparent [27].

There are two different types of flotation cells used in the mining industry, *i.e.*, mechanically agitated flotation cells and flotation columns. Traditionally, flotation had been conducted in the mechanically agitated cells until columns were first used in practice in Canada in 1980 [28]. The characteristics of froths observed in the two may not be too much different from each other in essence. Therefore, the froth recovery model to be developed in this report should work for both. However, the model developed in the present work is more suitable for in mechanically agitated cells. Operated in deeper froth than mechanical cells, columns have advantages of improving product grade after introducing wash water into the froth. On the other hand, the hydrodynamics in columns becomes more complex than the one in mechanically agitated cells because the resultant froth instability from adding the wash water and deeper froth induce convective flow inside [29], which is not considered in the present model. Efforts have been made to develop the model from first principles.

2. Froth recovery model development

2.1 Overall froth recovery

The present froth recovery model accounts for two independent mechanisms*, i.e.*, recovery due to attachment and recovery due to entrainment. Thus, the overall froth recovery, R_F, becomes,

$$R_F = R_{F-a} + R_{F-e} \tag{1}$$

where $R_{F\text{-}a}$ is the recovery due to attachment, and $R_{F\text{-}e}$ is the recovery due to entrainment. Warren [9] has shown experimentally that the two are independent, and found $R_{F\text{-}a}$ changes with mineral type and particle size, while $R_{F\text{-}e}$ changes with water recovery and particle size.

2.1.1. Froth recovery due to attachment

Gorain *et al*. [7] proposed an empirical expression for overall froth recovery after analyzing numerous experimental data. The authors found that froth recovery decreases with longer residence time of air in a froth phase. Therefore, one can write the following relation,

$$R_{F-a} = R_{F-max}\exp\left(-\alpha t_f\right) \tag{2}$$

where t_f is the retention time of air in froth phase, and $R_{F\text{-}max}$ represents the maximum fractional recovery in the froth. In Gorain's model, $R_{F\text{-max}}$ was taken to be unity, In the present model it is considered to change with bubble size along the depth of a froth phase. As is well known, bubble size is small at the base of a froth phase but increases as the bubbles rise along the height due to coalescence. Therefore, the surface area rate of the bubbles, S_b, will decrease along the height and so will the capacity of the froth to carry particles upward. The surface area rate can be given as follows [30].

$$S_b = \frac{6V_g}{d_2} \tag{3}$$

where V_g is the superficial gas velocity, and d_2 is bubble diameter. In the present work, $R_{F\text{-}max}$ is considered to be the ratio of the surface area rate at the top of the froth to the one at the pulp-froth interface [31], *i.e*.,

$$R_{F-max} = \frac{S_{b-f}}{S_{b-0}} = \frac{d_{2-0}}{d_{2-f}} \tag{4}$$

where the subscripts -0 and *–f* indicates that the parameters are pertaining to the bottom and top of the froth, respectively. Eq. (4) suggests that the froth recovery can be maximized by minimizing bubbles coalesce, which can be achieved by increasing frother dosage. Forth recovery can also be increased by employing shallow froth depth to minimize bubble coalescence.

It has been shown that froth recovery increases as the froth residence time decreases [7]; therefore, α may be considered the rate constant for particles dropping back to the pulp phase due to coarsening. Assuming that each bubble carried N particles initially, α may be given as,

$$\alpha = -\left(\frac{Nd_1^2}{d_{2-0}^2}\right)\left(S_{b-f} - S_{b-0}\right) \tag{5}$$

where d_1 is particle diameter, $d_{2\text{-}0}$ is the initial bubble diameter (at the bottom). The second term in the parenthesis represents the change in surface area rate (S_b) as bubble size grows from $d_{2\text{-}0}$ at the bottom to $d_{2\text{-}f}$ at the top. Substituting Eq.(3) into (5), one obtains:.

$$\alpha = N\frac{6V_g}{d_{2-0}}\left(1-\frac{d_{2-0}}{d_{2-f}}\right)\left(\frac{d_1}{d_{2-0}}\right)^2 \tag{6}$$

Note here that N should vary depending on both physical (e.g., bubble size, particle size, turbulence) and chemical (e.g.,hydrophobicity, surface tension) properties of the system. Therefore, it may be treated as as an adjustable parameter.

As for the retention time, t_f, in Eq.(2), one may use the retention time of air, which can be given as the froth height (h_f) divided by superficial gas velocity, i.e., $t_f = h_f/V_g$, in the same manner as Gorain *et al*.'s [7]. Eq.(2) can then be rewritten as,

$$R_{F-a} = R_{F-max}\exp\left(-\alpha\frac{h_f}{V_g}\right) = \frac{d_{2-0}}{d_{2-f}}\exp\left(-N\frac{6h_f}{d_{2-0}}\left(1-\frac{d_{2-0}}{d_{2-f}}\right)\left(\frac{d_1}{d_{2-0}}\right)^2\right) \tag{7}$$

According to Eq. (7), $R_{F\text{-}a}$ should be a function of the ration between the bubble sizes at the base ($d_{2\text{-}0}$) and at the top ($d_{2\text{-}f}$) of a froth, where $d_{2\text{-}0} < d_{2\text{-}f}$. In a froth (or foam), bubbles coarsen due to drainage and rupture of intervening water films. The drainage occurs primarily in plateau borders [15, 17, 18], although drainage through plateau border junctions and lamella films may also be significant depending on bubble sizes involved. When the thickness of the lamella film becomes smaller than the critical rupture thickness (H_{cr}), the film ruptures and bubbles become coarser.

The number of plateau borders per unit cross-sectional area of foam should be proportional to the number of bubbles. Therefore, one can derive the following relationship,

$$\frac{N_{PB-f}}{N_{PB-0}} = \frac{4S/\pi {d_{2-f}}^2}{4S/\pi {d_{2-0}}^2} = \left(\frac{d_{2-0}}{d_{2-f}}\right)^2 \tag{8}$$

where N_{PB} is the number of plateau borders at a cross-section, S the cross-sectional area of a foam column, and d_2 is the bubble diameter with the subscripts -0 and *–f* representing the same as in Eq.(4).

It has been shown experimentally that the number of bubbles in a foam changes exponentially with time [32]. Therefore, the number of plateau borders may be estimated as follows,

$$N_{PB} = n_0\exp\left(-C\sqrt{A_{cr}/A}\right) \tag{9}$$

where N_{PB} is the total number of plateau borders at a given cross-sectional area of a flotation cell, n_0 the initial number of plateau borders, C a fitting parameter representing bubble coalescence, A the plateau border cross-sectional area, and A_{cr} is the critical value of A at which bubbles

coalesce. It has been shown experimentally that foam bubbles coarsen at a critical liquid fraction [33]. It would, therefore, be reasonable to assume that there is a critical value of A, i.e., A_{crit}, at which the lamella film between two bubbles rupture at a critical rupture thickness (H_{cr}) and become one [22, 26, 34, 35] The use of A_{cr} may be convenient in modeling foam (or froth) stability, as plateau boarders can be related to liquid fraction or measured optically. The measurement of $H_{cr,}$ on the other hand, requires sophisticated devices such as thin-film pressure balance (TFPB) [36].

Substituting Eq.(9) into Eq.(8), and assuming that A_{cr} is approximately the same as the plateau border area (A_f) at the top of a foam, one can write the following relation,

$$\frac{d_{2-0}}{d_{2-f}} = \sqrt{\exp\left(C\sqrt{A_f/A_0} - C\right)} \tag{10}$$

where A_0 the plateau border areas at the bottom of the foam. The plateau boarder area can be related to the average drainage velocity (U) in the plateau boarders [17, 18, 37],

$$U = \frac{1}{\mu}\left(\rho g A - \frac{f\gamma}{2}\frac{1}{\sqrt{A}}\frac{\partial A}{\partial x}\right) \tag{11}$$

where ρ is the liquid density, g the gravity, γ surface tension, and μ is dynamic viscosity of liquid, and f is a parameter related to plateau border shape. For well-structured, mono-dispersed foams, f = 0.4. In the present work, where coarsening foams (or froth) are considered, it is assumed that f = 2.

At steady state, the downward liquid velocity (U) given by Eq. (11) should be equal to the superficial gas velocity, -V_g, which is upward. One can, therefore, derive the following relation,

$$\frac{dA}{dx} = \frac{\rho g}{\gamma} A\sqrt{A} + \frac{\mu V_g}{\gamma}\sqrt{A} \tag{12}$$

which can be solved to obtain,

$$\sqrt{A_f} = \sqrt{\frac{V_g\mu}{\rho g}}\tan\left(\tan^{-1}\left(\sqrt{\frac{\rho g A_0}{V_g\mu}}\right) - \frac{h_f}{2}\frac{\sqrt{\rho g \mu V_g}}{\gamma}\right) \tag{13}$$

with boundary conditions: $A = A_f$ at $x = 0$ (top of a froth), and $A = A_0$ at $x = h_f$ (bottom of a forth). Eq. (13) can be used to obtain the value of $\sqrt{A_f/A_0}$, which in turn can be substituted into Eq.(10) to predict the coarsening of foam (or froth) bubbles. All of the parameters of Eq. (14) are known except A_0. In the present work, it is considered that $\sqrt{A_0} \approx d_{2-0}$, which is an approximation based on the observation that for stable foams the radius of curvature of plateau border ($\sqrt{A}$) is proportional to the radius of the bubbles by a factor less than 2, depending on the wetness of a foam under consideration [38].

2.1.2. Froth recovery due to entrainment

Fine particles in a flotation cell flow with water due to their small masses. In principle, therefore, the recovery ($R_{F\text{-}e}$) due to entrainment for fine particles should be the same as water recovery (R_w). The latter should in turn be a function of the liquid fraction of the foam at the top, which should decrease as bubbles coarsen along the height of a froth phase. Once a group of bubbles reach the top, however, they will start flowing laterally toward the overflow lip, during which time bubble coarsening continues and, hence, the liquid fraction decreases further. Thus, R_w should be given as,

$$R_W = F_W F_B \tag{14}$$

where F_W is the liquid fraction at the top of a foam as soon as bubbles arrive at the top, and F_B is the fraction of bubbles that do not burst during their lateral flow.

In principle, F_w should be a function of the surface area rate of the bubbles ($S_{b\text{-}f}$) at the top of a froth phase. This relationship may be given as follows,

$$F_W = \varepsilon_0 \mathrm{S}_{b-f} t_{cf} = \varepsilon_0 \frac{6V_g}{d_{2-f}} \frac{4\mu h_f}{\rho g \delta^2} \tag{15}$$

where ε_0 is the liquid fraction at the bottom of a froth phase, t_{cf} is the time scale over which a thick liquid film thins to a thickness δ [39], and h_f is the froth height. Typically, ε_0 varies in the range of 0.26-0.36, depending on the packing condition of bubbles at the bottom [40]. In the present work, a value of 0.33 has been chosen for ε_0 [14, 41], while δ has been approximated by the following relation,

$$\delta = \frac{3}{4}\left(\frac{\varepsilon_0}{1-\varepsilon_0}\right) d_{2-0} \tag{16}$$

which has been derived assuming that all of the bubbles at the pulp-froth interface have diameter $d_{2\text{-}0}$ and film thickness δ.

As for F_B in Eq. (15), one may use the following form,

$$F_B = \exp\left(-\frac{h_f}{L}\right) \tag{17}$$

where h_f is the froth height at a steady state, and L is a length scale representing transport of froth across a flotation cell, which may be represented by,

$$L = \frac{\mu}{\rho_2 U_f} \tag{18}$$

where μ is the liquid viscosity, ρ_2 is air density, and U_f is the velocity of froth moving laterally toward overflow lip. Eqs. (17) and (18) suggest that as froth height increases the lateral velocity of froth should decrease, which is consistent with industrial experience.

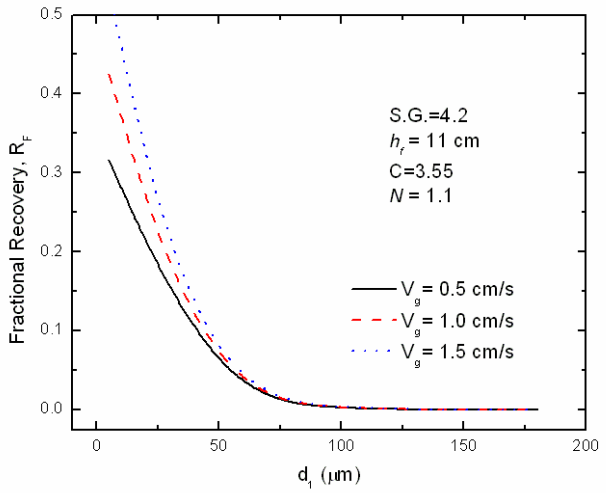

Figure 1. Effect of superficial gas flow rate on froth recovery. Higher superficial gas flow is beneficial to fine particles froth recovery.

As discussed above, Eq. (14) gives the water recovery (R_w), which should be equal to the recovery of fine particles. However, coarse particles deviate from fluid flow due to inertia force; therefore, Eq. (14) may be rewritten as follows,

$$R_{F-e} = F_W F_B \exp\left(-0.0325\Delta\rho - 0.063 d_1\right) \tag{19}$$

where $\Delta\rho$ is the specific gravity difference between mineral and medium (water), and d_1 is particle diameter in μm. The terms in the parenthesis are designed to make corrections for the S.G. and size of particles, as determined empirically by Maachar and Dobby [10].

Substituting Eqs. (7) and (19) into Eq. (1), one obtains an expression for the overall froth recovery as follows:

$$R_F = \frac{d_{2-0}}{d_{2-f}} \exp\left(-\alpha \frac{h_f}{V_g}\right) + R_W \exp\left(-0.0325\Delta\rho - 0.063 d_1\right) \tag{20}$$

Most of the parameters of Eq.(20) are readily available from operating conditions.

3. Effect of Various Parameters on Froth Recovery

In the following, the effects of various parameters used in the model are presented. Figure 1 shows the effect of particle size on froth recovery at different superficial gas flow rates. As shown, froth recovery increases with decreasing particle size mostly due to increased entrainment of fine particles. As particle size (d_1) becomes smaller, the recovery due to entrainment ($R_{f\text{-}e}$) increases as shown in Eq. (19). Eq. (15) shows that as the superficial gas velocity (V_g) increases, water recovery (F_w) increases, which in turn causes an increase in the

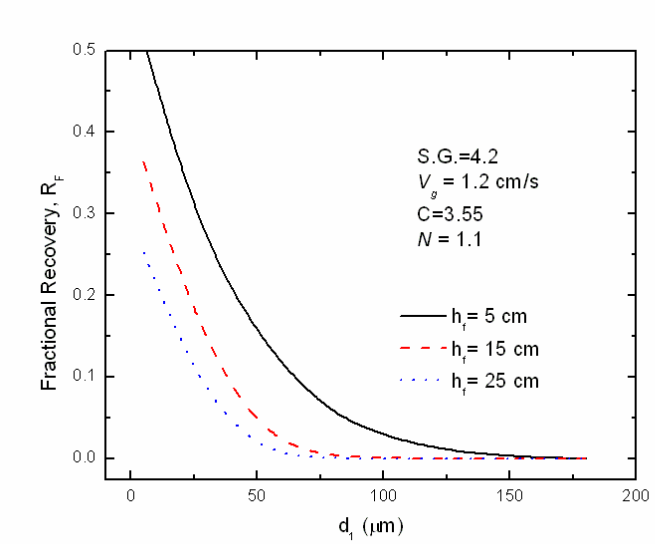

Figure 2. Effect of froth height on froth recovery. Shallow froth height is helpful for froth recovery of coarse particles.

overall froth recovery (R_f), as shown in Eq. (20). An increase in V_g should also increase the recovery due to attachment ($R_{F\text{-}a}$) as shown in Eq. (20). Its benefit is small, however, at larger particle sizes, which can be attributed to the high detachment probabilities associated with coarse particles.

Figure 2 shows the effect of changing froth heights. As shown in Eq. (17), a decrease in froth height causes F_B increase, which in turn causes the entrainment recovery ($R_{F\text{-}e}$) to improve as

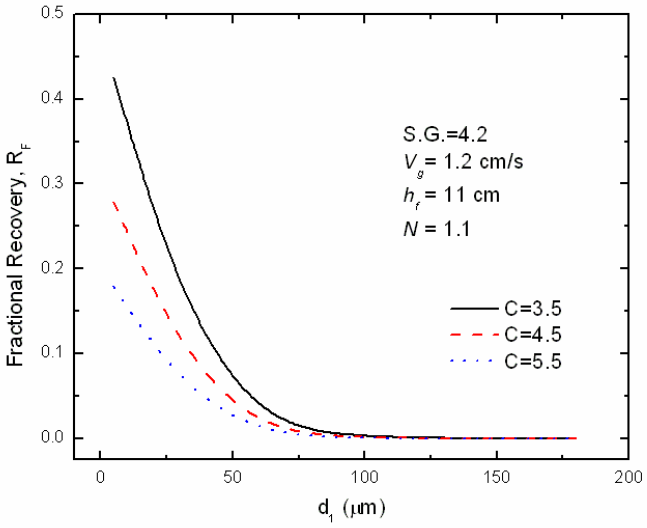

Figure 3. Effect of coarsening on froth recovery. Higher coarsening factor, meaning unstable froth, shows lower froth recovery.

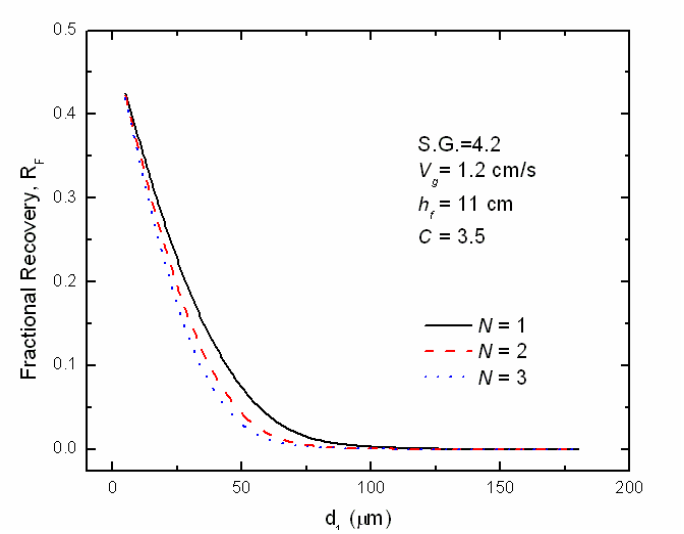

Figure 4. Effect of mineralization on froth recovery. The degree of mineralization in fine particles and coarse particles has less significant effect than other particle sizes.

shown in Eq. (19). The predictions shown in Figs. 1 and 2 agree with industrial experience that increasing superficial gas velocity and decreasing froth height in flotation is beneficial to froth recovery [30]. It should be noted here that the simulation results presented in Figures 1 and 2 have been obtained by assuming that the lateral velocity (U_f) of froth on the top of a froth phase is 1 cm/s. It has been reported that for a 50 m^3 conventional flotation cell U_f is in the range 2~12 cm/s [42].

The effects of coarsening and the degree of mineralization of bubbles are presented in

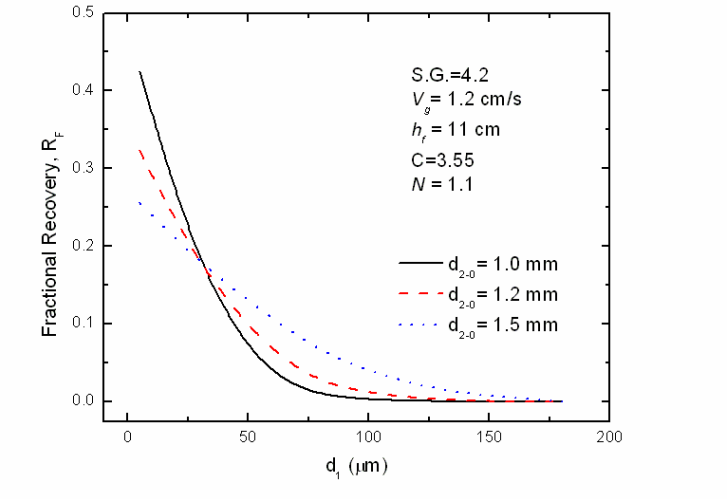

Figure 5. Effect of bubble size entering the interface (d_{2-0}) on froth recovery. Small entering bubbles are helpful for the froth recovery of particles as fine as 25μm, while large entering bubbles are for larger particles than 25 μm.

Figures 3 and 4, represented by the changes of parameters C in Eq.(9), the fitting parameter representing coalescence, and N in Eq.(6), the fitting parameter representing the number of particles returning to the pulp. Eq. (9) suggests that higher values of C represent less stable froth, and hence the froth recovery should decrease with increasing C. This is shown to be the case in Fig. 3.

On the other hand, as the drop-back rate (Eq.(6)) increases with increasing N. N represents the number of particles dropping back to pulp-phase. Thus, froth recovery decreases with increasing N, as shown in Fig. 4. However, the effect of changing N is minimal when particles are very fine (<1μm) or coarse (>100μm). This may be because at fine particle sizes particle drop rate is low regardless of the degree of mineralization, and the drop-back rate is high at coarse particle sizes. Parameters C and N work as independent parameters in the present model, although the two may have certain relationship to each other. However, the present work did not account for this relationship.

The effect of bubble size entering froth is shown in Figure 5. Eqs.(4) and (7) suggests that small bubbles entering the froth should yield low froth recovery. In figure 5, on the contrary, smaller entering bubbles are shown to be beneficial for the recovery at d_1<25 μm. Therefore, the simulation results for particles for those sizes are attributed to the recovery due to entrainment ($R_{F\text{-}e}$), rather than due to attachment. As shown in Eq.(14)~(16), small entering bubbles induce high water recovery, and hence high $R_{F\text{-}e}$. This model prediction agrees well with Ata *et al*.'s [43] experiment, in which fine silica particles showed significantly low recovery rate with large bubbles entering the froth, while the recovery of hydrophobic particles did not change much in the same environment.

The various parameters studied in the present work are interdependent with each other in practical froths. Therefore, the predictions made in Figures 1~5 may not be valid for certain cases, because the present model has been derived by assuming that all the parameters are independent from each other. Experimental data for verifying the model for all of the parameters are not available as yet. In the following section, some of the model predictions will be compared with experimental data reported in the literature.

4. Comparison with experimental work

In this section, the model for overall froth recovery is compared with experimental data reported in other literature. Seaman *et al*. [1] reported size-by-size froth recovery data. The authors measured froth recovery using two different methods and found that the pulp-froth interface is responsible for the recovery loss of recovery. Their device could effectively capture particles subject to true flotation, and corresponding data showed that true froth phase recovery varies with particle sizes. The data may be helpful for verifying the present model, but may not be the best because entrainment should give rise to the total recovery. Therefore, the entrainment part of the model is compared with other data reported by Zheng *et al*.[44, 45]. Both authors used the Outokumpu 3m^3 (OK3) cell. Typical operational values of OK3 cell such as specific air rate, and specific area were used in the simulation to provide the same conditions with the report. Any

physical conditions of OK3 may be found in the literature [46]. Any unspecified information but necessary for the current model was selected from other references.

In model predictions, the bubble size entering the froth was assumed to be 1 mm. The coalescence parameter *C* in Eq.(10) was chosen 3.55 for chalcopyrite flotation and 4 for galena flotation. These values are close to the data obtained for beer foams, for which the equivalent empirical parameter vary between 3 and 5 [47]. The model predictions for the froth recoveries of chalcopyrite are shown in Figures 6-A and 6-B, and those for galena are shown in Figures 7-A and 7-B. As shown, the model shows good agreement with experimental data represented by

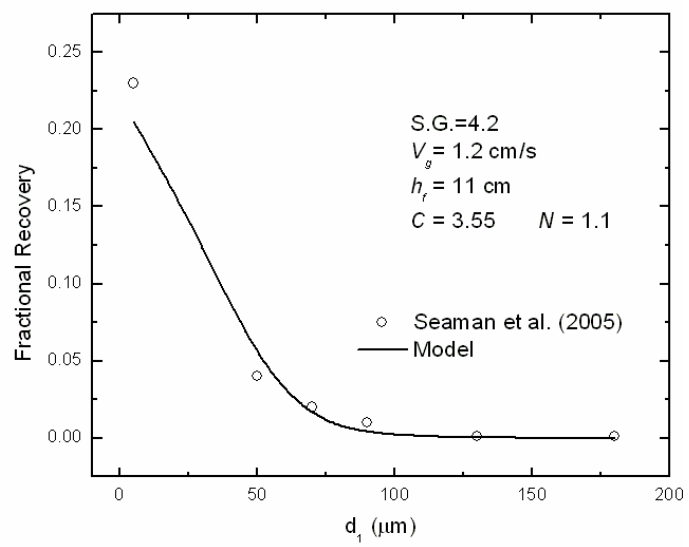

Figure 6-A. Comparison of the model, froth recovery due to attachment, with the chalcopyrite froth recovery data reported by Seaman et al.

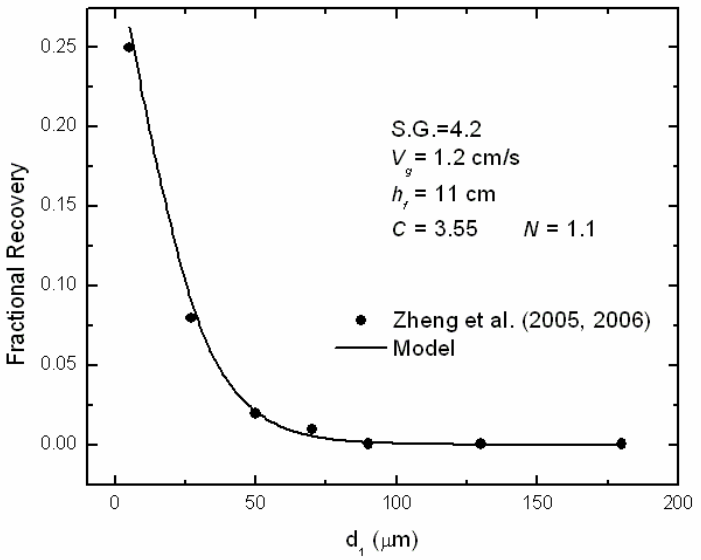

Figure 6-B. Comparison of the model, froth recovery due to entrainment, with the chalcopyrite froth recovery data reported by Zheng et al.

symbols. As shown, the recovery due to entrainment is as significant as attachment recovery when particles are small, but the significance diminishes as particles become as large as 50μm. This observation is consistent with what is reported in the literature [8, 48]. The predictions for the recovery due to attachment are not as good as those for the recovery due to entrainment, which may be attributed to the possibility that the adjustable parameter N from Eq.(7) may actually be a variable.

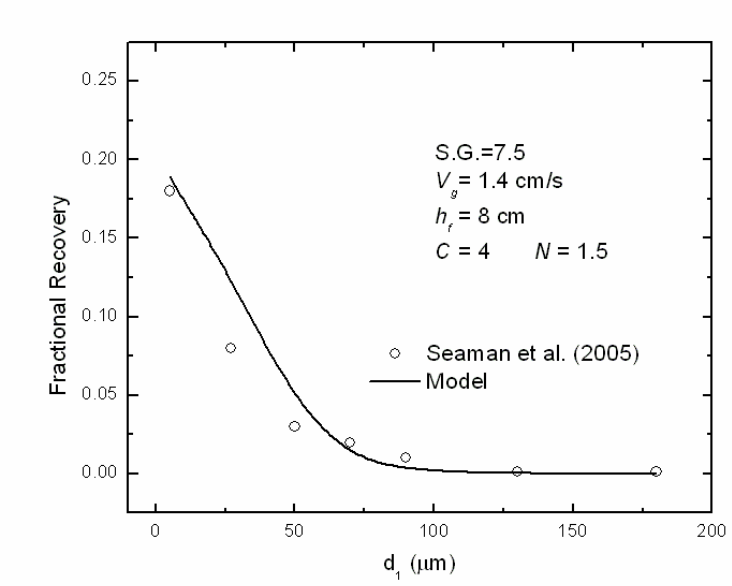

Figure 7-A. Comparison of the model, froth recovery due to attachment, with the galena froth recovery data reported by Seaman et al.

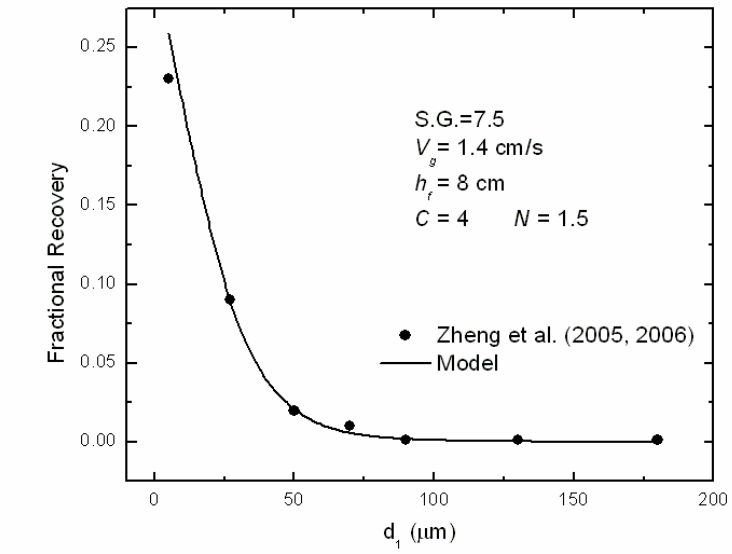

Figure 7-B. Comparison of the model, froth recovery due to entrainment, with the galena froth recovery data reported by Zheng et al.

5. Summary and conclusion

A froth recovery model for the conventional flotation cell has been developed and compared with experimental data. The model includes two major mechanisms for froth recovery, i.e., bubble-particle attachment and particle entrainment. For the froth recovery by attachment, a maximum recovery factor was considered from the idea that attachment is proportional to available surface area. A new definition of the particle drop-back rate in the froth was derived to account for the changes in bubble surface area and froth retention time for air bubbles. The recovery due to entrainment has been modeled by deriving a relationship between water recovery and fraction of water at the top of a froth phase and the fraction of bubble unburst during the process of bubble-particle aggregates being transported to overflow lip. The model predictions show that entrainment becomes significant with fine particles.

The model predictions show also that froth recovery decreases with increasing particle size due to detachment of particles, which in turn can be related to the decrease in bubble surface area as bubbles rise along the height of a froth phase due to bubble coalescence. Thus, coarse particle recovery in the froth phase can be improved by decreasing froth height or letting large bubbles enter the froth, as Eq.(7) indicates in case of high particle dropping rates.

6. References

1. Seaman, D.R., E.V. Manlapig, and J.P. Franzidis, *Selective transport of attached particles across the pulp-froth interface.* Minerals Engineering, 2005. **19**(6-8): p. 841-851.
2. Waters, K.E., et al., *Positron emission particle tracking as a method to map the movement of particles in the pulp and froth phases.* Minerals Engineering, 2008. **21**(12-14): p. 877-882.
3. Mathe, Z.T., et al., *Review of froth modelling in steady state flotation systems.* Minerals Engineering, 1998. **11**(5): p. 397-421.
4. Yoon, R.H., *The role of hydrodynamic and surface forces in bubble-particle interaction.* International Journal of Mineral Processing, 2000. **58**(1-4): p. 129-143.
5. Craig, V.S.J., B.W. Ninham, and R.M. Pashley, *The effect of electrolytes on bubble coalescence in water.* The Journal of Physical Chemistry, 1993. **97**(39): p. 10192-10197.
6. Ata, S., N. Ahmed, and G.J. Jameson, *Collection of hydrophobic particles in the froth phase.* International Journal of Mineral Processing, 2002. **64**(2-3): p. 101-122.
7. Gorain, B.K., et al., *The effect of froth residence time on the kinetics of flotation.* Minerals Engineering, 1998. **11**(7): p. 627-638.
8. Trahar, W.J., *A rational interpretation of the role of particle size in flotation.* International Journal of Mineral Processing, 1981. **8**(4): p. 289-327.
9. Warren, L.J., *Determination of the contributions of true flotation and entrainment in batch flotation tests.* International Journal of Mineral Processing, 1985. **14**(1): p. 33-44.
10. Maachar, A. and G.S. Dobby, *Measurement of feed water recovery and entrainment solids recovery in flotation columns.* Canadian Metallurgical Quarterly, 1992. **31**(3): p. 167-172.

11. Savassi, O.N., et al., *An empirical model for entrainment in industrial flotation plants.* Minerals Engineering, 1998. **11**(3): p. 243-256.
12. Lynch, A.J., M.W. Johnson, and E.V. Manlapig, eds. *Mineral and coal flotation circuits: their simulation and control*. Developments in mineral processing 3. 1981, elsevier.
13. Pugh, R.J., *Experimental techniques for studying the structure of foams and froths.* Advances in Colloid and Interface Science, 2005. **114-115**: p. 239-251.
14. Weaire, D. and S. Hutzler, *The physics of foams*. 1999: Oxford university press.
15. Leonard, R.A. and R. Lemlich, *A study of interstitial liquid flow in foam. Part I. Theoretical model and application to foam fractionation.* AIChE Journal, 1965. **11**(1): p. 18-25.
16. Koehler, S.A., S. Hilgenfeldt, and H.A. Stone, *A Generalized View of Foam Drainage: Experiment and Theory.* Langmuir, 2000. **16**(15): p. 6327-6341.
17. Verbist, G., D. Weaire, and A.M. Kraynik, *The foam drainage equation.* Journal of Physics: Condensed Matter, 1996. **8**(21): p. 3715-3731.
18. Gol'dfarb, I.I., K.B. Kann, and I.R. Shreiber, *Liquid flow in foams.* Fluid Dynamics, 1988. **23**(2): p. 244-249.
19. Verbist, G. and D. Weaire, *A Soluble Model for Foam Drainage.* EPL (Europhysics Letters), 1994. **26**(8): p. 631-634.
20. Do, H., et al., *Coarsening foam- Numerical modeling and experimental results*, in *Flotation 07 symposium*. 2007: Cape town, South Africa.
21. Wang, L. and R.-H. Yoon, *Hydrophobic forces in thin aqueous films and their role in film thinning.* Colloids and Surfaces A: Physicochemical and Engineering Aspects, 2005. **263**(1-3): p. 267-274.
22. Angarska, J.K., et al., *Detection of the Hydrophobic Surface Force in Foam Films by Measurements of the Critical Thickness of the Film Rupture.* Langmuir, 2004. **20**(5): p. 1799-1806.
23. Vrij, A., *Possible mechanism for the spontaneous rupture of thin, free liquid films.* Discussions of Faraday Society, 1966. **42**: p. 23-33.
24. Ruckenstein, E. and R.K. Jain, *Spontaneous rupture of thin liquid films.* Journal of Chemical Society, Faraday Transactions 2, 1974. **70**: p. 132-147.
25. Ivanov, I.B., et al., *Theory of the critical thickness of rupture of thin liquid films.* Transactions of Faraday Society, 1970. **66**: p. 1262-1273.
26. Wang, L. and R.-H. Yoon, *Effects of surface forces and film elasticity on foam stability.* International Journal of Mineral Processing, 2008. **85**(4): p. 101-110.
27. Yoon, R.H. and L. Wang, *Hydrophobic forces in foam films*, in *colloids and interface science series*, Tadros, Editor. 2007, Wiley-VCH. p. 161-186.
28. Habashi, F., *A short history of mineral processing*, in *23rd International Mineral Processing Congress*. 2006: Istanbul, Turkey. p. 3-8.
29. Hutzler, S., D. Weaire, and R. Crawford, *Convective instability in foam drainage.* EPL (Europhysics Letters), 1998. **41**(4): p. 461-466.
30. Finch, J.A. and G.S. Dobby, *Column flotation*. 1990: Pergamon press.
31. Sherrell, I. and R.-H. Yoon. *Development of a turbulent flotation model*. in *Centenary of flotation symposium*. 2005. Barisbane, Australia.
32. Szekrenyesy, T., K. Liktor, and N. S?dor, *Characterization of foam stability by the use of foam models 1. Models and derived lifetimes.* Colloids and Surfaces, 1992. **68**(4): p. 267-273.

33. Carrier, V. and A. Colin, *Coalescence in Draining Foams.* Langmuir, 2003. **19**(11): p. 4535-4538.
34. Yoon, R.-H. and B.S. Aksoy, *Hydrophobic Forces in Thin Water Films Stabilized by Dodecylammonium Chloride.* Journal of Colloid and Interface Science, 1999. **211**(1): p. 1-10.
35. Hartland, S. and A.D. Barber, *A model for a cellular foam.* Trans. Instn Chem. Engrs, 1974. **52**: p. 43-52.
36. Scheludko, A. and D. Exerowa, Kolloidnyi Zhurnal, 1959. **165**: p. 148.
37. Nguyen, A.V., *Liquid Drainage in Single Plateau Borders of Foam.* Journal of Colloid and Interface Science, 2002. **249**(1): p. 194-199.
38. Narsimhan, G. and E. Ruckenstein, *Structure, drainage and coalescence of foams and concentrated emulsions*, in *Foams: Theory, Measurments, and Applications*, R.K. Prud'homme and K.B. Kann, Editors. 1995, Marcel Dekker: New York.
39. Mysels, K.J., K. Shinoda, and S. Frankel, *Soap films, studies of their thinning and a bibliography*. 1959, New York: Pergamon Press.
40. Neethling, S.J., H.T. Lee, and J.J. Cilliers, *The recovery of liquid from flowing foams.* Journal of Physics: Condensed Matter, 2003. **15**(10): p. 1563-1576.
41. Prud'homme, R.K. and S.A. Khan, eds. *Foams: theory, measurement, and applications*. surfactant science series. 1995, Marcel Dekker.
42. Zheng, X. and L. Knopjes, *Modelling of froth transportation in industrial flotation cells: Part II. Modelling of froth transportation in an Outokumpu tank flotation cell at the Anglo Platinum Bafokeng-Rasimone Platinum Mine (BRPM) concentrator.* Minerals Engineering. **17**(9-10): p. 989-1000.
43. Ata, S., N. Ahmed, and G.J. Jameson, *A study of bubble coalescence in flotation froths.* International Journal of Mineral Processing, 2003. **72**(1-4): p. 255-266.
44. Zheng, X., N.W. Johnson, and J.P. Franzidis, *Modelling of entrainment in industrial flotation cells: Water recovery and degree of entrainment.* Minerals Engineering, 2006. **19**(11): p. 1191-1203.
45. Zheng, X., et al., *Modelling of entrainment in industrial flotation cells: the effect of solids suspension.* Minerals Engineering, 2005. **18**(1): p. 51-58.
46. Fallenius, K., *Turbulence in flotation cells.* International Journal of Mineral Processing, 1987. **21**(1-2): p. 1-23.
47. Sauerbrei, S., E.C. Haß, and P.J. Plath, *The Apollonian decay of beer foam bubble size distribution and the lattices of young diagrams and their correlated mixing functions.* Discrete Dynamics in Nature and Society, 2006: p. 1-35.
48. Smith, P.G. and L.J. Warren, *Entrainment of particles into flotation froths.* Mineral Processing and Extractive Metallurgy Review, 1989. **5**: p. 123-145.

Chapter 7. Summary and Suggestions for Future Research

1. Original Contributions

Five different topics have been presented in each chapter of this dissertation. However, all were in a consistent purpose: incorporating hydrophobic force into a flotation model. Therefore, the dissertation comprised mostly mathematical models pertaining to the fundamental theory of flotation. The original contributions by the present research are summarized as follows.

- ☐ Modeling flotation
  - A comprehensive turbulent flotation model has been developed for the first time.
  - The model incorporates both surface forces and hydrodynamic forces.
  - The model includes input parameters changing interdependently.
  - Extended DLVO theory has been verified from induction time measurement
- ☐ Modeling foam
  - The drainage equation incorporates bubble coalescence and PB area change for the first time.
  - Foam film rupture is modeled by incorporating hydrophobic force with fundamental theories.
- ☐ Froth recovery model
  - The model considers two distinctive mechanisms: particle attachment and entrainment.
  - Attachment mechanism is a function of bubble coarsening, which can be predicted from A_{cr} and h_{cr} models.
  - Entrainment mechanism is a function of water recovery, which can be predicted from a model.
- ☐ Dynamic simulator development
  - Flotation model and froth recovery model are ready to be implemented to the simulator.
  - Models can be used for circuit simulation, plant optimization and control.

2. Suggestions for Future Research

Even though experimental evidences were given to verify the models developed in this dissertation, they may be insufficient. In addition, the models are not complete since a lot of assumptions and simplifications were made to render the model work. In this regard, several suggestions are made for further research.

In chapter 2, the probability of aggregates entering froth (P_f) was introduced for the first time. It has been well known that the pulp-froth interface behaves like a barrier, and some particles collected by bubbles in the pulp phase fail to be recovered and hence fall back. However, there are no reports in the literature yet, that has systematically investigated the drop-back phenomenon in a flotation cell. Therefore, it is suggested that the P_f model may be validated by using an experimental technique similar to Heweitt *et al.'s* [1]. In a similar sense, the modified model for P_c may be validated as well if proper experimental method is present to account for all ranges of d_1/d_2.

In the flotation model, the value of K_{132} was estimated by known contact angles using an empirical relationship between the contact angle and hydrophobic force. However, this process may be substituted by a first principle since we have the extended DLVO theory. If the potential energy between bubble and mineral surfaces can be predicted by the theory, it may be incorporated with the Frumkin-derjaguin equation [2] to calculate the contact angle, when system properties are given. The reverse relationship may be found also because the original relationship would be derived from first principles.

The velocity increase factor of the flow inside a channel of hydrophobic walls was derived in chapter 4, but it was not validated by an independent experiment. However, it may be possible by a simple experiment. For example, one can evaluate the increase by studying the flow rate of water through a cylindrical plug made of a bunch of capillary glass tubes or sintered glass with certain porosity. Because glass surface can be hydrophobized and corresponding interfacial forces are relatively well known, flow through the hydrophobized media can be analyzed and compared with the untreated media.

In the foam drainage model, the interchangeability between the critical plateau border area (A_{cr}) and the critical rupture thickness (h_{cr}) was discussed. A_{cr} was preferred in the model because the other required more unknown parameters to be substituted in the drainage model. The number of unknown parameters may be reduced if one can devise an equation to correlate them. It can be done by analyzing the relationship between foam lifetime data and the critical rupture thickness data obtained from independent experiments.

References

1. Hewitt, D., D. Fornasiero, and J. Ralston, *Bubble-particle attachment.* Journal of Chemical Society, Faraday Transactions, 1995. **91**: p. 1997-2001.
2. Churaev, N.V. and V.D. Sobolev, *Physical chemistry of wetting phenomena*, in *Colloid stability: the role of surface forces, part 2*, F. Tadros, Editor. 2007, Wiley-VCH. p. 130.